VYSOKÉ UČENÍ TECHNICKÉ V BRNĚ

BRNO UNIVERSITY OF TECHNOLOGY

FAKULTA STROJNÍHO INŽENÝRSTVÍ
ENERGETICKÝ ÚSTAV

FACULTY OF MECHANICAL ENGINEERING
ENERGY INSTITUTE

SUSPENSION FLOW MODELING

MODELOVÁNÍ PROUDĚNÍ SUSPENZÍ

DIPLOMOVÁ PRÁCE
MASTER'S THESIS

AUTOR PRÁCE — Bc. ATTILA HIDEGHÉTY
AUTHOR

VEDOUCÍ PRÁCE — doc. Ing. PAVEL RUDOLF, Ph.D.
SUPERVISOR

BRNO 2013

Vysoké učení technické v Brně, Fakulta strojního inženýrství

Energetický ústav
Akademický rok: 2012/2013

ZADÁNÍ DIPLOMOVÉ PRÁCE

student(ka): Bc. Attila Hideghéty

který/která studuje v **magisterském navazujícím studijním programu**

obor: **Fluidní inženýrství (2301T036)**

Ředitel ústavu Vám v souladu se zákonem č.111/1998 o vysokých školách a se Studijním a zkušebním řádem VUT v Brně určuje následující téma diplomové práce:

Modelování proudění suspenzí

v anglickém jazyce:

Suspension flow modeling

Stručná charakteristika problematiky úkolu:

Práce je zaměřena modelování pohybu pevných částic ve vysoce vířivém proudění hydrocyklonu. Hydrocyklon je konstrukčně a provozně jednoduché zařízení sloužící k separaci částic od kapaliny nebo k jejich třídění dle velikosti a hustoty.

Cíle diplomové práce:

1. Rozbor silových poměrů na částici pohybující se v poli odstředivých sil.
2. Návrh základních rozměrů hydrocyklonu pro odlučování nemagnetických kovových částic.
3. Modelování proudění v hydrocyklonu modelem Euler-Lagrange a tvarová optimalizace hydrocyklonu.

Seznam odborné literatury:

1.Narasimha, M., Brennan, M. S., Holtham, P. N: A review of CFD modelling for performance predictions of hydrocyclone, Engineering Applications of Computational Fluid Mechanics, Vol. 1, No 2, pp. 109-125, 2007.

2. Rudolf, P.: Simulation of multiphase flow in hydrocyclone, Proceedings of conference Experimental fluid mechanics, 2012.

3. Rieger, F., Novák, V., Jirout, T.: Hydromechanické procesy II. 1. vyd. Praha: Vydavatelství ČVUT, 2005. 167 s. ISBN 80-01-03302-3.

Vedoucí diplomové práce: doc. Ing. Pavel Rudolf, Ph.D.

Termín odevzdání diplomové práce je stanoven časovým plánem akademického roku 2012/2013.

V Brně, dne 20.11.2012

L.S.

_____	_____
doc. Ing. Zdeněk Skála, CSc.	prof. RNDr. Miroslav Doupovec, CSc., dr. h. c.
Ředitel ústavu	Děkan fakulty

Abstract

This master thesis deals with the investigation of flow in a hydrocyclone, which is a separator device for separating solid phase from a fluid (mainly water). Due to the tangential inlet to the device high swirling flow is gained, which results the suction of air through the over and underflow, where the air core plays an important role in separating particles. The investigation is carried out with the aid of CFD.

Keywords:
hydrocyclone, DPM, RSM, separation, air core

Abstrakt

Diplomová práce se zabývá prouděním v hydrocyklónu. Hydrocyklón je separační stroj, kterým slouží k oddělování pevných částice z kapaliny (nejčastěji z vody). Díky tangenciálnímu vstupu do zařízení nastává silné vířivé proudění, které způsobuje přisávání vzduchu přes horní a dolní výtok. Toto vzduchové jádro hraje důležitou roli v separaci částic. Výpočty jsou provedeny pomoci CFD.

Klíčová slova:
hydrocyklón, DPM, RSM, separace, vzduchové jádro

Bibliografic citation:

HIDEGHÉTY, A. *Modelování proudění suspenzí.* Brno: Vysoké učení technické v Brně, Fakulta strojního inženýrství, 2013. 96 s. Vedoucí diplomové práce doc. Ing. Pavel Rudolf, Ph.D..

Affirmation:

I declare that this master thesis results of my own work and knowledge, led by doc. Ing. Pavel Rudolf, Ph.D. and all used sources are duly listed in the bibliography.

In Brno, 24th May 2013 Attila Hideghéty

Acknowledgements

I would like to thank my supervisor doc. Ing. Pavel Rudolf Ph.D for all support, which escorted me through the whole writing.

Content

1. Introduction

This master thesis aims on investigating the flow in a hydrocyclone. The task is to carry out CFD simulations in the software FLUENT. The complexity of such a calculation is significant, because of the interaction of water, air and dispersed solid phase. A detailed view of decomposition of forces acting on particles has to be carried out.

Hydrocyclones are used long time ago, thus experimental data and empirical equations are available. The initial design shall respect these equations. After it the optimization will be needed, to investigate the effect of changing the particular dimension on the hydrocyclones work.

2. Suspension

Before the start, the meaning of the expression suspension has to be cleared. The first thing is to understand the fact, that in the nature does not exist absolute clean water or other continuum phase. In the water there are located small particles (such as dust), microorganisms (such as bacteria) and gases (both soluble and insoluble), which can be invisible for the naked eye, hence the notion dispersed multiphase systems has to be introduced. However these systems can be divided into classes according to phases that are mixed:

1. Liquid + solid phase
2. Liquid + another immiscible liquid
3. Liquid + gas

1. The first dispersed system (liquid + solid phase) has priority for this work, therefore this case will be investigated onwards. This system is the mixture of continuum (mostly water) and solid phase, and can be divided into more subsystems:

    1.1. Solution: When two or more substances are ideally mixed. This homogenous mixture is called the solution. If assuming spherical particles the diameter is under 10^{-9} metres. An example can be salty water, where the water dissolves the salt. In this case the water is the solvent. The salt loses its solidity [1].

Figure 1: Salt added to water [2]

1.2. Colloid: It is important to know that a different science branch deals with colloids, which was founded by a chemist from Scotland named Thomas Graham. The size of solid particles ranges from 10^{-9} to 10^{-6} metres, they are invisible for the naked eye and an optical microscope, too. This system can be defined as heterogeneous, in which the substance (in this case dispersed solid phase) is dispersed in another continuous phase (often water, oil). An important phenomenon is connected with colloids, called the Tyndall effect. This effect is a light scattering phenomenon, the upcoming light into the colloid is scattered by small particles [3], [4].

Figure 2: The glass on the left contains colloid, showing Tyndall effect, the glass on the right probably contains solution or suspension [5].

1.3. Suspension is for this thesis the most relevant part of these systems, because later the flow of such a suspension has to be investigated. To understand the difference between suspension and colloid is very important. The simplest explanation is on an example, let assume a vessel of water, if sand is thrown into it, consequently the sand will settle if left undisturbed, due to the effect of gravity. However, colloids will act differently compared to suspensions. The dispersed phase in colloids will not settle.
The size of the solid phase usually is above 10^{-6} metres. These particles can be observed by an optical microscope.
In addition we will describe the flow of suspension with a small amount of non-magnetic particles (such as aluminium) with water [3].

Property	True Solution	Colloidal Solutions	Suspension
Size of the particles	< 1nm	1 – 1000nm	> 1000nm
Nature	Homogeneous	Heterogeneous	Heterogeneous
Filterability (Diffusion through parchment paper)	Particles of true Solution diffuse rapidly through filter paper as well as parchment paper.	Colloidal particles pass through parchment paper.	Suspension particles do not pass through filter paper and parchment paper.
Visibility	Particles of True Solution are not visible to naked eye.	Colloidal particles are not seen to naked eye but can be studied through ultra microscope.	Suspension particles are big enough to be seen by naked eye.
Tyndall effect	True Solution does not show Tyndall effect.	Colloids shows Tyndall effect.	Suspension may or may not show Tyndall effect.
Appearance	Transparent	Translucent	Opaque

3. Forces acting on particles in fluids

The mathematical model is based on the Lagrangian concept [6]. The velocity and trajectory of the particles is only the function of time. In accordance with Newton's second law the following equation can be written [7]:

$$m_p \cdot \vec{a}_p = \vec{F}_i \tag{1}$$

Where $\vec{F}_i$ is the vector of sum of forces acting on the particle, m_p is the mass and $\vec{a}_p$ is the vector of acceleration of the particle. Expression (1) can be extended:

$$\rho_p \cdot V_p \cdot \frac{d\vec{u}_p}{dt} = \vec{F}_V + \vec{F}_S \tag{2}$$

The term on the righthand side of equation (1) is divided into forces acting on volume $(\vec{F}_V)$ and forces acting on surface $(\vec{F}_S)$. ρ_p, V_p, u_p – correspond to the density, the volume and the velocity of the particle, respectively. From now on the volume forces will be indicated with blue and surface forces with red colour [8].

$$\rho_p \cdot V_p \cdot \frac{d\vec{u}_p}{dt} = \vec{F}_g + \vec{F}_c + \oiint_S \boldsymbol{\sigma} \cdot \vec{n} \cdot dS \tag{3}$$

Where $\vec{F}_g$ is the gravitational and $\vec{F}_c$ the centrifugal force. $\boldsymbol{\sigma}$ is the stress tensor of liquid on the particles surface.

$$\rho_p \cdot V_p \cdot \frac{d\vec{u}_p}{dt} = \vec{F}_g + \vec{F}_c + \underbrace{\oiint_S (\mathbf{p} - \mathbf{\Pi}) \cdot \vec{n} \cdot dS}_{\vec{F}_{Surface}} \tag{4}$$

Stress tensor consists of pressure (**p**) and shear stress (**Π**). Although this equation is simple and beautiful, it is unusable for further applications. There is the absence of the pressure and shear stress distribution along the surface, that is because of the impossibility of analytical solution of the Navier – Stokes equation [9].
In order to solve the equation of force equilibrium, the surface integral on the right hand side of the equation has to be substituted with another forces, in other words this can be considered as a mathematical modelling. In the past several authors provided a more detailed investigation of this problem, this knowledge will be the base of the ongoing analysis.

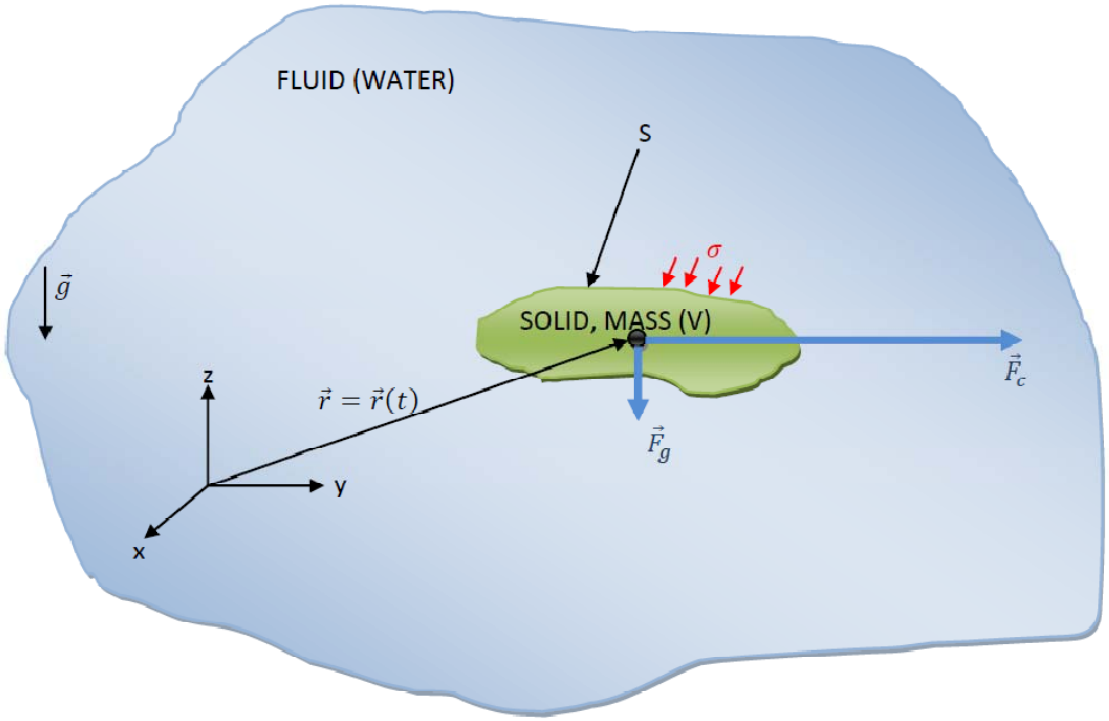

Figure 3: Scheme of a rigid body supplemented with forces acting on it

This decomposition according to Vejražka [9] is applied on large bubbles dynamics:

$$\rho_p \cdot V_p \cdot \frac{d\vec{u}_p}{dt} = \vec{F}_G + \vec{F}_C + \vec{F}_{BG} + \vec{F}_{BC} + \vec{F}_D + \vec{F}_{AM} + \vec{F}_H + \vec{F}_T + \vec{F}_L + \cdots \tag{5}$$

This substitution is valid for bubbles in the flow. The influence of wall, free surface and other bubbles in the neighbourhood is not included.

- $\vec{F}_G$ – is the gravity force of the particle.

$$\vec{F}_G = \rho_p V_p \vec{g} \tag{6}$$

Where $\rho_p, V_p, \vec{g}$ denote density, volume of the solid particle and gravitational acceleration [9].

- $\vec{F}_{BG}$ – is the buoyant force acting on the particle (Archimedes) in gravity field and acts in the opposite direction [9].

$$\vec{F}_{BG} = -\rho V_p \vec{g} \tag{7}$$

Where ρ denotes fluid density.

- $\vec{F}_C$ – is the centrifugal force acting on the particle. The best suited coordinate system for calculating this force is the cylindrical, however all other forces are derived in Cartesian coordinate system.

$$\vec{F}_C = \rho_p V_p \frac{v_\varphi^2}{r} \vec{\varsigma} \qquad a_\varphi = \frac{v_\varphi^2}{r} \tag{8}$$

Where v_φ is the tangential velocity of the particle, r the diameter of its trajectory and $\vec{\varsigma}$ represents the unit vector in cylindrical coordinate system for radial direction (figure 10). The decomposition in Cartesian coordinate system [10] (figure):

$$r^2 = x^2 + y^2 \qquad v_\varphi^2 = v_x^2 + v_y^2$$

$$\cos\varphi = \frac{x}{r} = \frac{x}{\sqrt{x^2 + y^2}} \qquad \sin\varphi = \frac{y}{r} = \frac{y}{\sqrt{x^2 + y^2}}$$

$$a_{\varphi x} = \frac{v_\varphi^2}{r}\cos\varphi \qquad a_{\varphi y} = \frac{v_\varphi^2}{r}\sin\varphi$$

$$a_{\varphi x} = \frac{v_x^2 + v_y^2}{x^2 + y^2}\, x \qquad a_{\varphi y} = \frac{v_x^2 + v_y^2}{x^2 + y^2}\, y$$

$$\vec{F}_C = \rho_p V_p \frac{v_x^2 + v_y^2}{x^2 + y^2}\, x\, \vec{\imath} + \rho_p V_p \frac{v_x^2 + v_y^2}{x^2 + y^2}\, y\, \vec{\jmath} \tag{9}$$

Where v_x and v_y is the velocity in direction $\vec{\imath}$ and $\vec{\jmath}$, x and y is the position of the particle. The suggested equation (8) for this approach has got a crucial insufficiency, because the forces are derived for particles trajectory, which are circles, nevertheless in a real application (hydrocyclone) the shape of trajectory is some kind of a helical form. However we do not know the trajectory apriori, therefore this simplification has to be introduced.
The approach presented in [11] assumes the motion of particle on the wall of the cone section in the hydrocyclone, hence the trajectory is quasi-known.

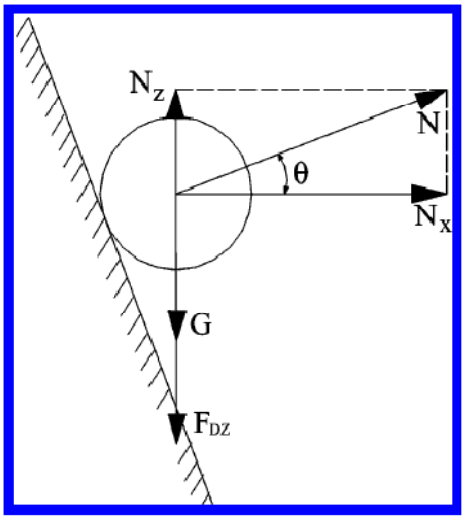

Figure 4: The force decomposition on the wall [11]

- $\vec{F}_{BC}$ – the buoyant force in the centrifugal field, the only change comparing to $\vec{F}_C$ is that we swap particles density for fluids density.

$$\vec{F}_{BC} = \rho V_p \frac{v_x^2 + v_y^2}{x^2 + y^2}\, x\, \vec{\imath} + \rho V_p \frac{v_x^2 + v_y^2}{x^2 + y^2}\, y\, \vec{\jmath} \tag{10}$$

- $\vec{F}_D$ - is called the drag force and arises from viscosity of the fluid (Stokes drag law). The drag force represents the resistance of the fluid, hence it is derived from the energy conservation equation. To get the particle into motion we have to exert a force on it, from this idea the force does work, due to viscosity the energy dissipates [9].

$$\vec{F}_D = -\pi\, \rho\, C_D \frac{d^2}{8} \left(\vec{u}_p - \vec{u}\right) \left|\vec{u}_p - \vec{u}\right| \tag{11}$$

Where C_D is the drag coefficient and can be calculated from correlated equations which can be found in [12], $\vec{u}$ and $\vec{u}_p$ is the velocity of liquid and particle, d is the diameter of the spherical particle. The coefficient C_D mainly depends on the Reynolds number, the shape and the size of the particle [12].

- $\vec{F}_{AM}$ - represents the force accelerating the apparent mass of particle relative to fluid. Let us assume that the particle accelerates the surrounding fluid too, hence there must be an interaction between the particle and the fluid acceleration. It involves only inviscid processes, that means the potential flow is investigated for obtaining the influence of fluid on the particle [9]. Prandtl elucidated the reason and took some pictures:

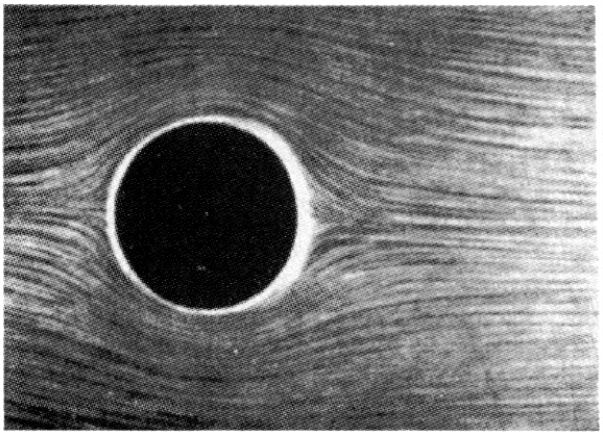

Figure 5: The flow right after the start, reproduced from [13]

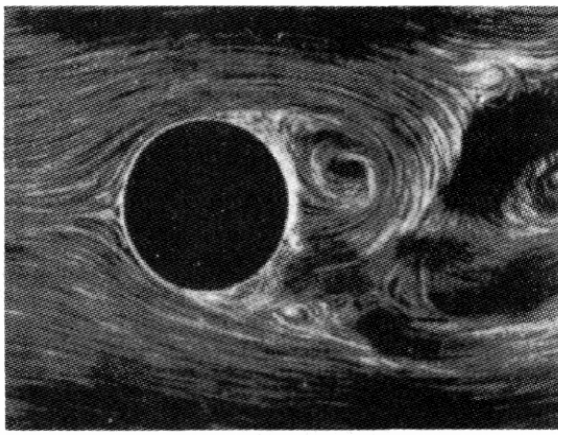

Figure 6: The flow after a few seconds, reproduced from [13]

The photo on the left was taken right after the start of the flow, it is very common to the potential flow, but the photo on the right was shot after a few seconds. The answer of this phenomenon is hidden in the equation for vorticity transport, because vorticity is produced on the boundaries (walls) and transporting the vortices from the boundary layer, which is time dependant. This viscous effects cannot be neglected so these reactions will be present in the next force (history force) [9].

$$\vec{F}_{AM} = -\frac{d}{dt}\left[\rho\, C_A\, V_p(\vec{u}_p - \vec{u})\right] \tag{12}$$

Where C_A is the coefficient of added-mass, for a spherical particle the value is usually $0{,}5$, $\vec{u}_p$ and $\vec{u}$ is the absolute velocity of the object and the fluid respectively. It is important to recognize the fact, that the fluid velocity differentiation must be substantial.

If ρ, C_A, V_p are constants, then:

$$\vec{F}_{AM} = -\rho\, C_A\, V_p \frac{d}{dt}(\vec{u}_p - \vec{u}) \tag{13}$$

- $\vec{F}_T$ – Tchen force is derived from the N-S equation for inviscid fluids and is sometimes implemented in the mass-added force. It shows the impact of the fluids local acceleration on the object [9].

$$\vec{F}_T = \rho\, V_p \frac{D\vec{u}}{Dt} \tag{14}$$

  It is also important to notice that for fluid substantial derivative is used.

- $\vec{F}_H$ – history force resembles the added-mass force, but it involves viscous processes only. The reaction to the change of velocity is included (unsteady motion). The force is shown in the picture below.

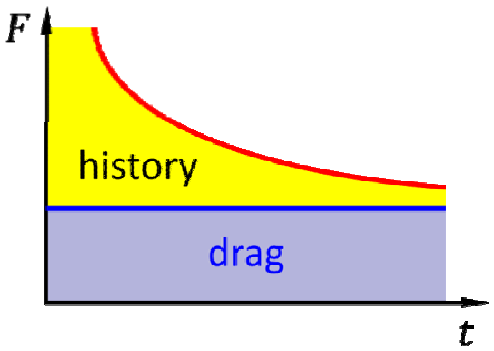

Figure 7: The distribution of history and drag force depending on time [9]

$$\vec{F}_H(t) = -6\pi\mu R \int_0^t \left(\frac{d\vec{u}_p}{dt_p} - \frac{d\vec{u}}{dt_p}\right) K\left[\frac{\nu(t-t_p)}{R^2}\right] dt_p \tag{15}$$

Where μ and ν denote dynamic and kinematic viscosity, respectively, K is the kernel function and t_p is the time in "past". The kernel function is available only in a few cases and its crucial feature is that the prediction is worthwhile only in short time. The advantage of it is, that for higher Reynolds number it can be neglected, but for low Reynolds numbers claims a computationally demanding problem (causes integro-differential equation) [9].

The substitution of forces was carried out by two Dutchman H. Meng and C. W. M. Van der Geld. They investigated the particles behavior around a cylinder in a steady non-uniform liquid flow. Particle diameter and its density play a significant role in particle trajectory computations [8]. The flow field was computed for an inviscid fluid for high Reynolds numbers. Forces, which are shown above will not be displayed once again $(\vec{F}_{AM}, \vec{F}_D)$

$$\vec{F}_{Surface} = \vec{F}_D + \vec{F}_{AM} + \vec{F}_{PG} + \vec{F}_B + \vec{F}_{LS} + \cdots \tag{16}$$

- $\vec{F}_{LS}$ – this force was introduced by Saffman (1968), sometimes called "shear-lift" too [8].

$$\vec{F}_{LS} = C_L \frac{d^2}{4} \sqrt{\rho\,\eta\,\kappa}\,\vec{e}_\kappa \times (\vec{u}_p - \vec{u}) \tag{17}$$

In equation above C_L is the lift coefficient, its value is $6{,}46$ and was determined by Saffman, κ is the liquid shear rate, in the form of liquid velocity gradients and $\vec{e}_\kappa$ is the unit vector of κ.

- $\vec{F}_{PG}$ – pressure-gradient force was revealed from the N-S equation, "represents the force required to accelerate the liquid which would occupy the space V_p if the particle were absent" [8], [12].

$$\vec{F}_{PG} = \rho\, V_p \left(\frac{d\vec{u}}{dt} - \frac{\eta}{\rho}\,\Delta\vec{u}\right) \tag{18}$$

- $\vec{F}_B$ – "Basset history force indicates the effect of the history of relative accelerations. This force actually accounts for the diffusion of the vorticity generated at the particles surface into the surrounding fluid." by Landau and Lifshitz in [8]. The Basset history force is valid for solid spheres and Stokes flow, that means $Re \ll 1$ [9].

$$\vec{F}_B = -\frac{3d^2}{2}\sqrt{\pi\,\rho\,\eta}\int_{t_0}^{t}\left(\frac{d\vec{u}_p}{dt}-\frac{d\vec{u}}{dt}\right)_{t=\tau}\frac{d\tau}{\sqrt{t-\tau}} \tag{19}$$

Another substitution of surface forces was published by Kraipech in [14]. Forces which distinguish from the previous overview will be indicated once again, for calculating the pressure-gradient force another formula is used here. This decomposition has got one advantage against the other, because it takes into account the rotation of the particle around its own axis, this phenomenon is considered by the Magnus lift force.

$$\vec{F}_{Surface} = \vec{F}_D + \vec{F}_{AM} + \vec{F}_{PG} + \vec{F}_B + \vec{F}_{LS} + \vec{F}_{LM} + \cdots \tag{20}$$

- $\vec{F}_{LS}$ – Saffman lift force is caused by the pressure distribution on the particle due to the rotation of fluid induced by the fluid velocity gradient ($\dot{\gamma}$ is the rate of fluid deformation) [14].

$$\vec{F}_{LS} = 1.615\,d^2\sqrt{\mu\,\rho\,\dot{\gamma}}\left(\vec{u}-\vec{u}_p\right) \tag{21}$$

- $\vec{F}_{LM}$ – Magnus lift force is caused by the particle rotation, the velocity varies on both sides of the particle due to the rotation, which induces uneven pressure distribution (force) [14].

$$\vec{F}_{LM} = \frac{1}{2}\,\rho\,C_L\left(\vec{u}-\vec{u}_p\right)^2\frac{\pi\,d^2}{4} \tag{22}$$

- $\vec{F}_{PG}$ – pressure gradient force is caused by the pressure gradient around the particle [14].

$$\vec{F}_{PG} = -\vec{u}_p\nabla p \tag{23}$$

4. The treatment of suspensions in engineering sciences - hydrocyclone

The first hydrocyclone was invented by a Dutchman M. G. Driessen in the time of the second world war. Immediately it gained significant task in raw mineral industry. The most common features of a hydrocyclone are thickening, sorting, classifying (by density or size) purging, last but not least separating. Thus it can be stated, that it is a useful and universal device, sometimes with the same or better outcome as a single-purpose mechanism [10]. The principle of operation in a hydrocyclone is represented by the large centrifugal acceleration, where the magnitude of the centrifugal force is severalfold (sometimes two or three thousand times) larger, than the gravitational, depending on the dimensions and operating conditions of the hydrocyclone [15].
Devices where the separating process is performed by the gravitational force are inadequate in industries dealing with fine-grained materials. This assertion is partly based on the fact, that gravity varies to third power of diameter and Stokes frictional force varies to the second power of diameter [6]. According to this fact the terminal velocity dramatically decreases depending on the size.
Nowadays hydrocyclones exist in several shapes and constructions. The most common construction is with a cone shape (figure 8.), nevertheless devices exist with another shapes such as cylindrical, helical, however the most general is the hydrocyclone with the cone part.
Hydrocyclones have been used for almost 90 years, mainly in chemical and mineral processing industries. In future it would be beneficial to extend the use of hydrocyclones to medical science and biotechnology applications [25].

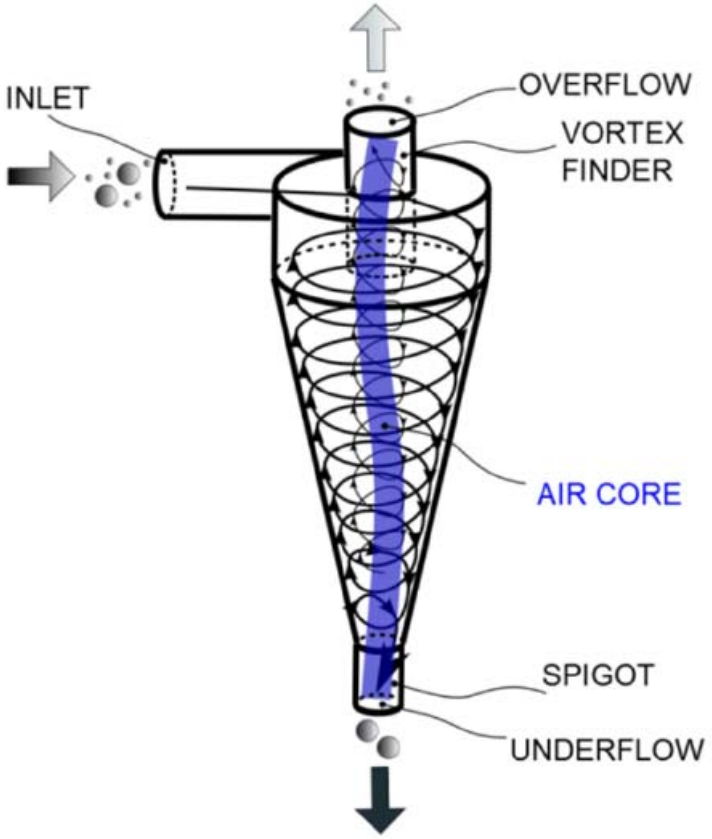

Figure 8: Hydrocyclone [24]

4.1 Construction of HC

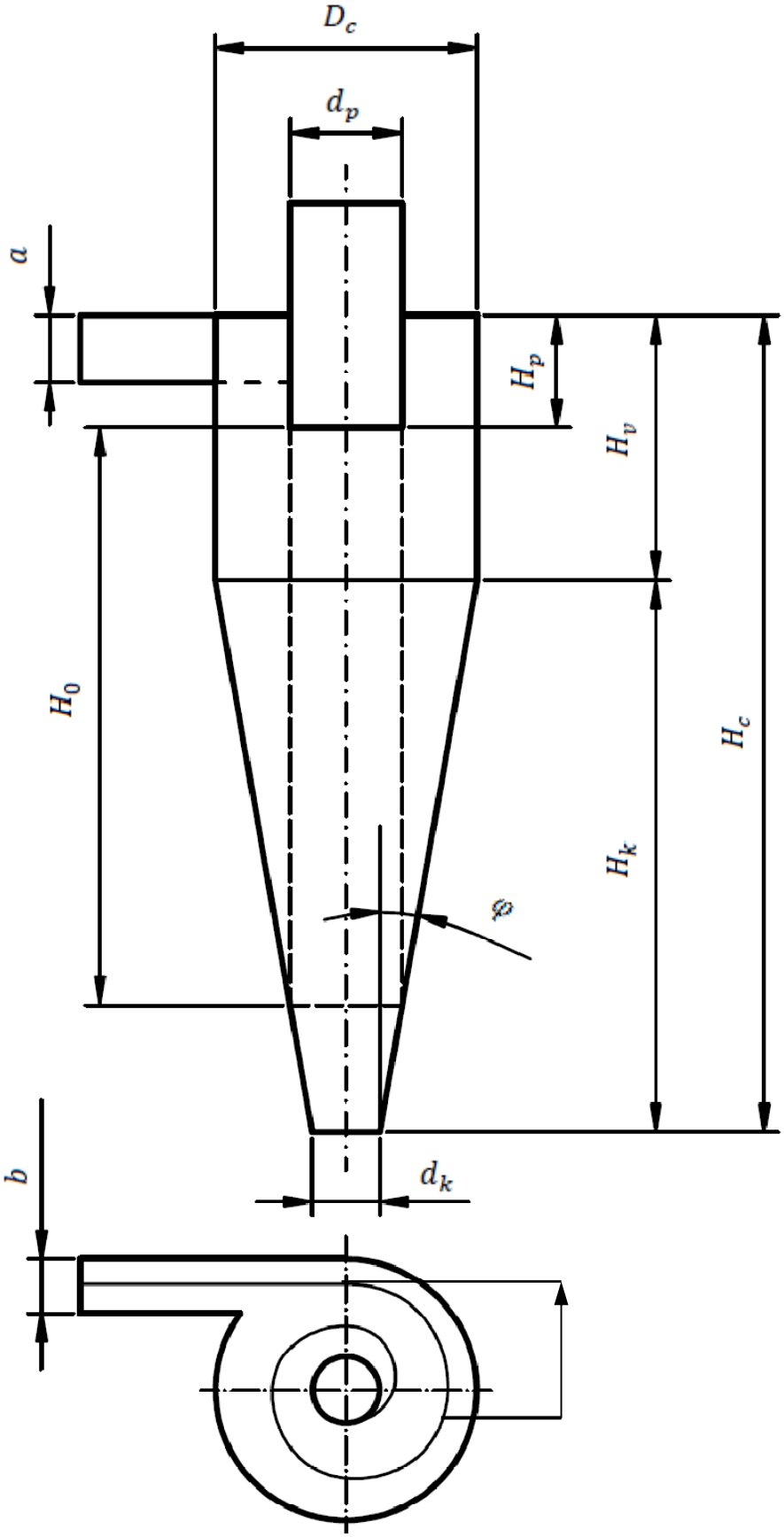

Figure 9: The design of a hydrocyclone

Legend:

D_c - diameter of the cylindrical section

d_p - diameter of the vortex finder

H_p - length of the vortex finder

H_v - length of the cylindrical section

H_c - length of the hydrocyclone

H_k - length of the conic section

φ - angle of the conic section

d_k - diameter of the spigot

a, b - dimensions of the inlet (rectangular shape)

4.2 Flow in hydrocyclones

The purpose of this master thesis is to describe the flow of a suspension flow in a hydrocyclone. The suspension will seem for observers as normal water from a water tap, although there will be dispersed small solid particles sized only micrometers and with a small weight ratio in contrast to the fluid. The aim is to optimize the main dimensions of the separating device, to separate the small particles from liquid. Generally, in more papers it is reported the fact, that the residence time of particles in such a device is very short, according to Thew and Smyth cited in [16] only a few seconds (sometimes under 2 seconds), depending on the design of the HC.
As the suspension enters the hydrocyclone, it has got a straight motion, after accessing the cylindrical part the fluid starts to flow spirally relative to the axis, hence the responsibility of the main separation process is taken by the cone and the cylindrical, which are responsible for the large centrifugal force. See figure 9. and On account of the spiral motion more recommended coordinate system is the cylindrical (r, θ, z) than the Cartesian (x, y, z).

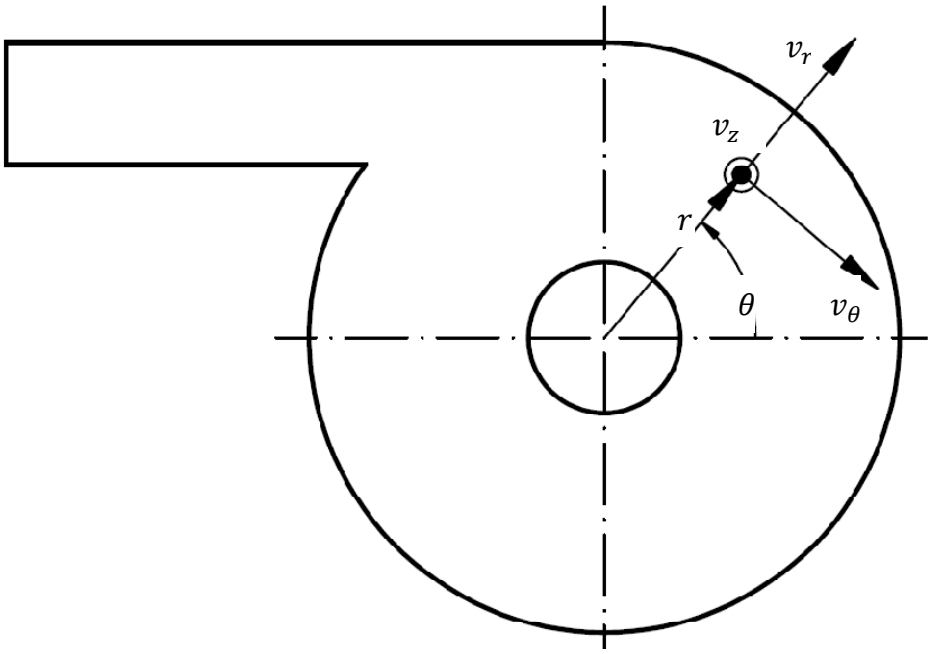

Figure 10: Radial, tangential and axial velocity

Thanks to this behaviour an outer (see figure 10.) and an inner vortex (see figure 12 c) is developed. The large centrifugal force field results in the decrease of static pressure along the axis (the mass is squeezed out to the wall), thus the suction of air from the vortex finder (overflow) and spigot (underflow) arises (equation 34). In addition this means creating an air core in the centre of the hydrocyclone, which increases the turbulence fluctuation and decreases the separation efficiency, as was presented e.g. Sripriya, Kaulaskar, Chakraborty and Meikap cited in [16].
The fully analytical investigation of the flow in a hydrocyclone remains still unclear, because the Navier Stokes eqation is cannot be solved analytically.

Particles which are resident in the flow domain, respecting the laws of physics can escape through the vortex finder or through the spigot. The lighter (solid phase with smaller diameter) fraction escapes the flow through the vortex finder and heavier (solid phase with bigger diameter) through spigot.
The most meaningful variables are velocity profiles, from which we can imagine the flow. Velocity profiles were first measured by Kelsall cited in [16]. According to his work, which establishes that tangential velocity profile resembles the Rankine vortex model. A few researchers addressed the problem of measuring velocity profiles in hydrocyclones, as a result in general they agreed on the fact, that measuring velocity profiles in the air core is a critical problem. The air core plays a key role in separating solid particles from fluid, on account of the spigot occlusion according to Sripriya, Kaulaskar, Chakraborty and Meikap cited in [16].

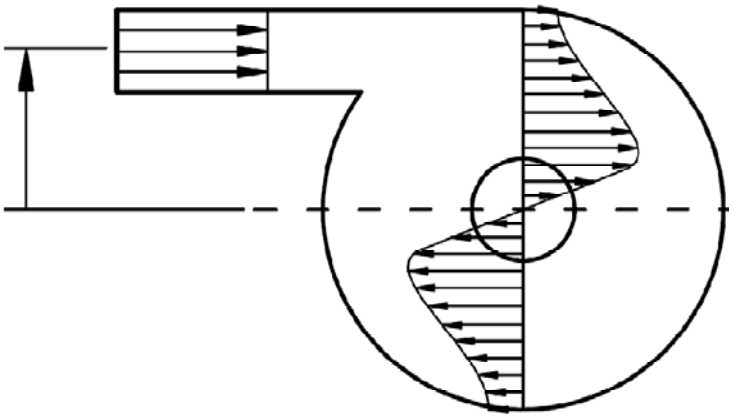

Figure 11: Tangential velocity profile shown (cross-section for $z = const.$)

To get a detailed overview for a better understanding of flow field within a hydrocyclone, the velocity profiles are plotted in the radi-axial cross section.

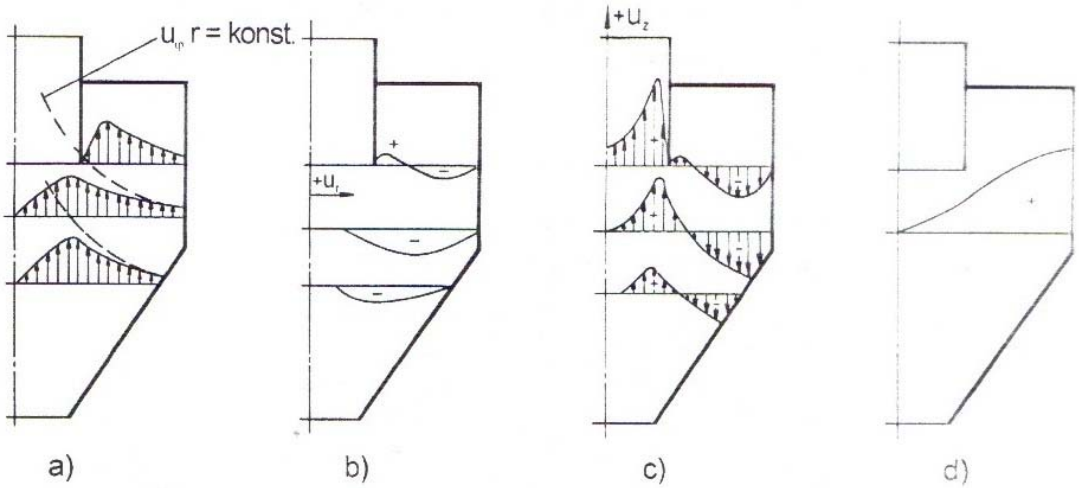

Figure 12: a.) distribution of tangential velocity, b.) distribution of radial velocity, c.) distribution of axial velocity, d.) distribution of static pressure [17]

Focusing on the picture above, it illustrates the following facts (from left to right):
a.) in the core section the tangential velocity increases, then decreases towards to the wall of the hydrocyclone.

b.) the radial velocity profile indicates the fluid motion in the direction of the axis (this phenomenon is achieved due to the shape of the separation device).

c.) the axial velocity profile is the most important, showing the creation of a secondary vortex. In addition the flow of fluid near to the wall of hydrocyclone flows in the direction of the spigot, however the fluid in the core flows to the vortex finder.

d.) the distribution of static pressure decreases from the wall to direction of the axis.

4.3 Determination of equations describing the flow

4.3.1 Tangential velocity

The most important impact on the pressure field and separation ability has got the tangential velocity [17], and it can be defined by the following half-empirical expression, which is valid in the annulus (between the wall of the hydrocyclone and wall of the vortex finder, see figure 8):

$$u_\varphi \cdot r^n = konst. \tag{24}$$

Where u_φ is the tangential velocity, r is the radius from the axis and n is an exponent, which value ranges from $-0{,}5$ to $0{,}8$ and depends mainly on the hydrocyclones dimensions and the suspensions physical properties. The definition of n will be explained in the next chapter [17].

$$u_\varphi \cdot r^n = u_{\varphi R} \cdot R^n \tag{25}$$

Where $u_{\varphi R}$ is the tangential velocity on the hydrocyclones wall, and can be specified from the equilibrium of angular momentums, but it is only valid for frictionless flows (dissipation is not assumed), therefore it has to be supplemented by correction coefficient α, see equation (27). Equilibrium of angular momentums (figure 10.) [17].

$$u_{\varphi R_c} \cdot R_c = u_1 \cdot R_S \tag{26}$$

$$u_{\varphi R_c} = \frac{u_1 R_S}{\alpha R_c} \tag{27}$$

Where u_1 is the inlet velocity to the hydrocyclone, R_S is the radius of the inlet surface centroid. After expanding expression (27) into equation (25), we can obtain [17]:

$$u_\varphi = \frac{u_1 R_S}{\alpha R_c}\left(\frac{R_c}{r}\right)^n \tag{28}$$

Furthermore the tangential velocity determination is possible on the boundary of hydrocyclones core $(r = r_p)$ [17]:

$$u_{\varphi_p} = \frac{2u_1 R_S}{\alpha D_c}\left(\frac{D_c}{d_p}\right)^n \tag{29}$$

Supposing approximation equation for tangential velocity in the core:

$$u_\varphi \cdot r^m = u_{\varphi_p} \cdot r_p^m \tag{30}$$

The evidence suggests that the value of exponent m should be $-0{,}5$ according to Loxham cited in [17].

$$u_\varphi = u_{\varphi_p} \left(\frac{r}{r_p}\right)^{0{,}5} \tag{31}$$

Apparently, after substituting u_{φ_p} (29) into expression (31), the following equation can be yielded:

$$u_\varphi = \frac{2u_1 R_S}{\alpha D_c} \left(\frac{D_c}{d_p}\right)^n \sqrt{\frac{r}{r_p}} \tag{32}$$

4.3.2 Pressure distribution equation

An alternative approach is necessary, consequently the starting point will be the Navier-Stokes equation in cylindrical coordinate system [18]. Generally the tangential velocity comparing to radial and axial velocity is the most significant, in addition they can be neglected.

$$u_\varphi = \frac{2u_1 R_S}{\alpha D_c} \left(\frac{D_c}{d_p}\right)^n \sqrt{\frac{r}{r_p}} \tag{33}$$

Simplifying the Navier-Stokes equation and assuming only tangential velocity the pressure distribution in differential form for direction r can be written:

$$\rho \frac{u_\varphi^2}{r} = \frac{dp}{dr} \qquad \Leftrightarrow \qquad dp = \rho \frac{u_\varphi^2}{r} dr \tag{34}$$

Where ρ denote density of the disperzum.
After the utilization of expressions (28) and (34), the following equation can be obtained:

$$dp = \rho \left(\frac{u_1 R_S}{\alpha R_c}\right)^2 R_c^{2n} r^{-2n-1}\, dr \tag{35}$$

To overcome this ordinary differential equation, integration has to be provided.

$$p = -\rho \left(\frac{u_1 R_S}{\alpha R_c}\right)^2 \frac{1}{2n} \left(\frac{R_c}{r}\right)^{2n} + C \tag{36}$$

Integration constant C can be derived the boundary conditions (for $r = R_c$ and $p = p_1$):

$$C = p_1 + \rho\left(\frac{u_1 R_S}{\alpha R_c}\right)^2 \frac{1}{2n} \tag{37}$$

Substituting the right hand side from (37) for C in (36), it can be gained:

$$p = p_1 - \rho\left(\frac{u_1 R_S}{\alpha R_c}\right)^2 \frac{1}{2n}\left[\left(\frac{R_c}{r}\right)^{2n} - 1\right] \tag{38}$$

This final equation represents the pressure distribution depending on variable r, but its authenticity is limited for the annulus (between the core and the wall of the hydrocyclone).

4.3.3 Correction coefficient α

As mentioned formerly this coefficient corrects the equilibrium of angular momentum, and was derived for tangential inlet depending on some dimensions of the separating device. For this dependence the following approximation equation was created [17]:

$$\alpha = [(-0{,}3467x + 0{,}462)x - 0{,}1484]x + [(0{,}048y - 0{,}1146)y + 0{,}0491]y + \\ +(0{,}4292x + 1{,}823y - 0{,}9444)xy + 1 \tag{39}$$

$$x = \frac{2b}{D_c} \text{ and } y = \frac{S_1}{S_p} \tag{40}$$

Where x should lie in the interval $0 < x < 0{,}8$ and y in the interval $0{,}45 < y < 1{,}8$.

4.3.4 The calculation of the parameter n

The study of Muschelknautzen presented the drop of the angular momentum in the flow area [17]. From his experimental data the following equation was formulated for calculating the exponent n:

$$n = 1 - \frac{\ln\left(\frac{S_1\alpha}{S_1\alpha + (\lambda_l + \lambda_S)\pi R_s H_c}\right)}{\ln\frac{d_p}{D_c}} \tag{41}$$

Where λ_l is the fluid friction coefficient, λ_S is the equivalent coefficient of friction of dispersed particles along the wall. From numerous experimental data a formula was established for calculation both coefficients by Muschelknautzen cited in [17]:

$$\lambda_l = \left\{ \left[\frac{0{,}628 H_c (D_c - d_p) \mu}{\dot{V}_l d_p \rho} \right]^{1{,}63} + \{40{,}3 + 5{,}4 \cdot 10^{-3} [-\ln(k^* + 10^{-6})]^5\}^{-2} \right\}^{0{,}4} \quad (42)$$

Where μ and ρ are the molecular viscosity and density of the fluid medium. The parameter k^* is the relative roughness on the wall of the hydrocyclone and can be computed:

$$k^* = \frac{k_{mid}}{D_c} \quad (43)$$

This formula is generally valid for pipes, it is evident that the sections of hydrocyclone are analogous to pipes. Parameter k^* is dimensionless and k_{mid} is the absolute roughness of the surface depending on the quality and the material.

material	quality of the wall	k_{mid} [mm]
steel	new, purified	0,1
	rusty (partially)	0,35-0,4
	rusty (after a long time)	1,2-3,0
cast-iron	new	0,5-1,0
	rusty (partially)	1,5

Chart 1: Absolute roughness [19]

According to Šob [19] the values in chart 1 for k_{mid} are proposed, however they are only indicative.

$$\lambda_S = 1{,}7 f \left(\frac{\rho_S - \rho}{\rho_S} \right) \frac{S_1 w_1 \alpha}{R_S \sqrt{D_c d_p}} \quad (44)$$

Although the determination of λ_S is possible according to equation (44), the weakness is that it is valid only if w_1 is smaller than 0,1 $(w_1 < 0{,}1)$, where w_1 is the mass fraction of solid phase in a fluid. In the same expression the variable f is called friction coefficient, and it is dependent on the type of liquid, the type of dispersed medium and on the material of the devices wall. Its value is estimated in the interval of 0,1 and 0,4.
In order to get desirable tangential velocity profile from equation (24) the obtained n (41) should be larger than -0,5 $(n > -0{,}5)$, otherwise if $n < -0{,}5$ the calcuted variable can result in inaccurate values [17].

4.3.5 Separation in cyclones

It is evident that defining the efficiency parameter for machines and devices is relevant, therefore a hydrocyclone is not an exception. The parameter shows the rate of "economical" operation. The efficiency of a hydrocyclone is characterized by 3 parameters: the critical diameter, fractional and total separability.
Critical diameter D_{50} concerns the size of the particle, and it means that the separability in the cyclone is 50%. If the particles diameter is bigger than D_{50}, it will be separated with the separability bigger than 50%. On the other hand, if the size is smaller than D_{50}, it will operate with lower separability.
The critical diameter is derived from Ljaščenkos and Reynolds number [17].

$$D_{50} = \frac{3}{\sqrt{\pi}} \sqrt{\frac{S_1\,\mu}{H_0(\rho_s - \rho)u_1}} \frac{\alpha\, D_c}{2\, R_s} \left(\frac{d_p}{D_c}\right)^n \tag{45}$$

H_0 represents the height of the core and can be written (see figure 8.):

$$H_0 = H_v - H_p + \frac{D_c - d_p}{D_c - d_k} H_k \tag{46}$$

Equation (45) represents the dependency of critical diameter mainly on the dimensions of hydrocyclone, inlet velocity and physical properties of fluid and solid phase.

Fractional (grade) separability φ_i
Is defined as the ratio of separated fractional mass sized D_i (particle diameter) to mass on the inlet of the same fraction.

$$\varphi_i = \frac{\dot{m}_{sik}}{\dot{m}_{si1}} \tag{47}$$

Where $\dot{m}_{sik}$ is the mass flow rate of solid phase sized D_i caught in the underflow (spigot) and $\dot{m}_{si1}$ is the mass flow rate of solid phase sized D_i entering the separator.

Total separability φ
Is defined as the ratio of separated mass by the hydrocyclone to the mass on the inlet.

$$\varphi = \frac{\dot{m}_{sk}}{\dot{m}_{s1}} \tag{48}$$

Where $\dot{m}_{sk}$ is the mass flow rate of solid phase separated in the underflow (spigot) and $\dot{m}_{s1}$ is the mass flow rate of solid phase entering the separator.

4.3.6 Efficiency of hydrocyclones

Unfortunately the approach used in this chapter does not enable the correct prediction of the efficiency η_h of hydrocyclones, furthermore it is important to concentrate on the fact that they are designed so that the 90% or more of fluid mass should escape the device through the vortex finder. In different literature several methods are explored, this thesis interprets the following evaluation of efficiency:

$$\eta_h = \frac{\dot{m}_{sk}}{\dot{m}_{s1}} \frac{\dot{m}_{lp}}{\dot{m}_{l1}} = \varphi \frac{\dot{m}_{lp}}{\dot{m}_{l1}} \tag{49}$$

Where $\dot{m}_{lp}$ is the mass flow rate of fluid escaping through the vortex finder and $\dot{m}_{l1}$ is the mass flow rate entering the hydrocyclone [17].

4.3.7 Distribution of fractional separability

Sometimes it is called the “recovery to underflow”. The distribution of fractional separability normally is determined from an experiment (hydrocyclone manufacturers should supply it), even so exists another possibility. With the aid of mathematics we can express the distribution with an exponential curve:

$$\varphi_i(D_i) = 1 - \exp\left[-\left(\frac{D_i}{D_{50}\, k_{\varphi t}\, k_{\varphi c}}\right)^{n_\varphi}\right] \tag{50}$$

Where $k_{\varphi c}, k_{\varphi t}$ and n_φ are the parametres of this exponential model, and $k_{\varphi c}$ for hydrocyclones has got the value $1{,}25$ and represents the quality of its implementation. For $k_{\varphi t}$ was established a regression equation from experimental data by Bauer presented in [17]:

$$k_{\varphi t} = 1{,}862 - 0{,}723n \tag{51}$$

The exponent n_φ can be computed for $\varphi_{50}(D_{50}) = 0{,}5$ and $D_i = D_{50}$ from equation (29), thus:

$$0{,}5 = 1 - \exp\left[-\left(\frac{D_{50}}{D_{50}\, k_{\varphi t}\, k_{\varphi c}}\right)^{n_\varphi}\right]$$

$$0{,}5 = \exp\left[-\left(\frac{1}{k_{\varphi t} 1{,}25}\right)^{n_\varphi}\right] \qquad /ln$$

$$\ln 0{,}5 = -\left(\frac{0{,}8}{k_{\varphi t}}\right)^{n_\varphi} \qquad |\cdot(-1)\,|ln$$

$$\ln 0{,}693147 = n_\varphi \cdot \ln\left(\frac{0{,}8}{k_{\varphi t}}\right)$$

$$n_\varphi = \frac{0{,}366513}{0{,}223144 + \ln k_{\varphi t}} \tag{52}$$

4.3.8 Pressure drop

The pressure drop is an important design parameter for every fluid device. Usually the drop can be calculated from Bernoulli equation between two points (neglecting the difference of hydrostatic pressure) [17]:

$$\frac{p_1}{\rho}+\frac{u_1^2}{2}=\frac{p_p}{\rho}+\frac{u_p^2}{2}+Y_{drop} \tag{53}$$

$$p_{drop}=p_1-p_p+\rho\frac{u_1^2-u_p^2}{2}=p_{tot1}-p_{totp} \tag{54}$$

Where p_1 and p_p denote the static pressures on the inlet respectively on the outlet of vortex finder, u_1 and u_p denote the velocity magnitude on the inlet and outlet of vortex finder.
An additional information is the difference of static pressure:

$$\Delta p=p_1-p_p=\frac{\rho}{2}\left(u_p^2-u_1^2\right)+\rho Y_{drop} \tag{55}$$

However this method cannot predict the correct pressure drop because it assumes the fact that fluid escapes the domain only through the vortex finder, which is not fully true, since it leaves through the spigot too.
Hydrocyclones should be designed so that the majority of the suspension should leave the separator through the vortex finder (sometimes more than 90% of the mass flow rate).
There exists another possibility how to evaluate the pressure drop, if the flow through the spigot becomes more important. It can be derived from the equilibrium of power.

$$\dot{m}_1Y_1=\dot{m}_pY_p+\dot{m}_kY_k+P_{drop} \tag{56}$$

$$\dot{m}_1\frac{p_{tot1}}{\rho}=\dot{m}_p\frac{p_{totp}}{\rho}+\dot{m}_k\frac{p_{totk}}{\rho}+\dot{m}_1\frac{p_{totdrop}}{\rho}$$

$$\dot{m}_1\,p_{tot1}=\dot{m}_p\,p_{totp}+\dot{m}_k\,p_{totk}+\dot{m}_1\,p_{drop}$$

$$p_{drop}=\frac{\dot{m}_1\,p_{tot1}-\dot{m}_p\,p_{totp}-\dot{m}_k\,p_{totk}}{\dot{m}_1} \tag{57}$$

Where $\dot{m}_1$ represents the mass flow rate on the inlet, $\dot{m}_p$ on the overflow and $\dot{m}_k$ on the underflow.
From the equations above, the determination of the pressure drop is possible, however the values of pressure and velocity are needed, which can be gained from a CFD simulation or an experiment.
If there are no simulations and data available, then it is an important issue, therefore a key technique was suggested by some writers how to evaluate the difference of pressure only from dimensions and operating conditions [10]. The disadvantage of these formulas is, that they are half empirical and are not valid under all circumstances.

- By J. J. Moder and D. A. Dahlstrom [10]:

$$\Delta p = \left[\frac{V}{1{,}25k\left(d_{vst}d_p\right)^{0{,}9}}\right]^2 \tag{58}$$

Where V is the volume flow performance in $\left[\frac{l}{min}\right]$, d_{vst} is the diameter of the inlet nozzle in $[cm]$, d_p is the diameter of the vortex finder in $[cm]$, k is a constant (depending on the ratio $\frac{d_p}{d_{vst}}$) and Δp is the pressure drop in $[m\ of\ water\ column]$.

The evaluation of k:

$$\frac{d_p}{d_{vst}} \in \langle 0{,}75; 1\rangle; k = 4{,}85e^{0{,}00537V_p} \tag{59}$$

$$\frac{d_p}{d_{vst}} \in \langle 1{,}25; 1{,}35\rangle; k = 7{,}16e^{0{,}00234V_p} \tag{60}$$

$$\frac{d_p}{d_{vst}} \in \langle 1{,}68; 2{,}11\rangle; k = 6{,}85e^{0{,}00163V_p} \tag{61}$$

V_p is a dimensionless number and represents the mass escaping through the vortex finder in percentages.

- By A. I. Povarov:

$$H = \frac{1}{g}\left[\frac{V\varphi^{0{,}2}}{9{,}1d_{vst}d_p}\right]^2 \tag{62}$$

Where $\varphi\ [deg]$ is the angle of the conical section (figure 8.), g is the gravitational acceleration in $\left[\frac{m}{s^2}\right]$ and H is the pressure on the inlet in $\left[\frac{kg}{cm^2}\right]$.

4.4 The initial design of hydrocyclone

Every device in mechanical engineering has to be designed for some operating conditions, thus a HC is not an exception. These conditions are the following:

- the volume flow rate of the suspension: $6\ l/s$
- the liquid phase: water
- the solid phase: aluminium (density: $\rho_{Al} = 2719 \frac{kg}{m^3}$)
- the mass fraction of aluminium particles in water, in this case this value was chosen: $w_1 = 0{,}001$
- aiming on separating particles from water, with size $1\ \mu m$ or less

In the figure 9 is shown a hydrocyclone with its corresponding dimensions, and from the same figure can be noticed the fact, that there are eight independent variables:
$H_c, H_p, a, b, D_c, d_p, d_k, \varphi$. The remaining (four) variables are dependent: H_0, H_v, H_k, R_s. Therefore H_k is possible to calculate with the aid of D_c, d_k and φ, H_v with the assistance of H_k and H_c and lastly H_0 from equation (46).

4.4.1 Supplementing equations

The separation in hydrocyclones depends highly on the diameter of the spigot and vortex finder, therefore their ratio should be chosen rationally. From experiments carried out by J. J. Moder a D. A. Dahlstorm [10] the following equation was constructed:

$$aD_c = 2d_{vst} + d_p \tag{63}$$

In this case a is a constant and its value is approximately $0{,}5$, d_{vst} is the diameter of the inlet nozzle, whereas this thesis aims on hydrocyclone with a rectangular shape of the nozzle. However this nuisance can be overcome with the support of surface equality, then:

$$d_{vst} = \sqrt{\frac{4ab}{\pi}} \qquad D_c = 8\sqrt{\frac{ab}{\pi}} + d_p \tag{64}$$

Furthermore Dahlstrom and Moder stated the optimal ratio of the vortex finder diameter and inlet nozzle diameter, its value should be 1:1 or 2:1.
Two more dimensional ratios are supplementing the initial design [10]:

$$\frac{D_c}{d_{vst}} \in \langle 4; 8 \rangle \qquad \frac{d_p}{d_k} \in \langle 1; 4 \rangle \tag{65}$$

The ratio on the left indicates the working pressure of the separator, if the inlet diameter is smaller than ratio increases, in addition the velocity increases. The pressure drop varies with the square of the velocity magnitude. The ratio on the right is from praxis.

4.4.2 Design

The initial design of the hydrocyclone was created with the assistance of equations (39) to (41), they were written in the commercial software *Microsoft Excel 2010*, and the independent variables were set up manually respecting the operating conditions.

1. Hydrocyclone number 1

The main independent dimensions: $H_c = 0{,}35m;\ H_p = 0{,}04m;\ a = 0{,}03142m;$ $b = 0{,}01m;\ D_c = 0{,}08m;\ d_p = 0{,}04m;\ d_k = 0{,}015m;\ \varphi = 15°$

The main dependent dimensions: $H_0 = 0{,}21505m;\ H_v = 0{,}10314m;$ $H_k = 0{,}24686m\ ;\ R_s = 0{,}07m$

The remaining parameters: $S_1 = 0{,}00031416m^2;\ x = 0{,}25;\ y = 0{,}25;$ $S_p = 0{,}00126m^2;\ \alpha = 0{,}96839; n = -1{,}01508; D_{50} = 0{,}4015\mu m; k_{\varphi c} = 1{,}25;$ $k_{\varphi t} = 2{,}5959;\ n_{\varphi} = 0{,}31138$ (calculated equivalent diameter $d_{vst} = 0{,}02m$ from S_1)

The determination of pressure drop:

- By J. J. Moder and D. A. Dahlstrom [10]:

$$\frac{d_p}{d_{vst}} = 2 \quad \Longrightarrow \quad k = 6{,}17506 \quad \Longrightarrow \quad \Delta p = 505371Pa$$

- By A. I. Povarov [10]

$$\Delta p = 722401{,}68Pa$$

Design number 1 does not take into consideration the equation (64), furthermore does not satisfy the criterion for y (chapter 4.3.3), and the condition for n given in chapter 4.3.4.

Figure 13: Rendered picture of hydrocyclone number 1

In the figure 13 (and 14) a model was created in the software *Autocad Inventor 2010*. On the left side is a cross section and on the right side is the full model of the separator device.

2. Hydrocyclone number 2

The main independent dimensions: $H_c = 0{,}5m;\ H_p = 0{,}0463m;\ a = 0{,}02356m;$ $b = 0{,}03m;\ D_c = 0{,}18m;\ d_p = 0{,}03m;\ d_k = 0{,}02m;\ \varphi = 20°$

The main dependent dimensions: $H_0 = 0{,}42535m;\ H_v = 0{,}0463m;$ $H_k = 0{,}4537m\ ;\ R_s = 0{,}15m$

The remaining parameters: $S_1 = 0{,}00070686m^2;\ x = 0{,}333;\ y = 1;$ $S_p = 0{,}00071m^2;\ \alpha = 1{,}3121; n = 0{,}0749; D_{50} = 0{,}393\mu m; k_{\varphi c} = 1{,}25;$ $k_{\varphi t} = 1{,}808;\ n_\varphi = 0{,}4496$ (calculated equivalent diameter $d_{vst} = 0{,}03m$ from S_1)

The determination of pressure drop:

- By J. J. Moder and D. A. Dahlstrom [10]:

$$\frac{d_p}{d_{vst}} = 1 \quad \Longrightarrow \quad k = 4{,}3885 \quad \Longrightarrow \quad \Delta p = 809440Pa$$

- By A. I. Povarov

$$\Delta p = 640396{,}86Pa$$

Figure 14: Rendered picture of hydrocyclone number 2

Hydrocyclone number 2 takes into account equation (64), in contrast to the first design, furthermore it satisfies the criterion for y (chapter 4.3.3) and the condition for n given in chapter 4.3.4.
With the help of $k_{\varphi c}$, $k_{\varphi t}$ and n_{φ} the distribution of fractional separability for hydrocyclone number 1 and 2 can be illustrated. From the graph is apparent the feature of the two separators, number 1 separates particles with smaller (smaller than D_{50}) diameter better than number 2, whereas for diameter bigger than D_{50} the opposite is valid.

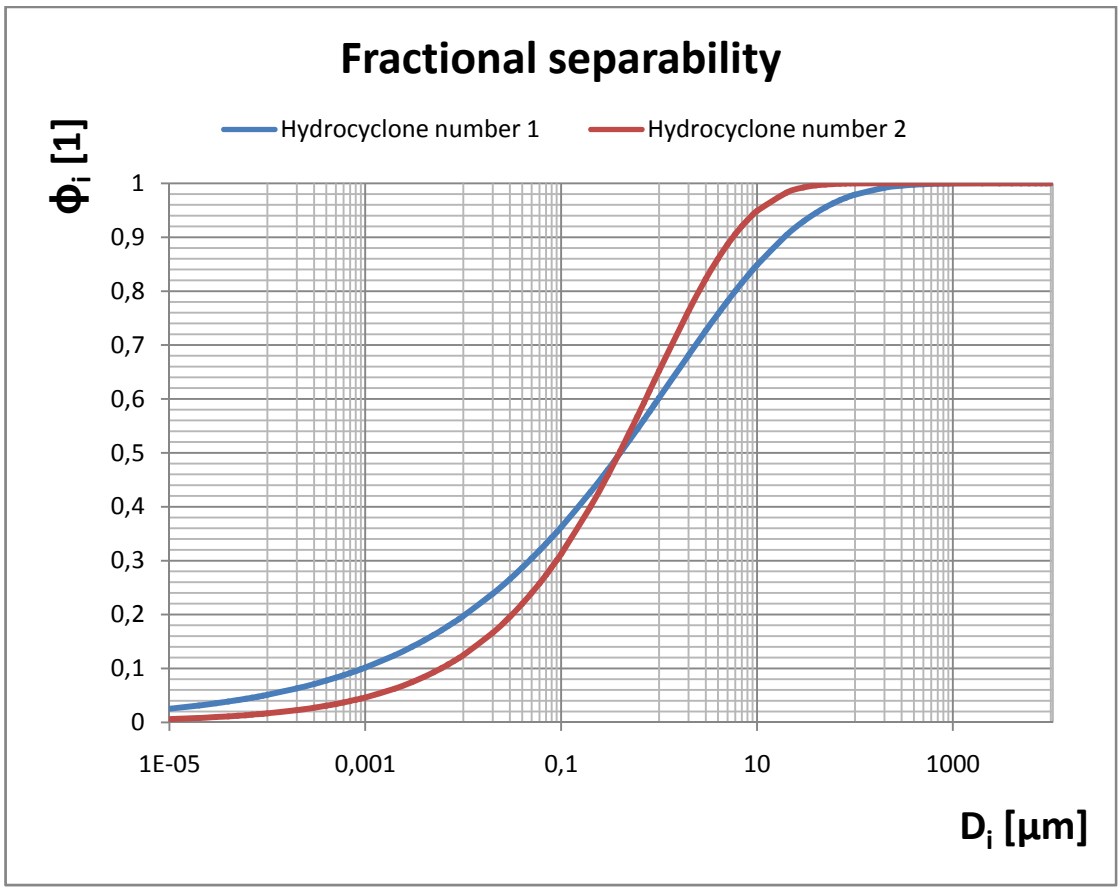

Graph 1: Distribution of fractional separability

5. Governing equations in computational fluid dynamics

The description of fluid flow mathematically is possible with the conservation laws of physics:

- the fluid mass conversation
- from Newton's second law the acceleration of the particles mass is equal to the sum of forces acting on it
- first law of thermodynamics [20]

The mass conservation law demonstrates the fact that mass in an isolated system throughout time will remain constant (called as continuity equation in fluid mechanics), in Cartesian coordinate system (on the left in Einstein summation convention, on the right compact vector notation) [6]:

$$\frac{\partial \rho}{\partial t} + \frac{\partial (\rho\, v_i)}{\partial x_i} = 0 \qquad or \qquad \frac{\partial \rho}{\partial t} + div(\rho\, \vec{v}) = 0 \tag{66}$$

Where ρ is the density of the medium, v_i $(\vec{v})$ is its velocity and is valid for compressible fluids [21]. However in most engineering problems for water is used the continuity equation in incompressible form (for $i = 1, 2, 3$):

$$\frac{\partial v_i}{\partial x_i} = 0 \qquad or \qquad div\, \vec{v} = 0 \tag{67}$$

The line above implies, that it is an algebraic differential equation and can be written:

$$\frac{\partial v_1}{\partial x_1} + \frac{\partial v_2}{\partial x_2} + \frac{\partial v_3}{\partial x_3} = 0 \tag{68}$$

This approach does not enable the full description of flow, it is only a supplementation of the Navier-Stokes equation.
The Navier-Stokes equation was first derived by Claude-Louis Navier and later complemented by George Gabriel Stokes hypothesis. Then later his hypothesis was verified for Newtonian fluid.

$$\frac{\partial v_i}{\partial t} + \frac{\partial v_i}{\partial x_j} v_j = -\frac{1}{\rho} \frac{\partial p}{\partial x_i} + \underbrace{\nu \frac{\partial^2 v_i}{\partial x_j \partial x_j}}_{\text{shear tensor}} + g_i \tag{69}$$

Where p is static pressure, g_i is acceleration of the fluid mass in a field force (for example gravity) and ν is the kinematic viscosity.
Analogically (69) it is a differential vector equation and can be expanded into 3 differential algebraic equations. In few situations the analytical solution of Navier-Stokes equation can be gained, but only for primitive boundary conditions and only in laminar flow regime.

The solution demands another approaches, so the aid of computers and numerical methods is needed.

Reynolds investigated the pure behaviour of the turbulent flow, after reasoning he introduced his argumentations, which included the statements, that properties (pressure and velocities) in the turbulent flow can be divided into 2 parts, one is the mean value of the property and second is the fluctuating part, which depends on time.

$$v(t) = \bar{v} + v'(t) \tag{70}$$

This is called the Reynolds decomposition. He derived the Reynolds-averaged Navier-Stokes equations (RANS) for incompressible flow, which are esentially time-averaged [21].

$$\frac{\partial \overline{v_i}}{\partial x_i} = 0 \tag{71}$$

$$\frac{\partial \overline{v_i}}{\partial t} + \frac{\partial}{\partial x_j}\left(\overline{v_i}\,\overline{v_j}\right) = -\frac{1}{\rho}\frac{\partial \bar{p}}{\partial x_i} + \nu\frac{\partial^2 \overline{v_i}}{\partial x_j \partial x_j} + \frac{1}{\rho}\frac{\partial \tau_{tij}}{\partial x_j} \tag{72}$$

$$\frac{\partial \overline{v_i}}{\partial t} + \frac{\partial}{\partial x_j}\left(\overline{v_i}\,\overline{v_j}\right) = -\frac{1}{\rho}\frac{\partial \bar{p}}{\partial x_i} + \nu\frac{\partial^2 \overline{v_i}}{\partial x_j \partial x_j} \underbrace{- \frac{\partial}{\partial x_j}\left(\overline{v_i' v_j'}\right)}_{\text{Reynolds stresses}} \tag{73}$$

In expression (73) the last term is called the Reynolds stress tensor, which is a new tensor with 9 new variables (for every direction 3 new variables). For a symmetric tensor it can be reduced to 6 variables.

$$\tau_{t11} = -\rho\overline{v_1'^2} \qquad \tau_{t22} = -\rho\overline{v_2'^2} \qquad \tau_{t33} = -\rho\overline{v_3'^2} \tag{74}$$

$$\tau_{t12} = \tau_{t21} = -\rho\overline{v_1' v_2'} \qquad \tau_{t13} = \tau_{t31} = -\rho\overline{v_1' v_3'} \qquad \tau_{t23} = \tau_{t32} = -\rho\overline{v_2' v_3'} \tag{75}$$

The meaning of these turbulent stresses can be found in [21]: "The terms involve products of fluctuating velocities and are associated with convective momentum transfer due to turbulent eddies."

This is a cardinal problem of RANS equation:

- only 4 equations are available (3xRANS for directions x_1, x_2 and x_3 and 1xcontinuity equation)

- but there are altogether 10 variables:
  - 3x $\overline{v_i}$ (mean velocities)
  - 1x $\bar{p}$ (mean static pressure)
  - and 6x τ_{tij} (turbulent stress components)

So called closure problem arises, which has to be solved by application of:

1. reduction the number of variables
2. devising new equations (''models'')

In year 1877 Boussinesq supposed that Reynolds stresses could be substituted with another tensor, which is analogous to the strain rate tensor included in N-S equation.
Boussinesq assumed that μ_t is a scalar isotropic quantity, on the other hand this is the disadvantage of this attitude and it may not be fulfilled in every occasion. For incompressible flow [20]:

$$\tau_{tij} = -\rho\overline{v_i' v_j'} = \mu_t\left(\frac{\partial \overline{v}_i}{\partial x_j} + \frac{\partial \overline{v}_j}{\partial x_i}\right) - \frac{2}{3}\rho k \delta_{ij} \tag{76}$$

Where k is the turbulent kinetic energy and δ_{ij} is the Kronecker delta.

Nowadays the most sturdy method for engineering applications is the RANS equations supplemented with k-ε turbulence or RSM model. Of course there exists other options to solve turbulent flow numerically, it is the LES (Large eddy simulation) and DNS (Direct numerical simulation) method. If we want to obtain satisfying values of the flow, then a very fine computational domain is needed, hence it leads to high computational costs.
For most problems in CFD the users are pleased with mean values, such as calculating surface integrals of static pressure, mean velocities, after it from these values mostly the efficiency can be evaluated of the given machine or mechanism. To gain these numbers the use of RANS equations satisfies our needs, however the effects of turbulence cannot be neglected in some situations, because instantaneous fluctuations can have an effect on the flow as well.

5.1 VOF model

The volume of fluid model is one of the three models which is available in FLUENT to manage multiphase flow (two and more phases) calculations. The VOF model is based on the Euler-Euler conception, different phases are treated as phase volume fractions. The sum of volume fractions in every mesh cell equals to one, and are handled as continuous functions of time and position (cell).
VOF was introduced by Hirt and Nichols in year 1981 (donor acceptor scheme) [22], and is the simplest method for computing multiphase flows according to convergence and calculation time, essentially. It is worth to note, that the use was set up for immiscible fluids, where between the density of fluids is a capital difference (for example water and air). FLUENT [23] guide recommends the usage of this model for free-surface flows, filling, large bubble motion in a fluid etc. The profitable benefits of this method should be the correct prediction of the interface between the eulerian phases.

The use of VOF is quite obvious and it can be seen in figure 18 and [24], that flows in hydrocyclones credibly imitate the free-surface flows, because the water and air core are visibly separated, also the interface between them is illustrated in the same picture.
The use of mixture model is also possible in hydrocyclones, however it has got a different numerical scheme for computation of the volume fraction equation.

It is important to remark that for all fluids the solution of a single set of momentum is required (N-S). The mathematical concept behind the VOF model, relies only on one transport equation for the volume fraction:

$$\frac{\partial \alpha}{\partial t} + \frac{\partial (\alpha\, v_i)}{\partial x_i} = 0 \tag{77}$$

After expanding the derivation for incompressible flow is valid [22]:

$$\frac{\partial \alpha}{\partial t} + v_i \frac{\partial \alpha}{\partial x_i} = 0 \tag{78}$$

Where α represents the volume fraction. The expression (77) can remind us of the continuity equation, the only change is that instead of density the volume fraction is the transported quantity. Naturally the sum of the volume fractions in computational element must be one. For a two phase flow:

$$\alpha_w = 1 - \alpha_a \tag{79}$$

Where α_w denotes to volume fraction of water and α_a volume fraction of air. Assuming only these two phases we can distinguish three states in each cell:

- $\alpha_w = 0$ and $\alpha_a = 1$, this element contains only one phase, which is air
- $\alpha_w = 1$ and $\alpha_a = 0$, this element contains only one phase, which is water
- $0 < \alpha_w < 1$ and $0 < \alpha_a < 1$, this element contains both phases (water and air), obviously the interface between them must be calculated. The formula for calculating the mean density in the element:

$$\rho = \rho_w \alpha_w + \rho_a \alpha_a = \rho_w \alpha_w + \rho_a (1 - \alpha_w) \tag{80}$$

Same formula is used for calculation of mean viscosity. Most of the methods in numerics has got some disadvantages, hence VOF is not any exception. Difficulties can occur at the interface discontinuity another problem is to calculate the curvature of interface.

5.2 $k-\epsilon$ model

This model is based on Boussinesq hypothesis and is the most widely implemented turbulence model in commercial CFD programs. This is a two equation model, which means that the 2 transport equations are derived for k and for ϵ, in addition with this technique the turbulence dynamics can be grasped, because k is the turbulent kinetic energy and ϵ is the rate of turbulent dissipation, moreover k and ϵ are instantaneous variables.

$$k(t) = \bar{k} + k \tag{81}$$

Where $\bar{k}$ is the mean kinetic energy of turbulence and k is the turbulent kinetic energy [21]. The kinetic energy essentially in physics is the velocity magnitude powered by two, multiplicated by mass and divided by two, although the mass in this situation does not figure, because it is evaluated per unit mass (for turbulence is hard to define the according mass). The expression for k and $\bar{k}$:

$$\bar{k} = \frac{1}{2}\left(v_1^2 + v_2^2 + v_3^2\right) \tag{82}$$

$$k = \frac{1}{2}\left(\overline{v_1'^2} + \overline{v_2'^2} + \overline{v_3'^2}\right) \tag{83}$$

Due to the use of isotropicity of turbulence $\overline{v_1'^2} = \overline{v_2'^2} = \overline{v_3'^2}$, so:

$$k = \frac{3}{2}\,\overline{v_1'^2} \tag{84}$$

A new feature had to be overtaken from the analogy of the fluid element deformation, which was used by the N-S equation derivation for Newtonian fluids, therefore tensor for the rate of deformation had to be proposed [21]:

$$s_{ij} = \begin{bmatrix} s_{11} & s_{12} & s_{13} \\ s_{21} & s_{22} & s_{23} \\ s_{31} & s_{32} & s_{33} \end{bmatrix} \tag{85}$$

This tensor reveals the fluid element deformation in a turbulent flow, analogically the matrix elements can be expressed:

$$s_{ij}(t) = \overline{s_{ij}} + s'_{ij}(t) \tag{86}$$

For elements of matrix $s_{ij}(t)$:

$$s_{ij}(t) = \overline{s_{ij}} + s'_{ij}(t) = \frac{1}{2}\left[\frac{\partial \overline{v_i}}{\partial x_j} + \frac{\partial v'_j}{\partial x_i}\right] + \frac{1}{2}\left[\frac{\partial \overline{v_j}}{\partial x_i} + \frac{\partial v'_i}{\partial x_j}\right] \tag{87}$$

On the diagonal on the matrix (for example element $s_{11}(t)$):

$$s_{11}(t) = \frac{1}{2}\left[\frac{\partial \overline{v_1}}{\partial x_1} + \frac{\partial v'_1}{\partial x_1}\right] + \frac{1}{2}\left[\frac{\partial \overline{v_1}}{\partial x_1} + \frac{\partial v'_1}{\partial x_1}\right] = \frac{\partial \overline{v_1}}{\partial x_1} + \frac{\partial v'_1}{\partial x_1} \tag{88}$$

An element off the diagonal (for example element $s_{12}(t)$):

$$s_{12}(t) = s_{21}(t) = \frac{1}{2}\left[\frac{\partial \overline{v_1}}{\partial x_2} + \frac{\partial v_2'}{\partial x_1}\right] + \frac{1}{2}\left[\frac{\partial \overline{v_2}}{\partial x_1} + \frac{\partial v_1'}{\partial x_2}\right] = \\ = \frac{1}{2}\left[\frac{\partial \overline{v_1}}{\partial x_2} + \frac{\partial \overline{v_2}}{\partial x_1}\right] + \frac{1}{2}\left[\frac{\partial v_1'}{\partial x_2} + \frac{\partial v_2'}{\partial x_1}\right] \tag{89}$$

Formerly a fundamental issue was the deduction of the dissipation rate of turbulence ϵ, later the powerful technique was used, which has facilitated the rate of viscous dissipation. The ϵ is pulled out from the N-S equation, so that all momentum equations are multiplied by the corresponding velocity (direction x_1 is associated with velocity v_1 etc), the same mathematical operations were carried out for Reynolds equations. After subtracting the equations from each other and demanding operations the equation for turbulent kinetic energy was gained by Tennekes and Lumley in 1972 cited in [21]. In this equation the following term is the rate of viscous dissipation:

$$\epsilon = 2\nu\overline{s_{ij}' \cdot s_{ij}'} \tag{90}$$

Substantial issue is that the value of this term will be always positive and represents the destruction of turbulent kinetic energy.
The k-epsilon turbulence model implemented in FLUENT has got 3 versions: standard, RNG and realizable. These modifications differ from each other mainly in three ways: the calculation of turbulent viscosity, the diffusion of k and ϵ and production, annihilation of terms in the ϵ equation [23].
The realizable $k-\epsilon$ model is one of the latest modifications, of $k-\epsilon$ model. FLUENT guide recommends the use in flows that involve rotation, separation and recirculation. This thesis uses this model only in the first few iterations to gain a better initialization and convergence of flow properties, which can be calculated by the RSM model onwards (the $k-\epsilon$ model fails to predict the correct flow [24]).
All three variations use the same formula to compute the eddy viscosity:

$$\mu_t = \rho C_\mu \frac{k^2}{\varepsilon} \tag{91}$$

Where C_μ is a dimensionless number, for realizable method is not constant and has to be evaluated from other formulas (for more informations see [23]).
For turbulence quantities k and ϵ transport equation can be written:

$$\underbrace{\frac{\partial(\rho k)}{\partial t}}_{\text{I}} + \underbrace{\frac{\partial\left(\rho k v_j\right)}{\partial x_j}}_{\text{II}} = \underbrace{\frac{\partial}{\partial x_j}\left[\left(\mu + \frac{\mu_t}{\sigma_k}\right)\frac{\partial k}{\partial x_j}\right]}_{\text{III}} + \underbrace{G_k + G_b}_{\text{IV}} \underbrace{- \rho\epsilon - Y_m}_{\text{V}} + S_k \tag{92}$$

$$\underbrace{\frac{\partial(\rho\epsilon)}{\partial t}}_{\text{I}} + \underbrace{\frac{\partial\left(\rho\epsilon v_j\right)}{\partial x_j}}_{\text{II}} = \underbrace{\frac{\partial}{\partial x_j}\left[\left(\mu + \frac{\mu_t}{\sigma_\epsilon}\right)\frac{\partial \epsilon}{\partial x_j}\right]}_{\text{III}} + \underbrace{\rho C_1 S\epsilon - \rho C_2 \frac{\epsilon^2}{k + \sqrt{\nu\epsilon}}}_{\text{IV}} + \underbrace{C_{1\epsilon}\frac{\epsilon}{k} C_{3\epsilon} G_b}_{\text{V}} + S_\epsilon \tag{93}$$

Where:

- term I is the k and ϵ rate of change
- term II is the k and ϵ transport by convection of fluid
- term III is the k and ϵ transport diffusion
- term IV is the k and ϵ rate of production (G_k - on account of mean velocity gradients, Boussinesq hypothesis used for calculation. G_b - on account of buoyancy)
- term V is the destruction term of turbulence

Further on:

$$C_1 = \max\left[0{,}43; \frac{\eta}{\eta + 5}\right];\ \eta = S\frac{k}{\epsilon}; S \equiv \sqrt{2\overline{S_{ij}}\overline{S_{ij}}} \tag{94}$$

Where $\overline{S_{ij}}$ is the mean rate of deformation (strain rate tensor), S is the corresponding modulus, Y_m this term plays a significant role in compressible flow, in incompressible flows it is neglected. S_ϵ and S_k are source terms and can be defined by the user, $C_{3\epsilon}$ has an impact on buoyancy and it is calculated from a formula. σ_k, σ_ϵ are turbulent Prandtl numbers (for k and ϵ), $C_{1\epsilon}$ and C_2 are constants of the model aiming on the credible prediction for canonical flows. The constant values are: $\sigma_k = 1$; $\sigma_\epsilon = 1{,}2$; $C_{1\epsilon} = 1{,}44$; $C_2 = 1{,}9$.

5.3 RSM

This model is not based on Boussinesq hypothesis [21]. The full name is Reynolds stress equation model. The „first" pioneer of developing this model was Launder et al in year 1975.
The most remarkable information is that the turbulent viscosity is here assumed as anisotropic [24], although the problem lies in its complexity, because for a 3D flow has to be solved seven additional equations [23]. Solving six equation for Reynolds stresses (equation 76) and one transport equation for the dissipation rate [23]. The use of this model may not produce satisfying results in all occasions must not satisfy the results in all occasions, in some situations the prediction is more suitable by a two equation model.
The use is recommended for highly swirling flow, for example the flow in a cyclone, where the Reynolds stresses are anisotropic. The exact transport equation for the Reynolds stresses is the following:

$$\frac{\partial\left(\rho\,\overline{u_i'u_j'}\right)}{\partial t}+\frac{\partial\left(\rho\,\overline{u_k}\,\overline{u_i'u_j'}\right)}{\partial x_k}=D_{T,ij}+D_{L,ij}+P_{ij}+G_{ij}+\phi_{ij}-\epsilon_{ij}+F_{ij} \qquad (95)$$

The previous equation is implemented in FLUENT, the terms on the left hand side are the local time derivative (rate of change) and the convection term (transport of Reynolds stresses by convection - C_{ij}). In addition the terms on the right hand side are: the first is turbulent diffusion (transport of Reynolds stresses due to turbulent diffusion), the second is molecular diffusion (transport of Reynolds stresses due to molecular diffusion), the third is stress production (rate of Reynolds stress production), the fourth is buoyancy term (rate of Reynolds stress production by buoyancy), the fifth is pressure strain, the sixth is dissipation (rate of Reynolds stresses dissipation) and the seventh is production by rotation (transport of Reynolds stresses by rotation of the system).
An important note to equation (95), is that not all terms require modeling. The terms which claim modeling are the following: $D_{T,ij}, G_{ij}, \phi_{ij}, \epsilon_{ij}$. Further terms, which do not need any modeling are: $D_{L,ij}, P_{ij}, C_{ij}, F_{ij}$. The calculation of dissipation rate is almost the same as in the standard $k-\epsilon$ model.
Because of the complexity of RSM model the formulas, the way of calculation of each term will not be displayed in this thesis, due to the equation amount. For the sake of the readers the additional equations can be found in FLUENT theory guide or in [21].

6. The optimization of hydrocyclone

6.1 Mesh and boundary conditions

The computational domain (mesh) was created in the commercial software *Gambit version 2.4.6*.

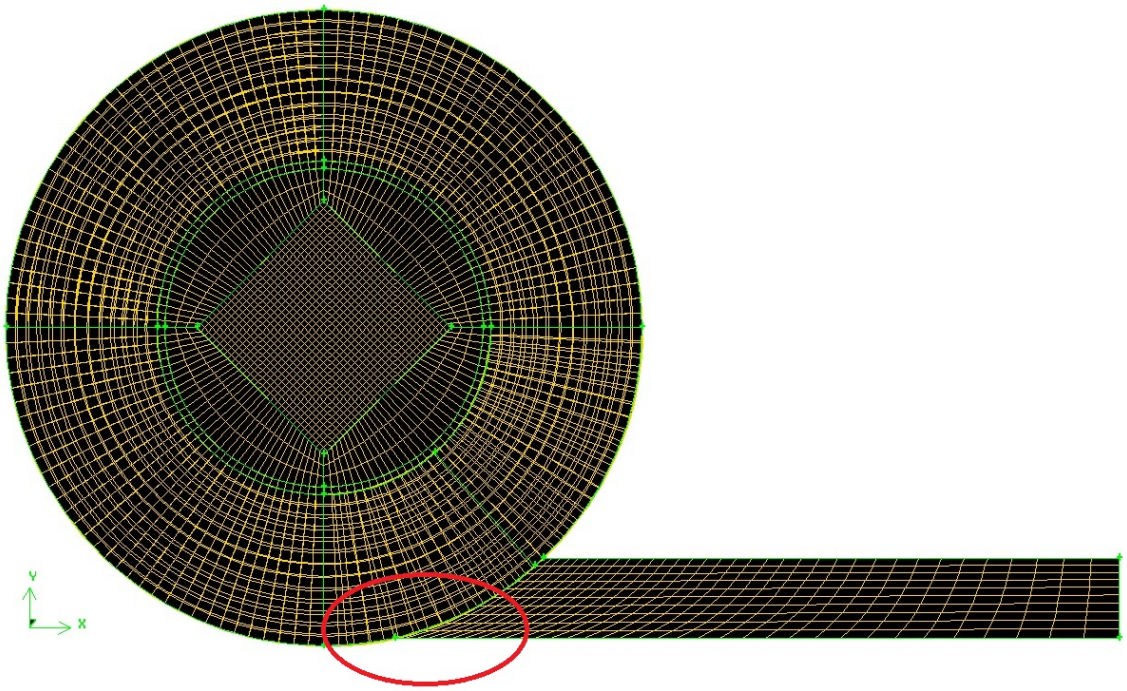

Figure 15: Computational mesh and the model of hydrocyclone number 1

Few researchers dealt with the problem of the mesh size [15], [24]. To obtain satisfying results from the simulation, the use of RSM on a relatively coarse mesh should be used.
After a long decomposition to get rid of hybrid and wedge elements the final version contains only hex elements, which is a big advantage concerning the quality of the elements. Another remarkable feature is, that the inlet pipe is not connected fully tangential to the cylindrical part, that is a leading cause of obtaining lower skewed elements. Skewness influences accuracy of the numerical solution. If the value is close to 0 it is a good element. FLUENT is capable to calculate the equations describing the flow on such an element if skewness is smaller than 0.93.
The hydrocyclone contains 353466 hex elements, and the measured maximum value of skewness is 0.834 (worst elements are on the boundary of the inlet nozzle and the cylindrical part).

Boundary conditions

Three types of boundary conditions were used: wall, velocity inlet and pressure outlet.

1. wall - wall of hydrocyclone, where the boundary layer is formed.
2. velocity inlet - the velocity profile is assumed as constant, it can be determined from the inlet surface and the volume flow rate, its value is $v = 19{,}1\,\frac{m}{s}$. There is no need to calculate Reynolds number because it will be surely turbulent flow.
3. pressure outlet:
    a. overflow (vortex finder): set up a constant gauge pressure on this boundary, its value $p = 0Pa$.
    b. underflow (spigot): the same condition as on the overflow.
    c. underflow (spigot): the same condition as on the overflow.

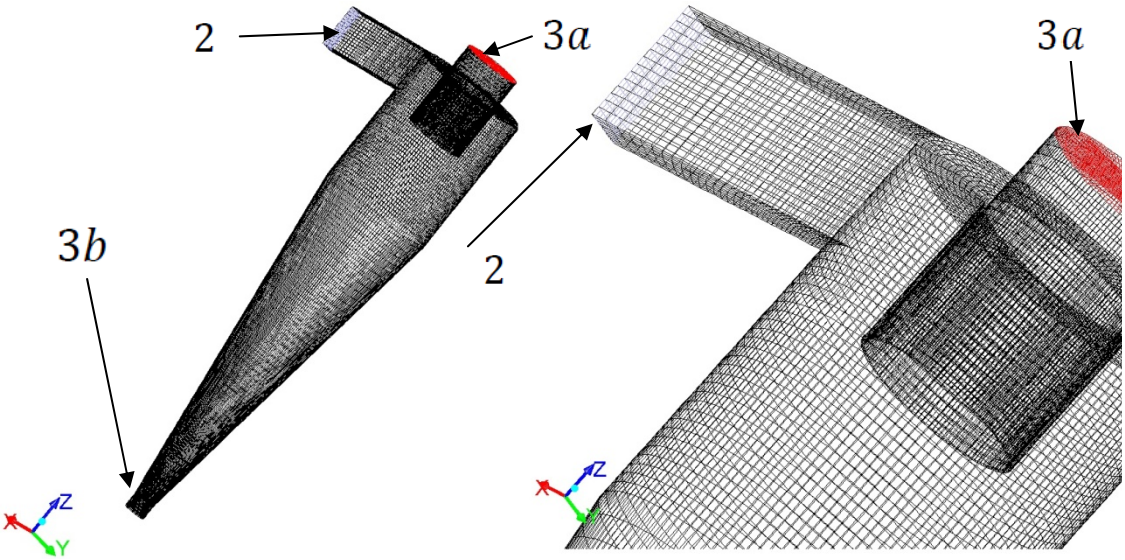

Figure 16: Boundary conditions + mesh (hydrocyclone number 1)

6.2 Processing

Lately much research has focused on modeling the flow within a hydrocyclone, therefore the basis of the FLUENT solver adjustment will respect these knowledges.
For initializing a problem it is good to start with the $k-\epsilon$ due to its robustness. However this model is unable to predict the correct flow properties, because of the anisotropic turbulence [24], therefore the RSM model has to be enabled on and later the VOF model too, which is calculated in transient formulation.
The air and water interaction is computed with the VOF model. The VOF model treats the coupled flow as Euler-Euler, on the other hand small aluminium particles are carried by the motion of fluids, which has to be dealt with Lagrangian approach. For tracking particles DPM (discrete phase modelling) is used.
For pressure-velocity coupling the SIMPLE algorithm was used. Although this algorithm is derived for steady flows, it was shown that for transient flow is also applicable. The problems were calculated in the beginning with 1st order, later higher accuracy discretization (2nd order) was set up for convective terms of the transport equation. For pressure the PRESTO! scheme was employed, which use is recommended for multiphase and highly swirling flows. In addition for VOF model the modified HRIC scheme was applied.
Generally in simulations of transient tasks a crucial problem occurs, choice of the size of the incremental time step, however the dynamical features of the given system are unknown in advance. It is recommended to choose the time step to be one hundred times smaller than the period of the dynamic phenomenon $\left(\Delta t=\frac{T_{period}}{100}\right)$. In this simulation the first choice of time step was $0{,}001s$ $(\Delta t=0{,}001s)$. It was shown that this value is insufficient and had to be decreased down to $\Delta t=0{,}0001s$. For a better understanding see the following section**.

6.2.1 Computation with time step 0,001s

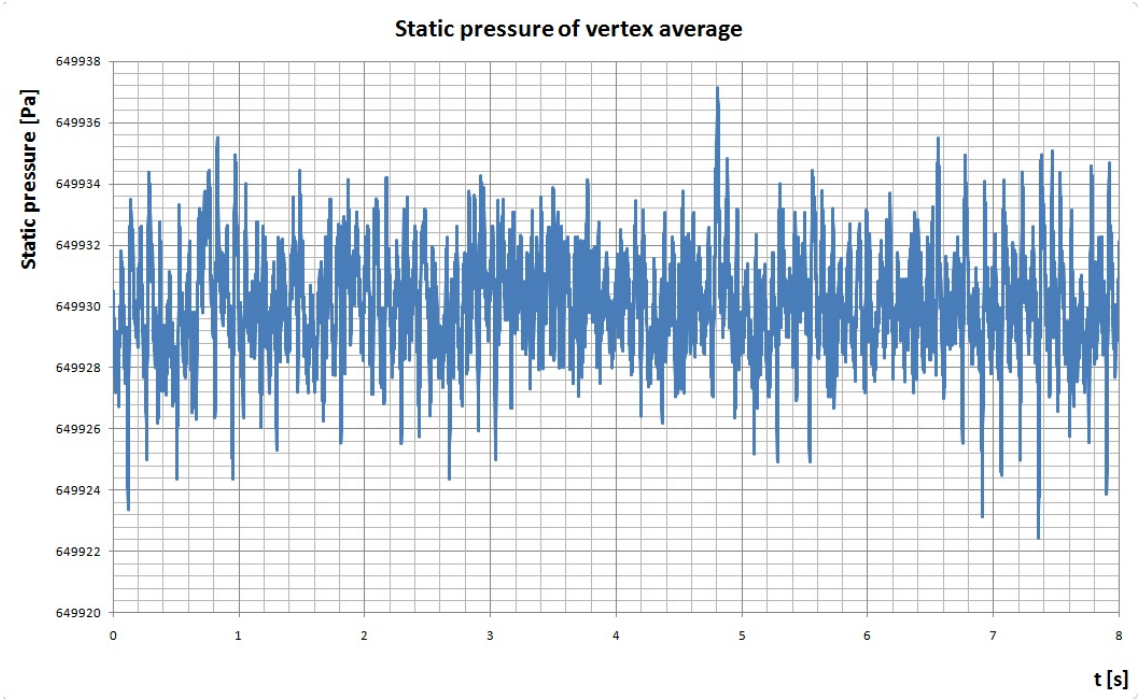

Graph 2: Static pressure of vertex average (hydrocyclone number 1 ,time step $0.001s$*)*

The graph 2 shows the static pressure obtained from FLUENT time step was brought $0{,}001s$, pressure varies only in a small range $649938 - 649922$. The pressure was monitored at a point between the wall and the axis of the hydrocyclone (in the conical section).

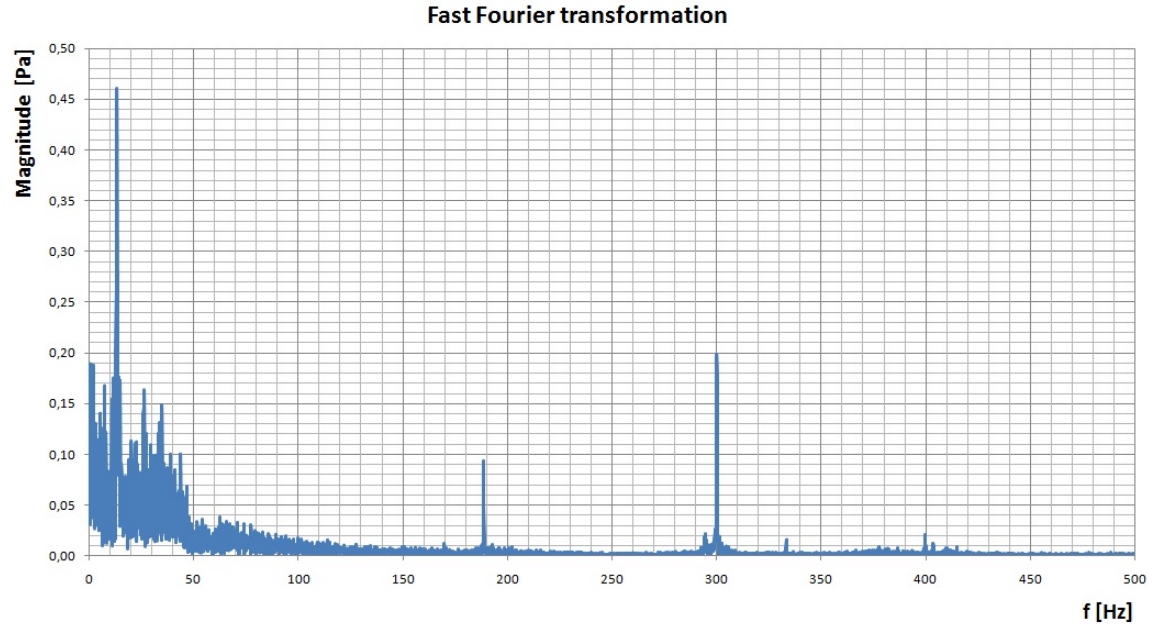

Graph 3: Fast Fourier transformation (hydrocyclone number 1, time step $0.001s$*)*

After applying fast Fourier transformation (from 8588 values) the steady value of static pressure $649930{,}06Pa$ at $0Hz$ (it is not shown in graph 3), the biggest magnitude is $0{,}46Pa$ at $13Hz$. The change in pressure is almost negligible, and it seems as the process would be steady. It was computed with Bounded Second Order Implicit scheme, and the results are valid for the incremental time step of $0{,}001s$.

6.2.2 Computation with time step0.0001s

Hydrocyclone number 1

Calculation carried out with the scheme Second Order Implicit (transient formulation) was impossible, because solution blew up. So another ways had to be found, an alternative solution was the Bounded Second Order Implicit scheme with an incremental time step of $0{,}0001\ seconds$. The bounded schemes are recommended to use with LES or with compressible multiphase flows, comparing to the Second Order Implicit formulation it brings the same accuracy with a better stability [23].

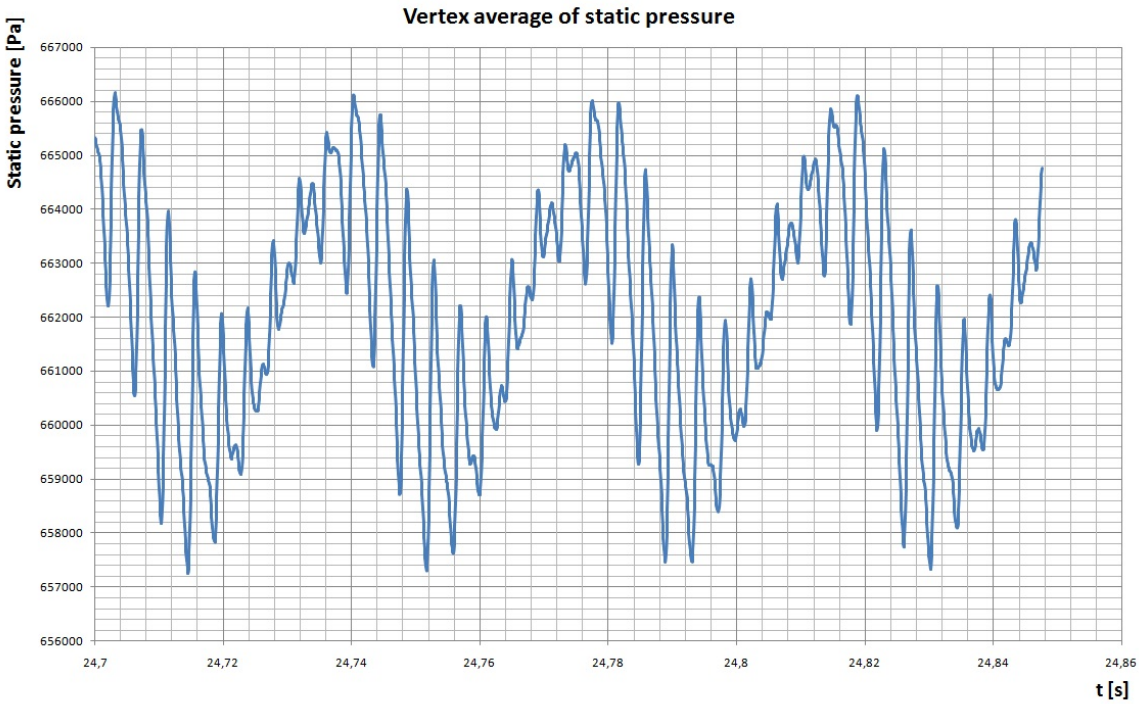

Graph 4: Static pressure of vertex average (hydrocyclone number 1 ,time step $0.0001s$)

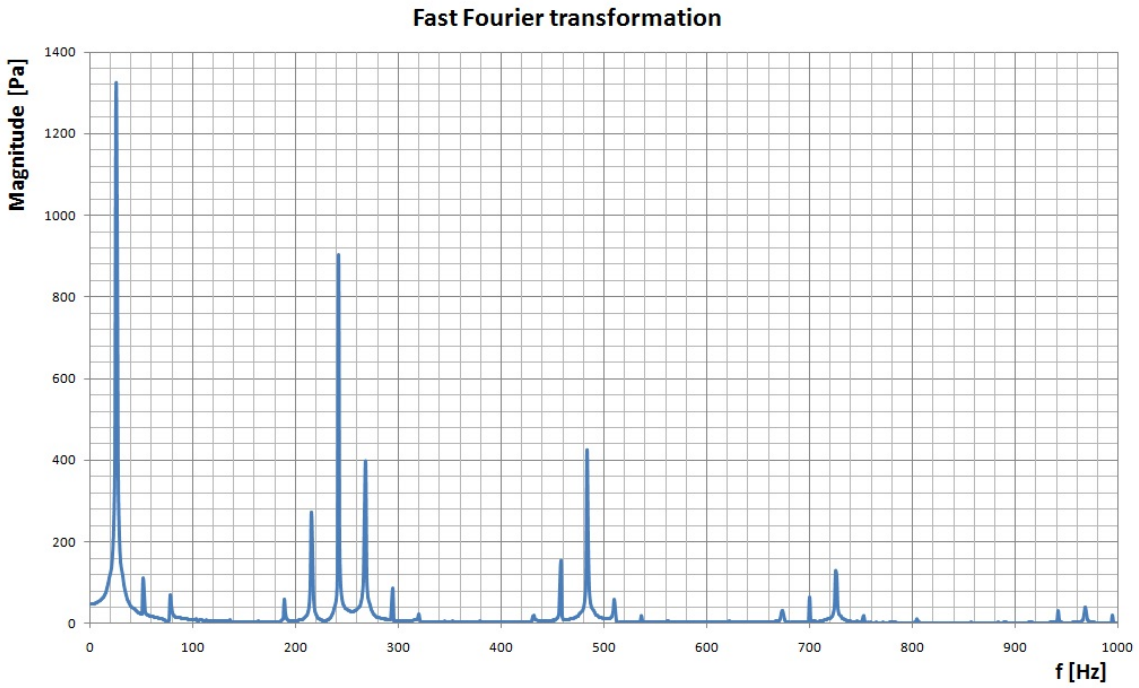

Graph 5: Fast Fourier transformation (hydrocyclone number 1, time step $0.0001s$)

From the recorded videos not only the pulsating intake of air, but also the rotating air core can be perceived. These two phenomena are connected, from FFT and with the aid of the videos their frequency can be determined. Both dynamical high-frequency phenoma belong to the second highest peak on the graph 5, the magnitude of pressure is $p = 903{,}14\ Pa$ at the monitored vertex and the frequency is $f = 241{,}76 Hz$.
The highest peak is presented by the values of magnitude $p = 1303{,}0558\ Pa$ and frequency $f = 25{,}641\ Hz$, nonethless its physical meaning remains unclear (one assumption is, that it could be axial pulsations).

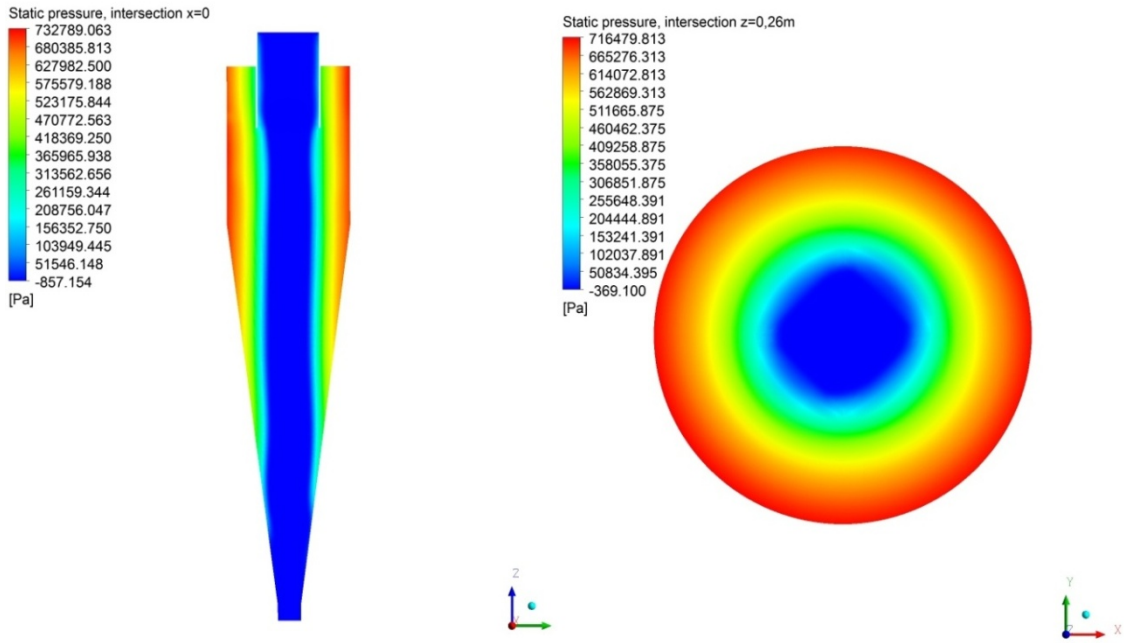

Figure 17: Contours of static pressure (intersection $x = 0$, $z = 0.26m$)

In figure 17 static pressure is displayed in two intersections. On the right hand side the distribution shows beautiful concentric circles, that explains the use of equation (34) (where the pressure varies only with radial coordinates). The static pressure can be displayed on a line (intersection $z = 0.26m$).

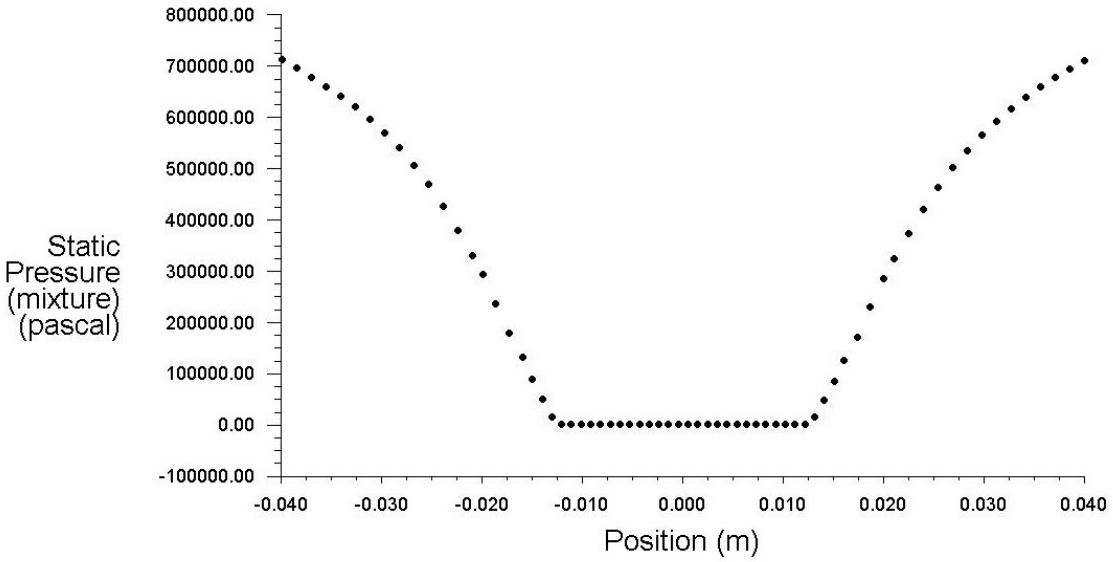

Graph 6: Distribution of static pressure (on a line, intersection $z = 0.26m$)

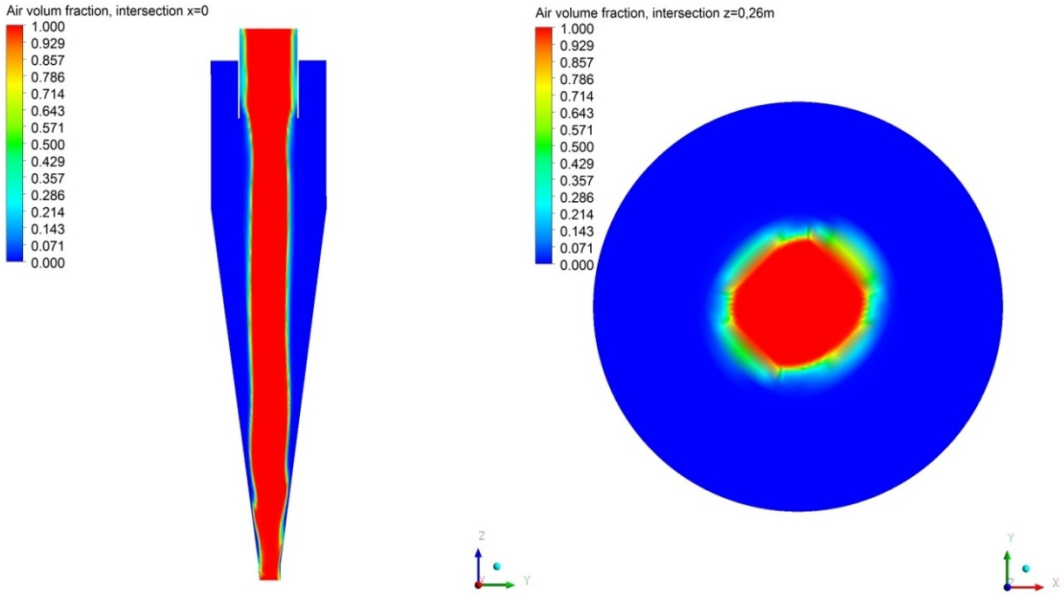

Figure 18: Contours of air volume fraction (intersection $x = 0$, $z = 0.26m$)

In figure 18 the air core is shown in two intersections (the modified HRIC scheme was used in VOF model). The red color represents the place where only air is present, the blue represents only water. On the right side the quality of transition from air to water is quite bad, contours are smeared that is caused by the mesh quality.
Another important remark is the air cores elliptical shape.

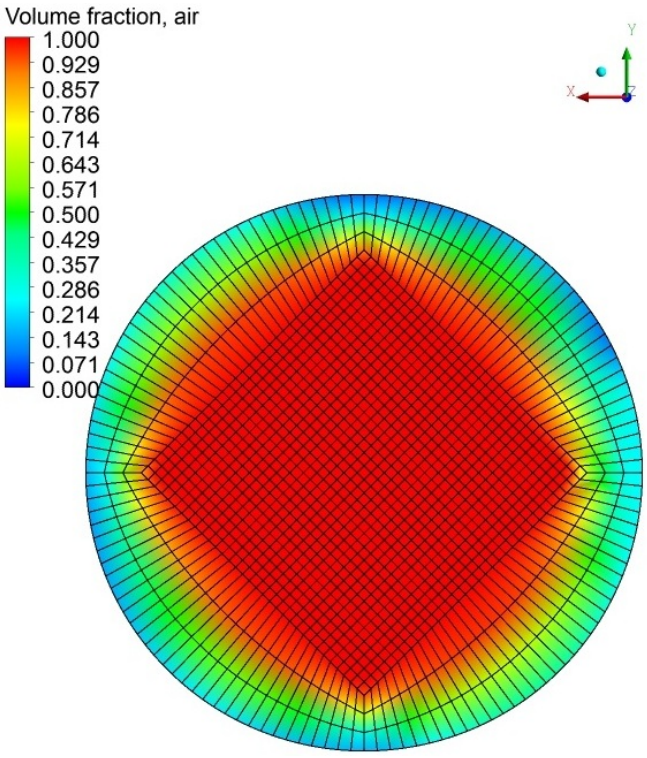

Figure 19: Mesh quality + contours of volume fraction (on boundary overflow)

In figure 19 the contours of air volume fraction are plotted on the overflow supplemented with the mesh. The effect of the elements on contours is remarkable. The mesh type and element shape is imprinted on the flow field.

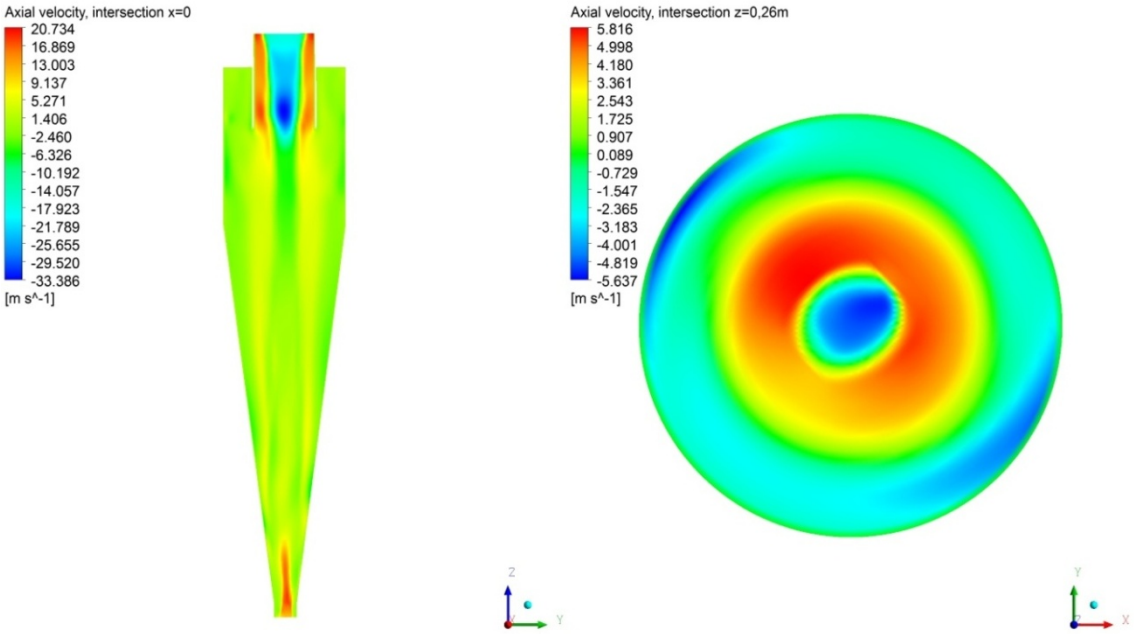

Figure 20: Contours of axial velocity (intersection $x = 0$, $z = 0.26m$)

The contours of axial velocity above, where negative and positive values denote that the fluid flows in the direction of the spigot or of the vortex finder, respectively. To understand the flow behaviour, the axial velocity profile is shown in the next graph, and is evaluated on a line of intersection shown in figures $(z = 0{,}26m)$. Position 0 is the axis of the hydrocyclone. The axial velocity plays a significant role in the air core motion, there is the intake of air is pulsating.

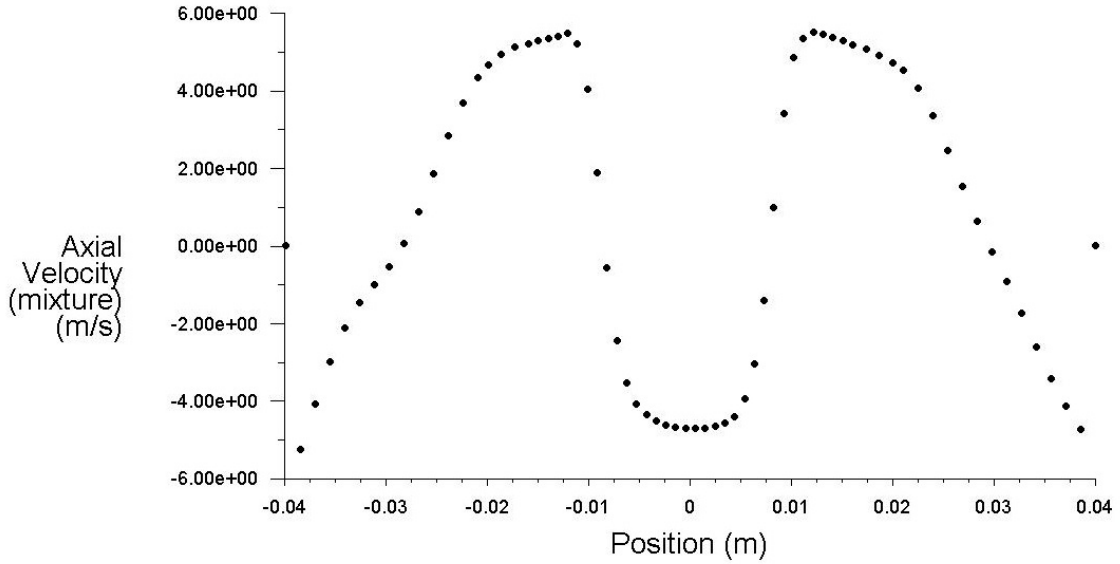

Graph 7: Distribution of axial velocity (on a line, intersection $z = 0.26m$)

The value of axial velocity on the wall of hydrocyclone is $0\frac{m}{s}$. Attentive readers can remark that between positions $(-0.03; -0.02)$ and $(0.02; 0.03)$ the direction of flow of the water changes from negative to positive or vice versa.
Another point is that air is sucked into the hydrocyclone through the vortex finder as it is shown in figure 20 and in graph 7 approximately between the positions $(0.01; 0.01)$. It is a fairly interesting phenomenon as water leaves the separator air enters in. The different flow directions and relatively high velocities (and their change) will result in high velocity gradients.
It is good to know that vorticity is the function of velocity gradients, therefore the plotted vorticity:

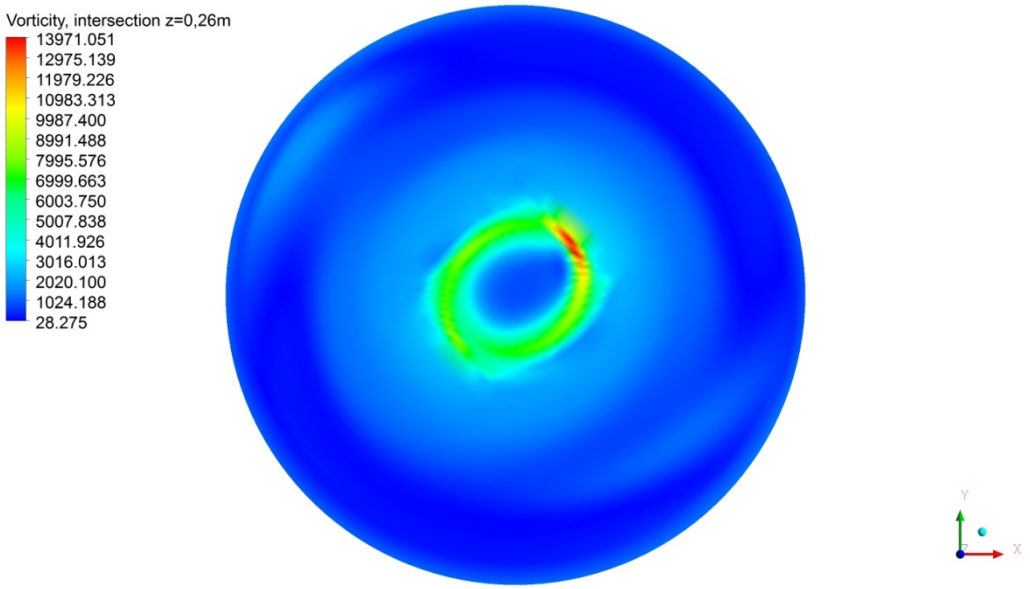

Figure 21: Contours of vorticity magnitude (intersection $z = 0.26m$)

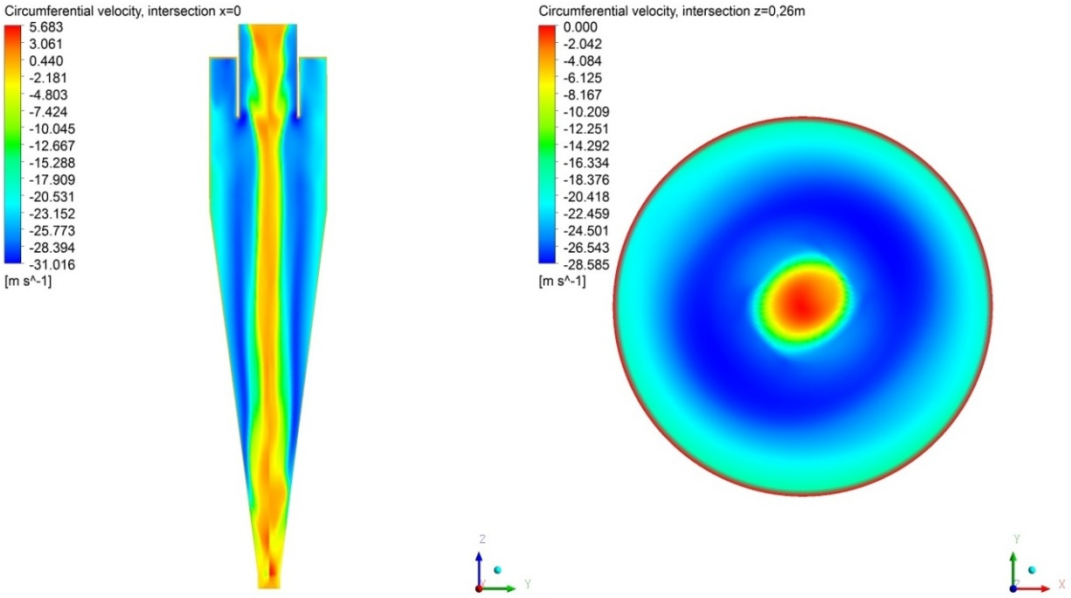

Figure 22: Contours of circumferential (tangential) velocity (intersection $z = 0.26m$)

Circumferential (tangential) velocity is plotted in figure 22, and the velocity distribution is displayed on the same line as for axial velocity.

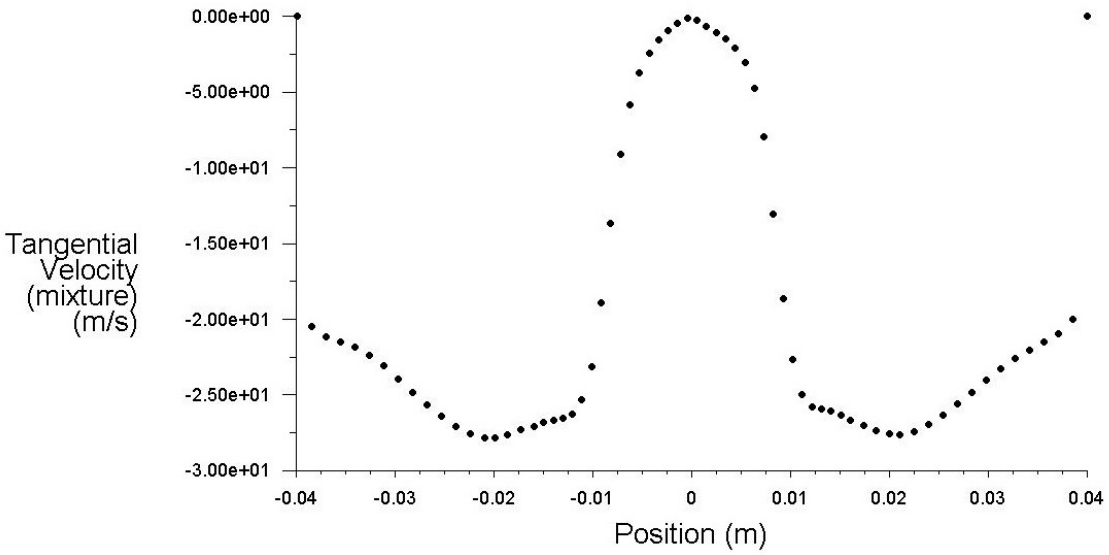

Graph 8: Distribution of tangential velocity (on a line, intersection $z = 0.26m$)

This graph shows the distribution of tangential velocities depending on the position. The velocity profile resembles the picture 11.
The simulations are confined to high Reynolds number.
The quality of the mesh is connected with its size and the Reynolds number due to description of smaller eddies. The indicator of the mesh quality along the walls called $wall\ y^+$. Its value should lie in the interval (20;120) for non-equilibrium wall functions. The reason of the high $wall\ y^+$ is the coarse mesh on the wall and big gradients of velocity.

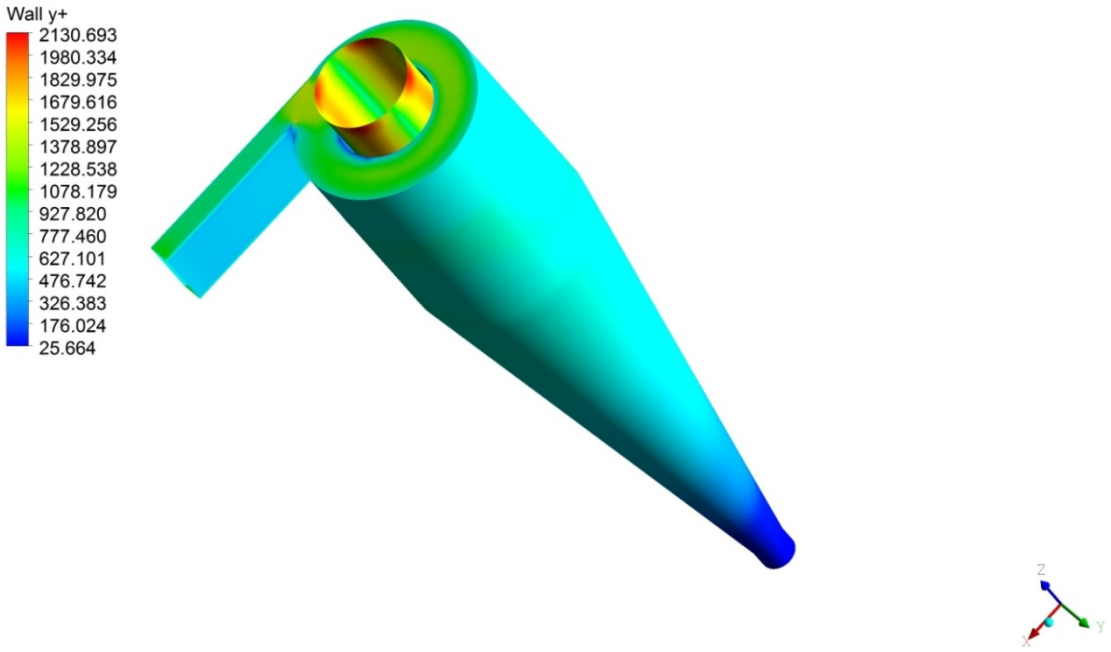

Figure 23: Wall y^+, hydrocyclone number 1

Trajectories of solid particles

The trajectory tracking of solid particles is possible in FLUENT with the discrete phase model. The model assumes the Lagrangian conception of continuum, it means the software integrates path of the particle throughout the flow domain [24].
The calculation of a particle track can be very time consuming. The use of DPM model makes sense only when the suspension is dilute (discrete phase max 10% mass fraction of solid phase).

The adjustment of the discrete phase model:

- assuming one-way coupling (only the fluid phase has influence on the solid phase, to fulfil this condition the particle must be small)
- injecting inert spherical aluminium particles $\left(\rho_{Al} = 2719 \frac{kg}{m^3}\right)$ with a diameter of $1 \mu m$
- single injection type was chosen, 5 injections were set up on the boundary velocity inlet to cover the whole surface (figure 24)
- the initial velocity and direction for the particle was supposed identical as the velocity of the fluid (that is some kind of simplification)

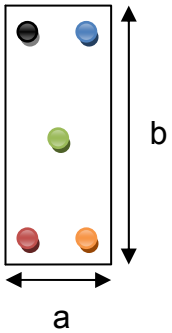

Adjusted single injections on the boundary velocity inlet:

Black - injection-0
Blue - injection-1
Green - injection-2
Red - injection-3
Orange - injection-4

Figure 24: Single injection on the boundary (velocity inlet), hydrocyclone number 1

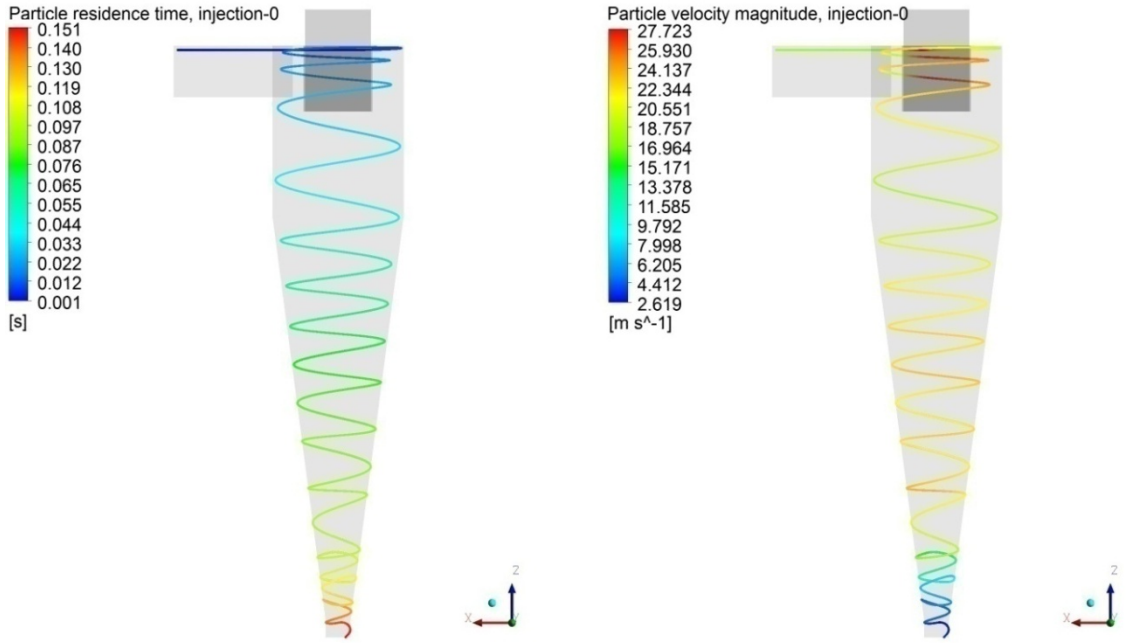

Figure 25: Trajectory of the particle (released from injection-0, without stochastic model), hydrocyclone number 1

On the right hand side of the picture the injection-0 is shown with its residence time in the separating device, in addition the particle escapes through the underflow after 0.151seconds. The calculation was carried out for spherically particles and diameter was $10^{-6}\,m$.
According to the simulation (righthand side of figure 25) the velocity magnitude of the particle in the inlet nozzle is almost invariable, whereas close to the vortex finder rapidly rises, furthermore it decreases significantly in the cylindrical section. After reaching the cone section the particle starts to accelerate and about at 80% of the hydrocyclone length it decelerates till it leaves the flow domain.

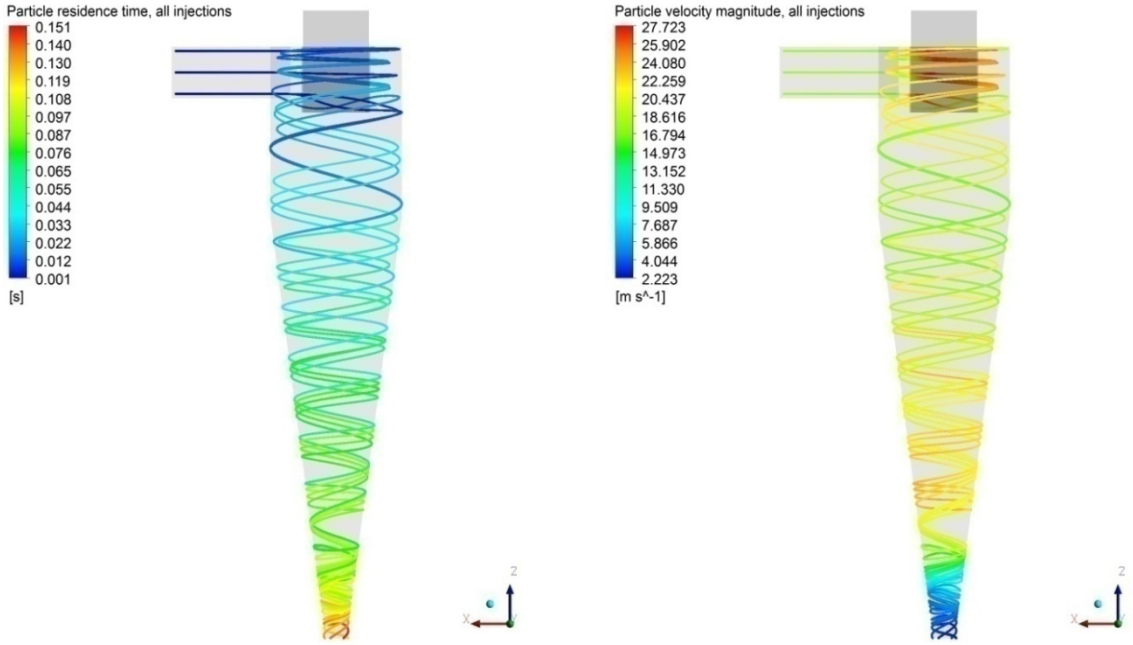

Figure 26: Trajectory of 5 particles (released from every injection, without stochastic model), hydrocyclone number 1

In illustration above the tracks of the particle are quite analogous, all particles fall out from the spigot.

As mentioned in chapter 5.3 RSM model supplements the time-averaged Navier-Stokes equation (RANS), however it is a crucial problem, in view of the fact that the fluctuations and turbulence behaviour can not be captured with this attitude (the inherent fluctuating behavior of turbulence id time averaged in this approach).
A worthwile study was carried out and interpreted in an earlier article by Chih-Yuan Hsu, Syuan-Jhih Wu and Rome-Ming Wu from Tamkang University (Taiwan):
"The dispersion of particles due to turbulence can be predicted using the stochastic tracking model, which includes the effect of instantaneous turbulent velocity fluctuations on the particle trajectory. FLUENT predicts the trajectory of a discrete phase particle by integrating the force balance on the particle." [16]
After this knowledge the stochastic tracking (implemented in DPM) was set up, which takes into account the turbulent dispersion and calculates it.
The same simulation was carried out with just one difference, the stochastic tracking was enabled.

The following trajectories:

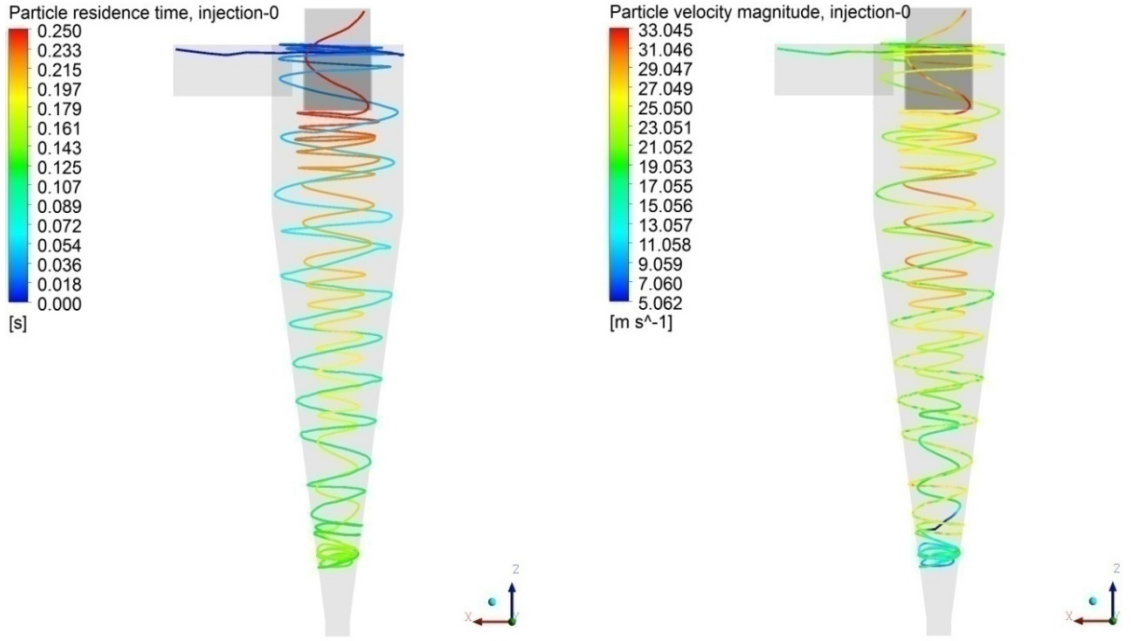

Figure 27: Trajectory of particle coloured by residence time and velocity magnitude (released from injection-0, with stochastic model), hydrocyclone number 1

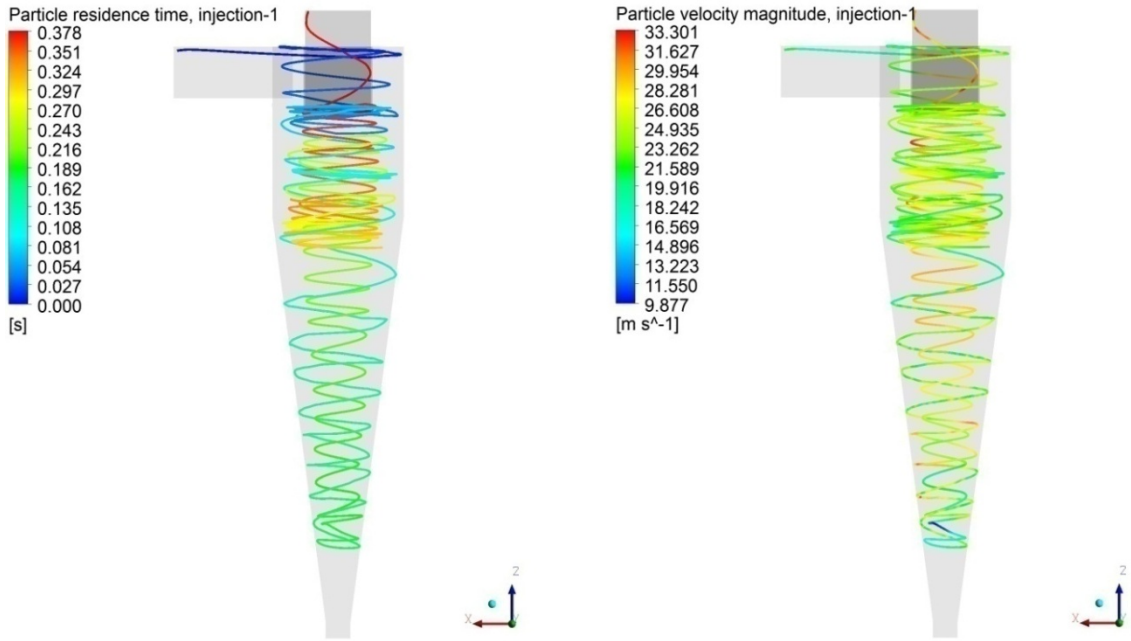

Figure 28: Trajectory of particle coloured by residence time and velocity magnitude (released from injection-1, with stochastic model), hydrocyclone number 1

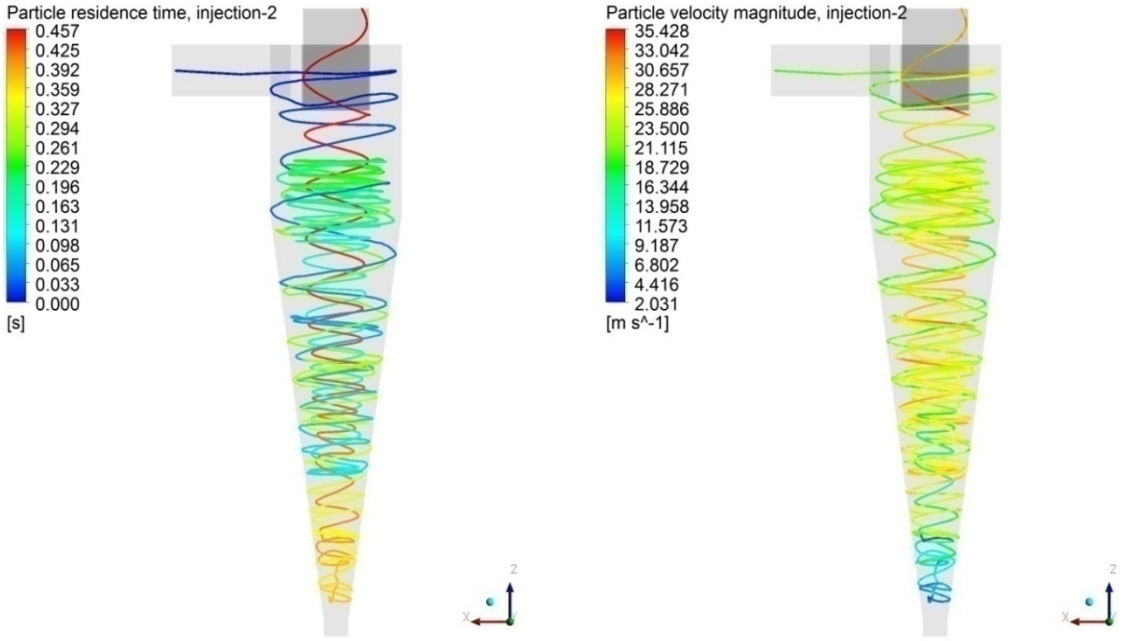

Figure 29: Trajectory of particle coloured by residence time and velocity magnitude (released from injection-2, with stochastic model), hydrocyclone number 1

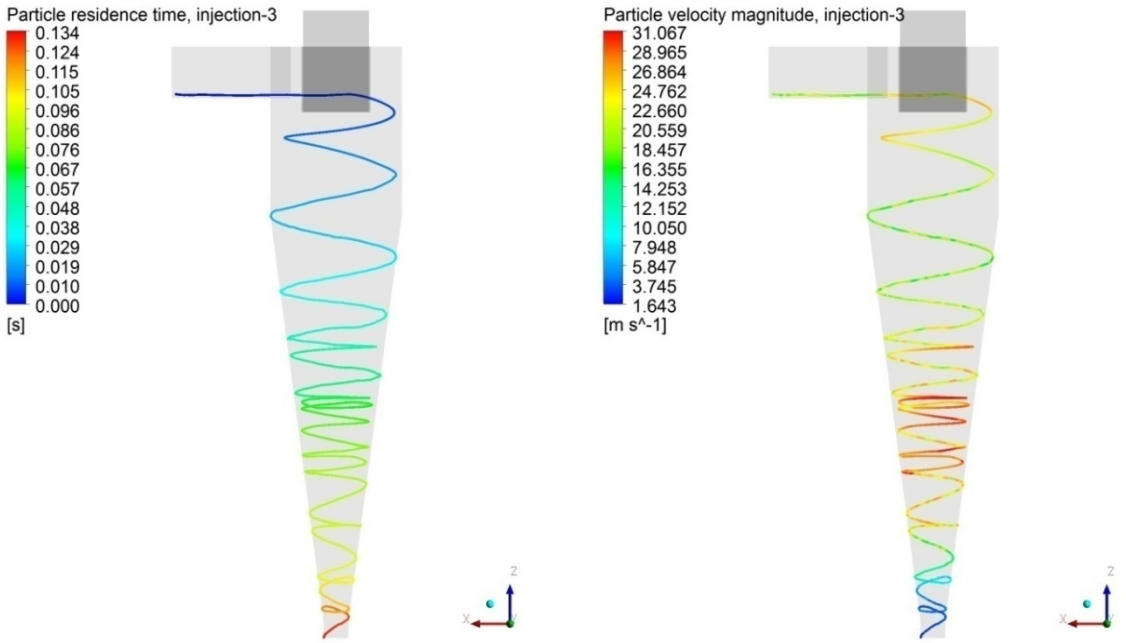

Figure 30: Trajectory of particle coloured by residence time and velocity magnitude (released from injection-3, with stochastic model), hydrocyclone number 1

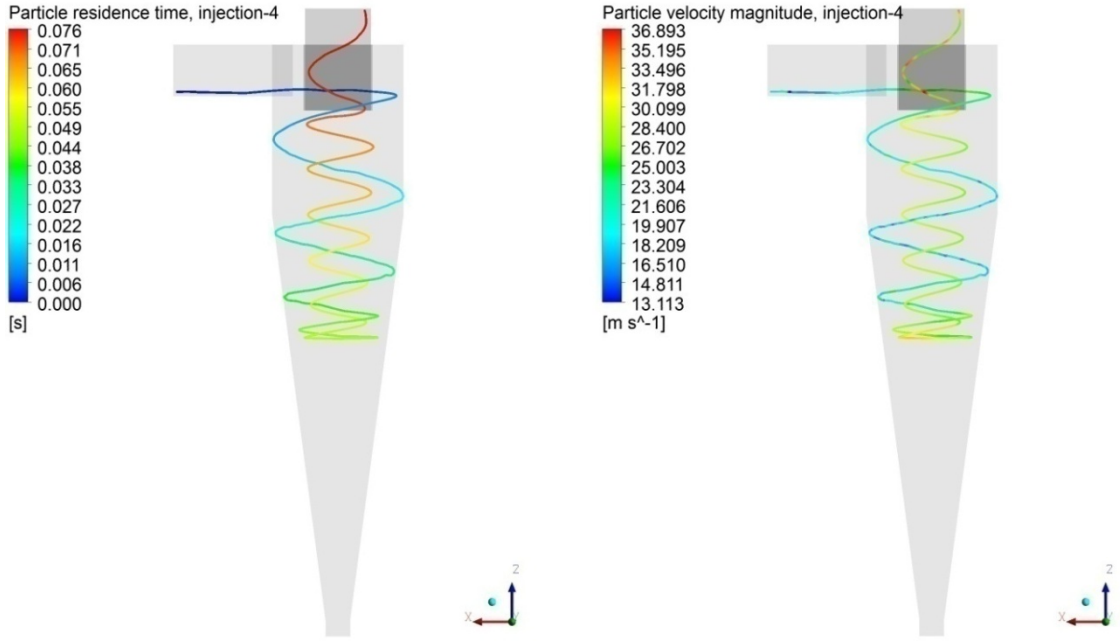

Figure 31: Trajectory of particle coloured by residence time and velocity magnitude (released from injection-4, with stochastic model), hydrocyclone number 1

In the previous five images the tracks of particles colored by velocity magnitude or by residence time are shown separately. After enabling the stochastic tracking the particle trajectories have become very chaotic, only one particle from five has left the flow domain through the spigot. From the right handed illustrations interesting fact is, that velocity magnitude varies substantially. The essential conclusion of this section is the relevancy of the turbulence impact. The figures above highlight the influence of turbulence, it causes local accelerating and decelarating of the particles along their trajectories.

	Particle residence time t_{res} $[s]$	Exit of particles through
Particle injected from injection-0	0.250	overflow
Particle injected from injection-1	0.378	overflow
Particle injected from injection-2	0.457	overflow
Particle injected from injection-3	0.134	underflow
Particle injected from injection-4	0.076	overflow

Chart 2: Residence time of particles and their fate, hydrocyclone number 1

The pressure drop
Can be determined from equation (54) and (57). The informations about the flow are obtained from the solver (mass weighted average values on given boundaries). Despite this, total pressure of air is included on boundaries (over- and underflow), the influence of air can be neglected, due to its density which is thousand times smaller than that of the water.

$$\dot{m}_1 = 5.9896412\,\frac{kg}{s};\ \dot{m}_p = 5.8745863\,\frac{kg}{s};\ \dot{m}_k = 0.043553838\,\frac{kg}{s}$$

$$p_{tot1} = 999670\ Pa;\ p_{totp} = 382100.13\ Pa;\ p_{totk} = 3715.5933\ Pa$$

From equation (57):

$$p_{drop} = \frac{\dot{m}_1\, p_{tot1} - \dot{m}_p\, p_{totp} - \dot{m}_k\, p_{totk}}{\dot{m}_1} = 624882.6058\ Pa$$

From equation (54):

$$p_{drop} = 617569.87\ Pa$$

The net flows through boundaries should be observed to check if the mass flow balance is achieved. The difference of mass flow rates, which indicates the convergence of the simulation:

$$\Delta\dot{m} = \dot{m}_1 - \dot{m}_p - \dot{m}_k = 0.071501062\,\frac{kg}{s} \qquad \frac{\Delta\dot{m}}{\dot{m}_1} = 1.194\%$$

This inaccuracy originates from the bad quality mesh (figure 19).

Efficiency and total separability
The efficiency and total separability of hydrocyclone number 1, for particles sized $1\mu m$ can be evaluated from the 5 injected particles, however the disadvantage is the small amount of particles. From equation (48) and (49).

$$\varphi = \frac{1}{5} = 0.2$$

$$\eta_h = \varphi\,\frac{\dot{m}_{lp}}{\dot{m}_{l1}} = 0.1962$$

Variant a

Mesh

The first variation of hydrocyclone number 1 differs from original in diameter of the spigot ($15mm$ was decreased to $10mm$). In addition the mesh was reconstructed to better capture boundary layer, because near wall region has large impact on boundary layer development and turbulence production. The number of elements was decreased, the total number of hex elements is 283440, which is about 70000 less, and the worst elements skewness was 0.8264.

Not all the pictures will be repated again. The aim is to point out the differences.

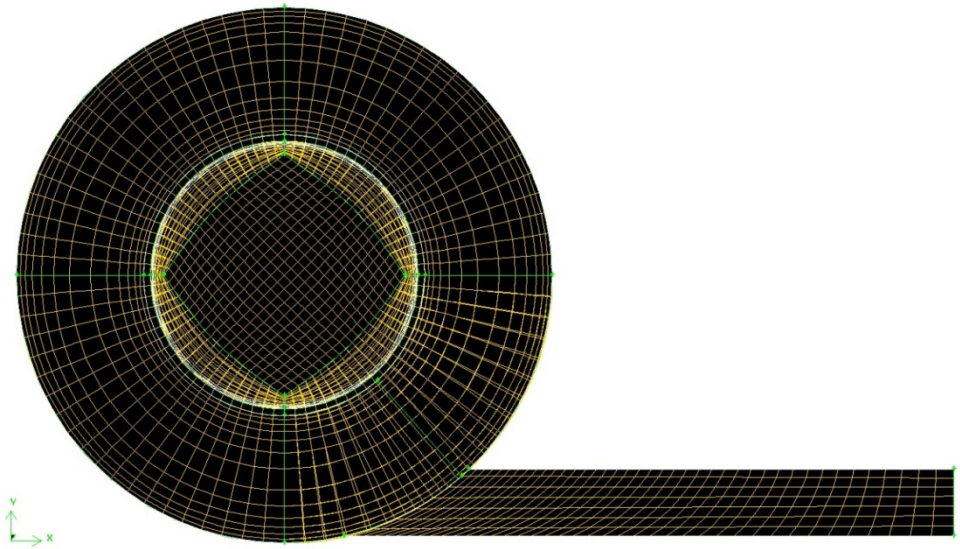

Figure 32: Computational mesh and the model of variant a

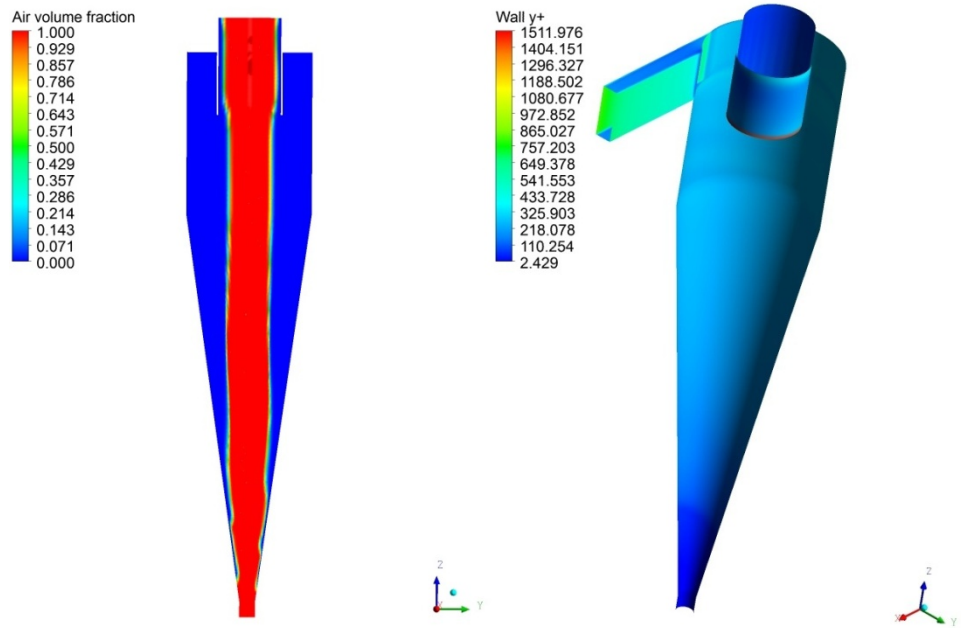

Figure 33: Air volume fraction and wall y^+ (variant a)

The picture above clearly shows that the spigot is fully blocked by the air, consequently water will leave the hydrocyclone through the vortex finder. For further application this variation is useless, because of the impossibility of separating particles. From the illustration displayed on the right, relatively high value of wall y^+ is present on the wall of the inlet nozzle (due to high velocity and a relatively coarse mesh). The highest value is on the entry to the vortex finder.

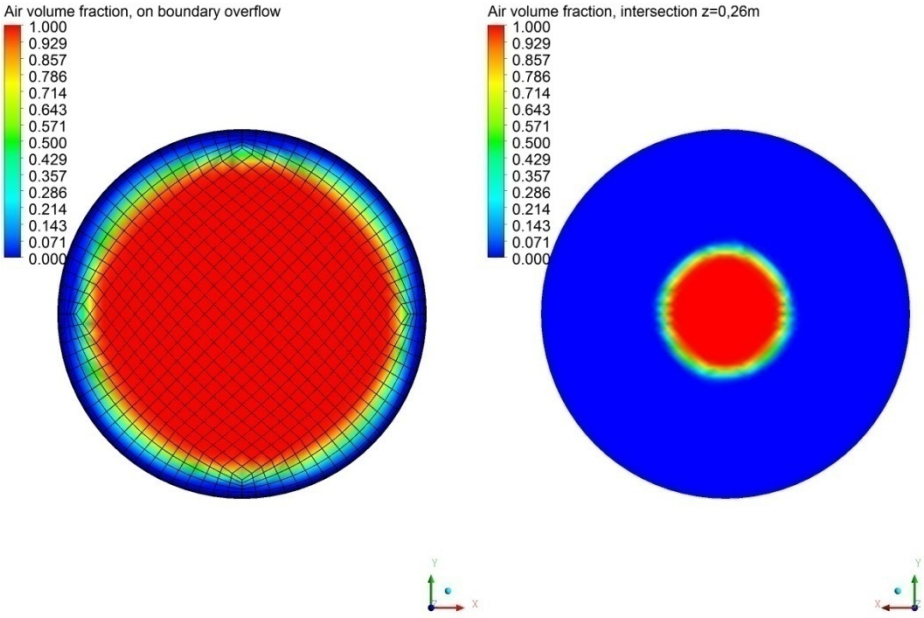

Figure 34: Air volume fraction is displayed on the boundary overflow (with the mesh) and on the intersection $z = 0.26m$ (variant a)

It is an important observation, that the air core has a circular air core, whereas the previous design had an elliptical shape.
The pictures of axial and circumferential velocity and static pressure will be not displayed due to similarity with previous designs (see hydrocyclone number 1).

The pressure drop
Informations about the flow:

$$\dot{m}_1 = 5{,}9896412\,\frac{kg}{s};\ \dot{m}_p = 5{,}9840955\,\frac{kg}{s};\ \dot{m}_k = 0\,\frac{kg}{s}$$

$$p_{tot1} = 961095{,}69\ Pa;\ p_{totp} = 443341{,}34\ Pa;\ p_{totk} = -0{,}2870343\ Pa$$

From both equations (57) and (54):

$$p_{drop} = p_{tot1} - p_{totp} = 517754{,}35\ Pa$$

The difference of mass flow rates $\Delta\dot{m} = \dot{m}_1 - \dot{m}_p - \dot{m}_k = 0{,}0055457\,\frac{kg}{s}$

$$\frac{\Delta\dot{m}}{\dot{m}_1} = 0.1\%$$

Variant b

Mesh

The number of elements, the scheme of the mesh (see figure 32) is the same, the only change is in diameter of spigot ($15mm$ was decreased to $20mm$).

Figure 35: Model of variant b

The static pressure was monitored at a point (between the axis and the wall of hydrocyclone), both schemes were used to highlight the differences between them. Both schemes Bounded Second Order Implicit, and Second Order Implicit were used.

Bounded Second Order:

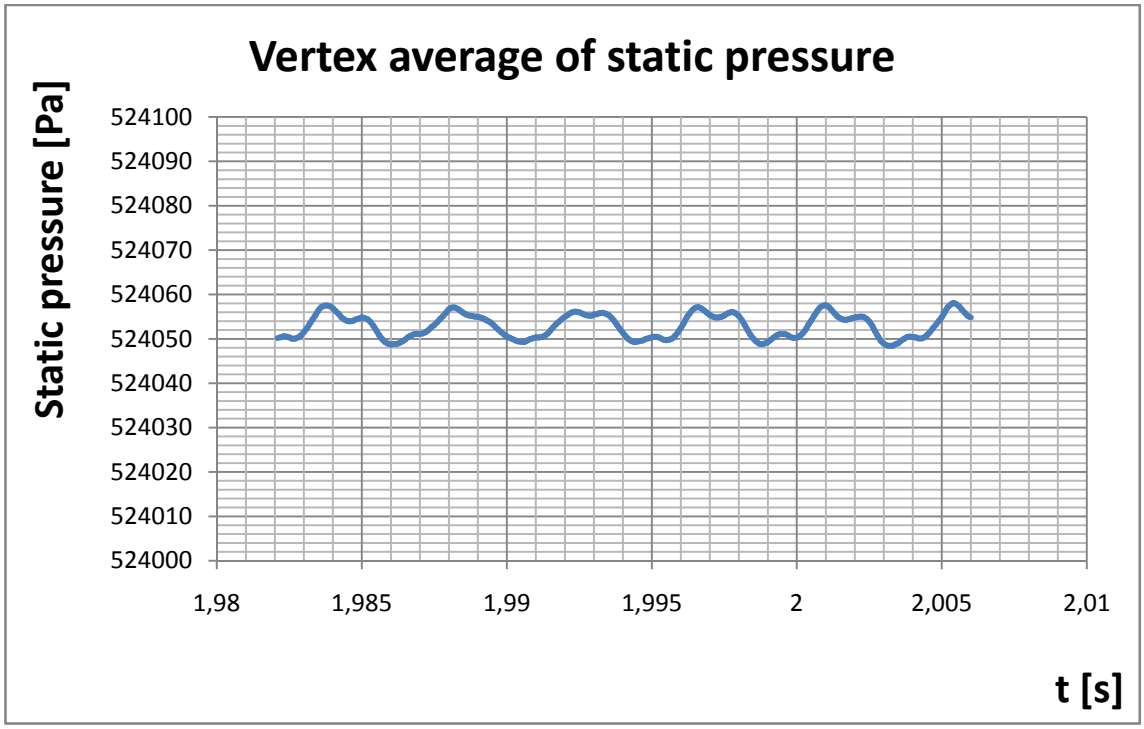

Graph 9: Static pressure of vertex average (variant b, time step $0.0001s$), Bounded Second Order Implicit scheme

Second order:

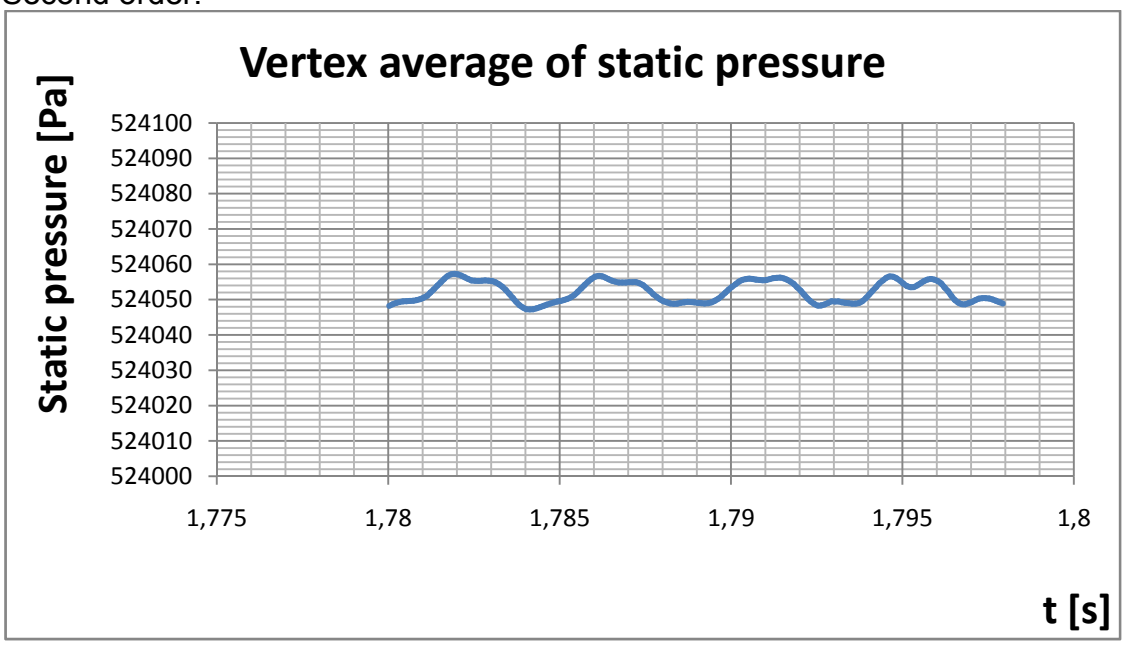

Graph 10: Static pressure of vertex average (variant b, time step $0.0001s$), Second Order Implicit scheme

From these two graphs the statement can declared, that both transient schemes produce similar results. Furthermore the dynamical effects can be neglected, because the change in static pressure is only $\pm 10\ Pa$, probably it is just a numerical noise, therefore the flow will be presumed as steady.

DPM
The tracking of particles was carried out for the same parameters and boundary conditions, as in previous calculation.

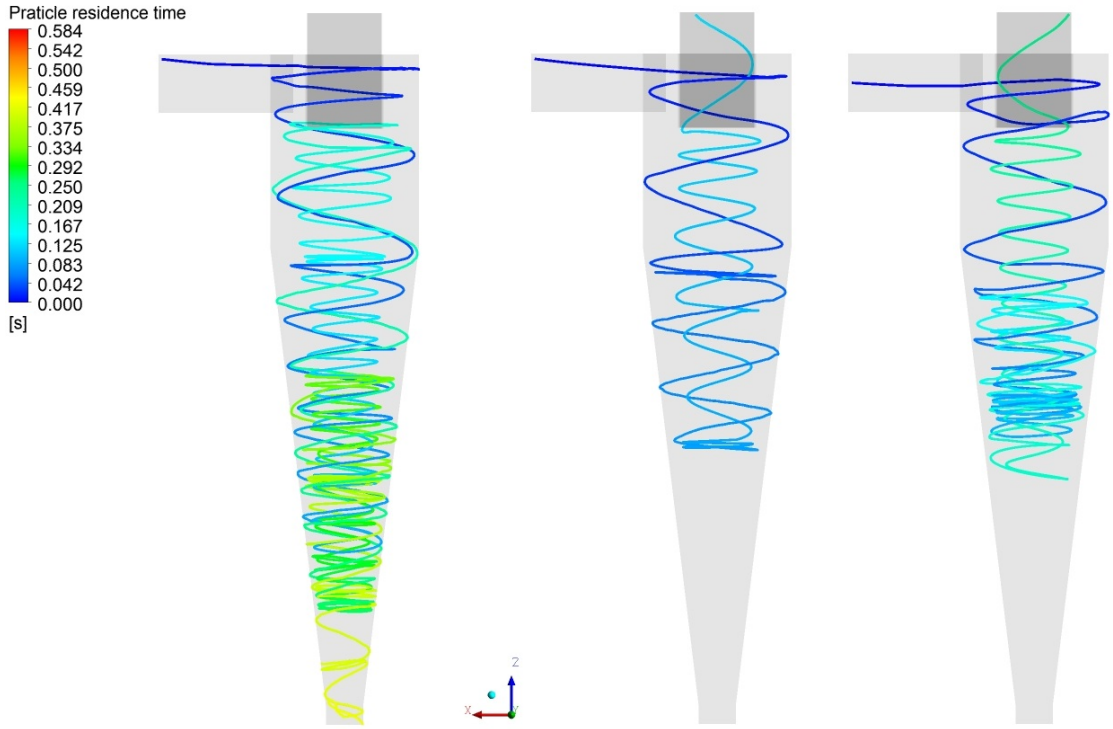

Figure 36: Trajectory of particle coloured by residence time (released from injection-0-1-2, with stochastic model), variant b

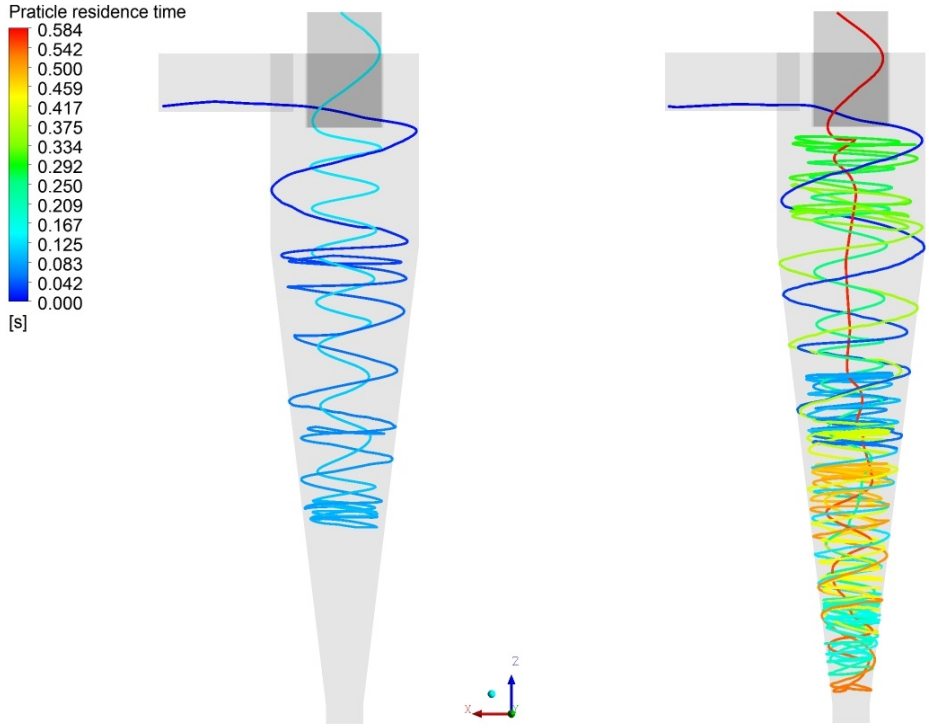

Figure 37: Trajectory of particle coloured by residence time (released from injection-3-4, with stochastic model), variant b

	Particle residence time t_{res} $[s]$	Exit of particles
Particle injected from injection-0	0.428	underflow
Particle injected from injection-1	0.123	overflow
Particle injected from injection-2	0.237	overflow
Particle injected from injection-3	0.137	overflow
Particle injected from injection-4	0.584	overflow

Chart 3: Residence time of particles and their exit, variant b

The pictures of axial and circumferential velocity and static pressure will not be displayed due to the "identity" of contour layouts (see hydrocyclone number 1). The contour of phases is identical as in figure 34 (same mesh, same characteristics).

The pressure drop
Informations about the flow:

$$\dot{m}_1 = 5{,}9896412\,\frac{kg}{s};\ \dot{m}_p = 5{,}9139766\,\frac{kg}{s};\ \dot{m}_k = 0{,}075740102\,\frac{kg}{s}$$

$$p_{tot1} = 939465{,}63\ Pa;\ p_{totp} = 425196{,}28\ Pa;\ p_{totk} = 24963{,}705\ Pa$$

From equation (57):

$$p_{drop} = \frac{\dot{m}_1\, p_{tot1} - \dot{m}_p\, p_{totp} - \dot{m}_k\, p_{totk}}{\dot{m}_1} = 519325{,}0039\ Pa$$

From equation (54):

$$p_{drop} = p_{tot1} - p_{totp} = 514269{,}35\ Pa$$

The difference of mass flow rates $\Delta\dot{m} = \dot{m}_1 - \dot{m}_p - \dot{m}_k = -0{,}000075502\,\frac{kg}{s}$

$$\frac{\Delta\dot{m}}{\dot{m}_1} = 0.00126\%$$

Efficiency and total separability
The efficiency and total separability of hydrocyclone number 1, for particles sized $1\mu m$ can be evaluated from the 5 injected particles, however the disadvantage is the small amount of particles. From equation (48) and (49).

$$\varphi = \frac{1}{5} = 0{,}2$$

$$\eta_h = \varphi\,\frac{\dot{m}_{lp}}{\dot{m}_{l1}} = 0{,}1975$$

Variant c

Mesh

The variant c differs from the original and the other two variations in the diameter of the spigot ($15mm$ was increased to $25mm$) and the size of the mesh. The number of hex elements is 314560. The measured maximum value of skewness is 0.8264. The top view from the mesh can be seen in figure (32).

Figure 38: Model of variant c

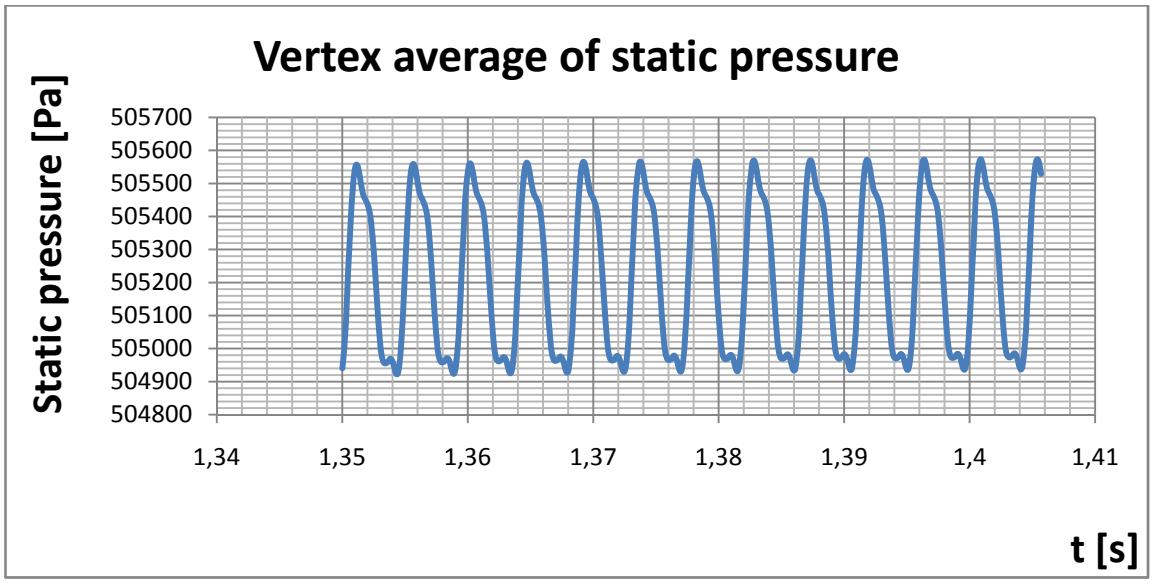

Graph 11: Static pressure of vertex average (variant c, time step $0.0001s$)

The graph displays the static pressure monitored at a point. The pressure varies from 504900 Pa to 505600 Pa, however the change is not essential. From FFT is possible to obtain the frequency of the given phenomenon (frequency of the rotating air core). The value of the frequency was confirmed from the video recorded in FLUENT. The frequency of the highest peak is $f = 219{,}78\ Hz$, which is quite close to the rotation of air core in the first design. In addition the shape of the air core was elliptical (the same situation as in the original design).

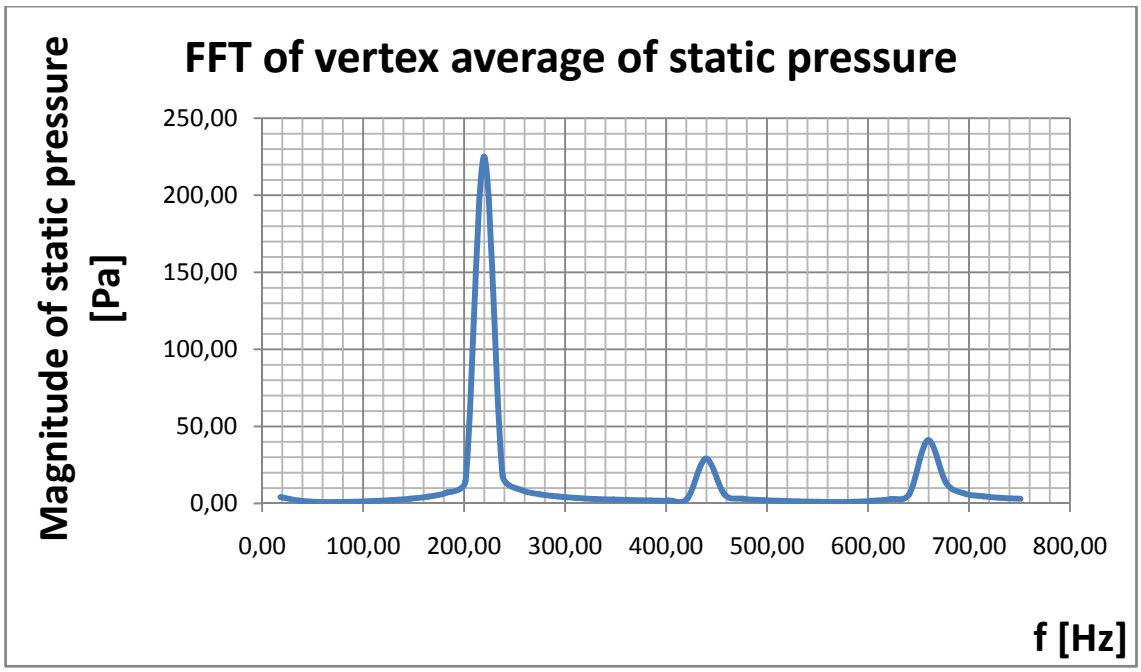

Graph 12: Fast Fourier transformation (variant c, time step $0.0001s$)

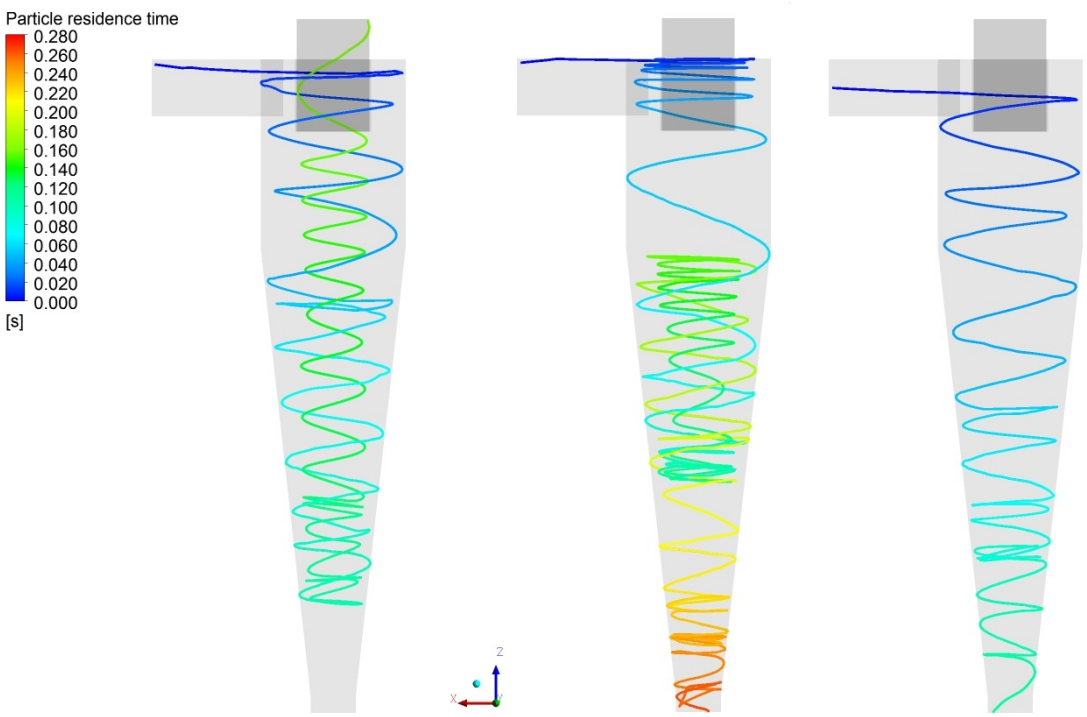

Figure 39: Trajectory of particle coloured by residence time (released from injection-0-1-2, with stochastic model), variant c

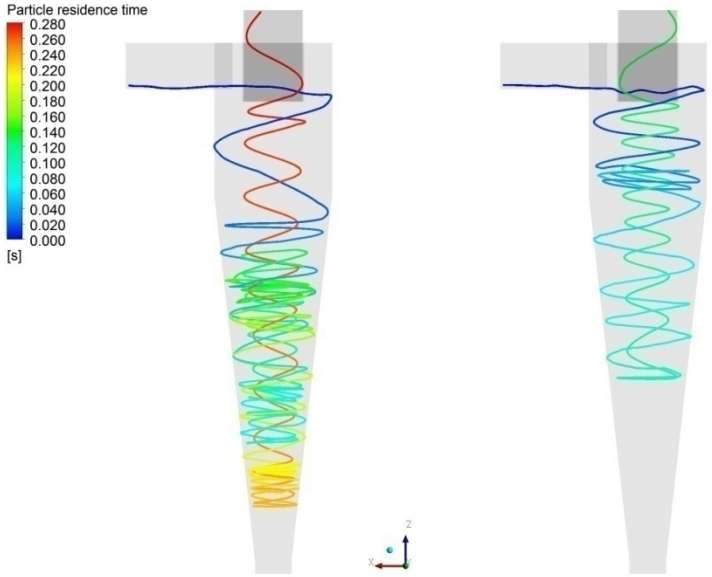

Figure 40: Trajectory of particle coloured by residence time (released from injection-3-4, with stochastic model), variant c

	Particle residence time t_{res} $[s]$	Exit of particles
Particle injected from injection-0	0.161	overflow
Particle injected from injection-1	0.264	underflow
Particle injected from injection-2	0.111	underflow
Particle injected from injection-3	0.280	overflow
Particle injected from injection-4	0.134	overflow

Chart 4: Residence time of particles and their exit, variant c

The pressure drop
Informations about the flow:

$$\dot{m}_1 = 5.9896412\frac{kg}{s};\ \dot{m}_p = 5.711115\frac{kg}{s};\ \dot{m}_k = 0.28977486\frac{kg}{s}$$

$$p_{tot1} = 921663.5\ Pa;\ p_{totp} = 409878.78\ Pa;\ p_{totk} = 96817.469\ Pa$$

From equation (57):

$$p_{drop} = \frac{\dot{m}_1\, p_{tot1} - \dot{m}_p\, p_{totp} - \dot{m}_k\, p_{totk}}{\dot{m}_1} = 526160.658\ Pa$$

From equation (54):

$$p_{drop} = p_{tot1} - p_{totp} = 511784.72\ Pa$$

The difference of mass flow rates $\Delta\dot{m} = \dot{m}_1 - \dot{m}_p - \dot{m}_k = -0{,}000075502\frac{kg}{s}$

$$\frac{\Delta\dot{m}}{\dot{m}_1} = 0.00126\%$$

The efficiency and total separability is evaluated from equations (48) and (49):

$$\varphi = \frac{2}{5} = 0{,}4; \qquad \eta_h = \varphi \frac{\dot{m}_{lp}}{\dot{m}_{l1}} = 0{,}3814$$

Summary of the 4 hydrocyclones

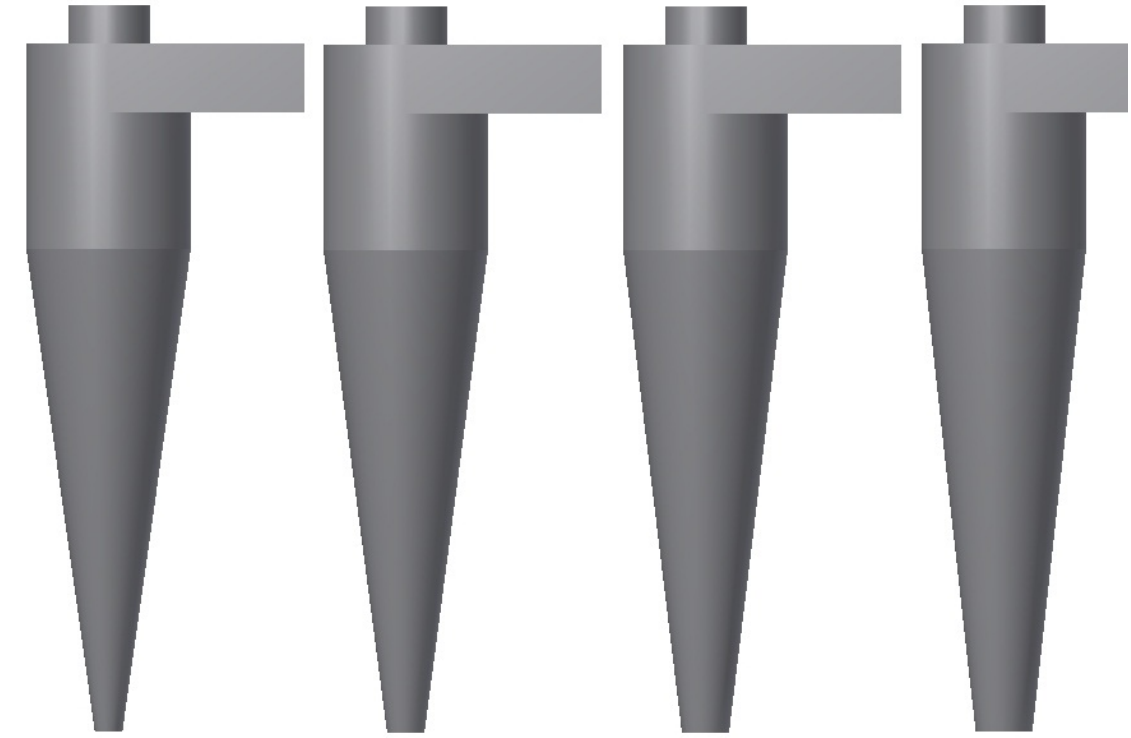

variant a hydrocyclone number 1 variant b variant c

Figure 41: Model of the original design 1 and its variants

	$\frac{d_k}{d_p}$	$p_{drop}\ [Pa]$	$\frac{\dot{m}_k}{\dot{m}_1}$
Original number 1	$\frac{0.015}{0.04} = 0.375$	642882.6058	0.007272
Variant a	$\frac{0.01}{0.04} = 0.25$	517754.35	0
Variant b	$\frac{0.02}{0.04} = 0.5$	519325.0039	0.012645
Variant c	$\frac{0.025}{0.04} = 0.625$	526160.658	0.048379

Chart 5: Summary of hydrocyclones

The pressure drop by the original design is extremely high compared to the other variants, which is caused by the bad quality of the mesh, therefore in the next graph is not included. Quadratic approximation provides inaccurate results, therefore linear approximation is used.

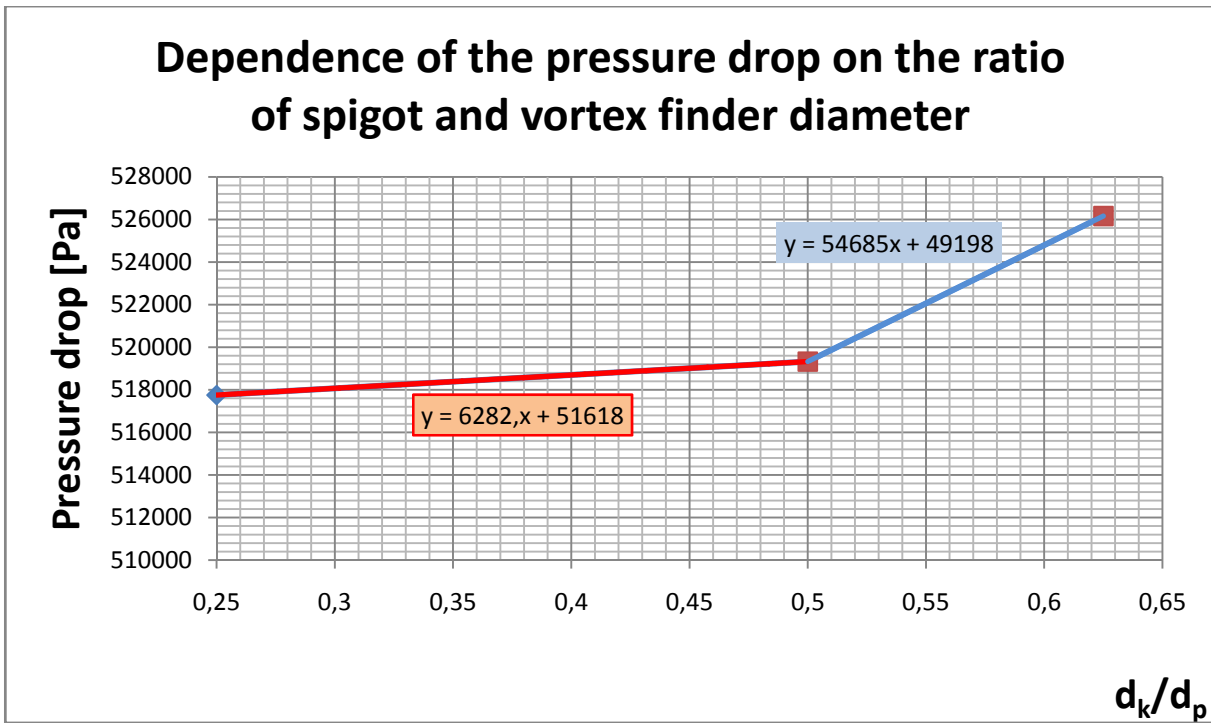

Graph 13: Dependence of the pressure drop on the ratio of spigot and vortex finder diameter

On the other hand plotting the graph of dependency of the mass flow rates does not include the variant a, because of the blocked underflow due to the air.

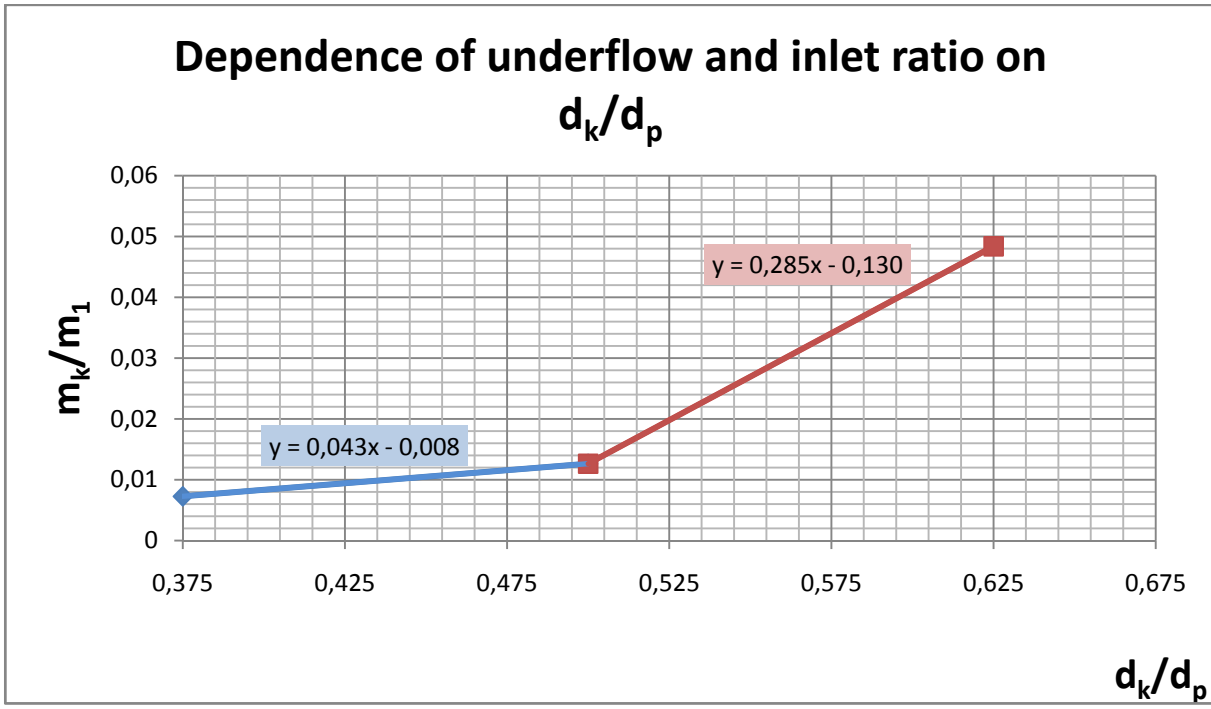

Graph 14: Dependence of underflow and inlet ratio on d_k/d_p

Hydrocyclone number 2

For this design the total number of elements is 317045, the worst elements skewness has the value of 0.766383, in addition a picture of the mesh and a cross section of the model is shown below. Length of the vortex finder is $0.0463m$.

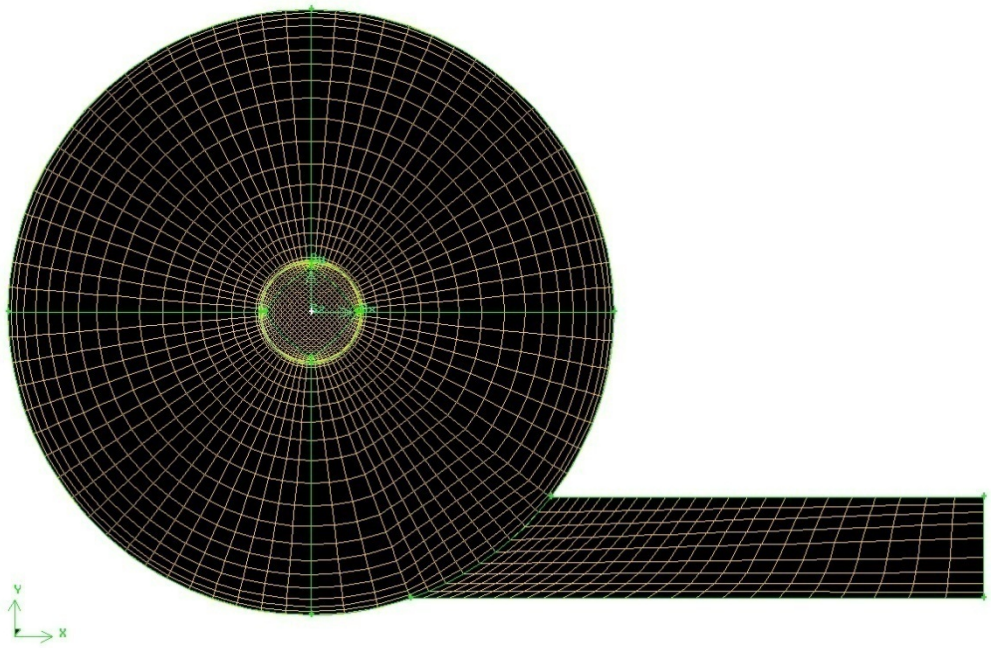

Figure 42: Computational mesh and the model of hydrocyclone number 2

Dynamical characteristics

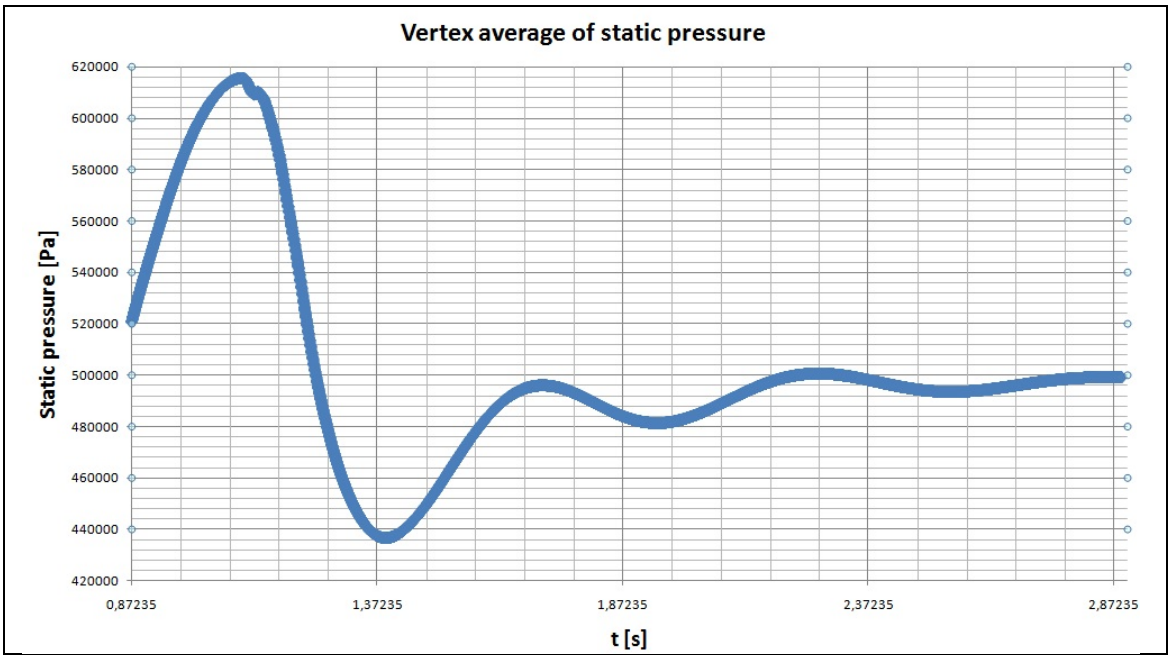

Graph 15: Static pressure monitored at a point

In the graph above the static pressure is monitored at a point, and it can be noticed as the pressure converges to an almost constant value. From this graph it can assumed the fact, that the flow characteristics are not changing in time (steady flow). The lenght of the
It is also remarkable, that this process needs about three seconds, what is a relevant drawback. The whole problem is computed with the time step 0.0001s. To achieve the value of three seconds 30000 time steps are needed, in addition the calculation of one time step took approximately 40 seconds (calculation carried out on Intel i7, 4 cores). The overall calculation of three seconds lasted 13.88 days. These calculations are highly time-consuming.

PARTICLE TRACKS:

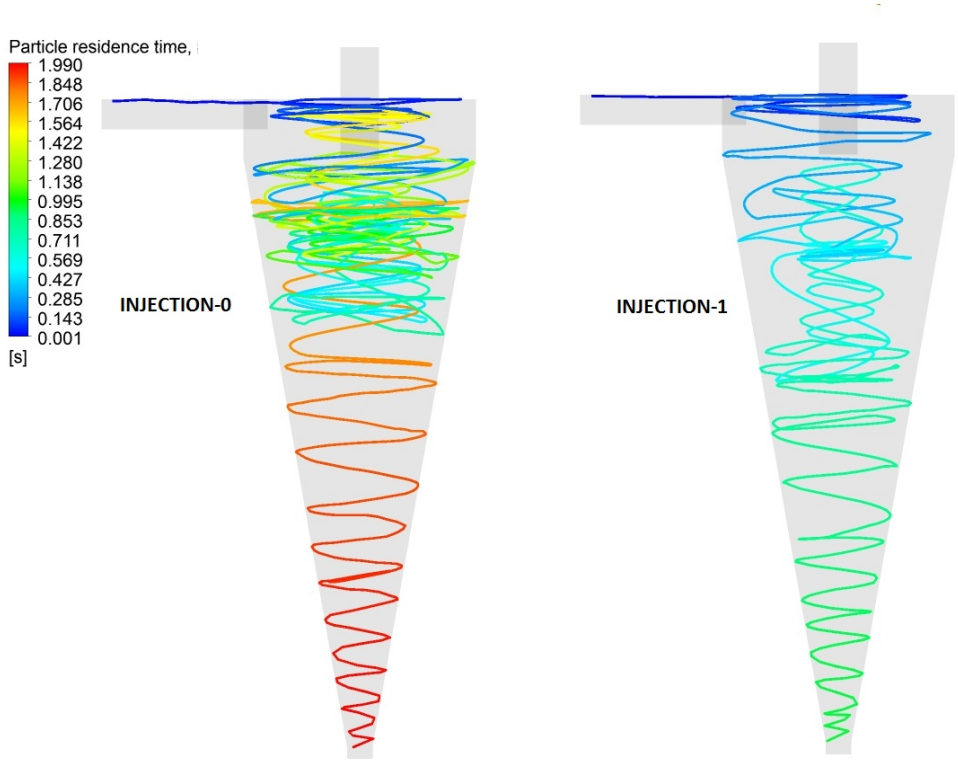

Figure 43: Particle trajectories colored by the residence time (injection-0 and injection-1)

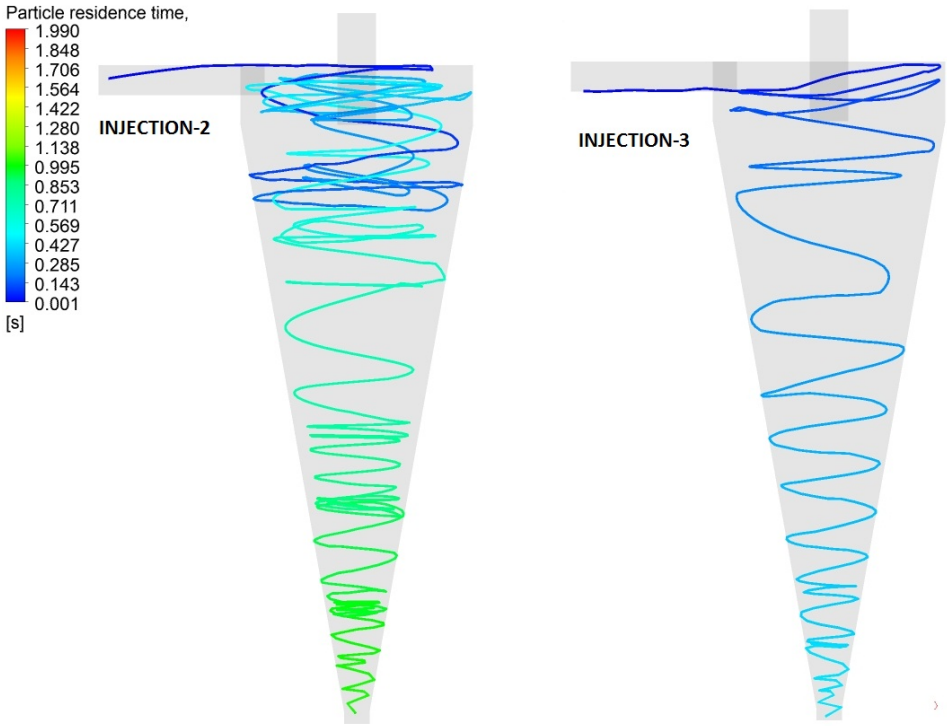

Figure 44: Particle trajectories colored by the residence time (injection-2 and injection-3)

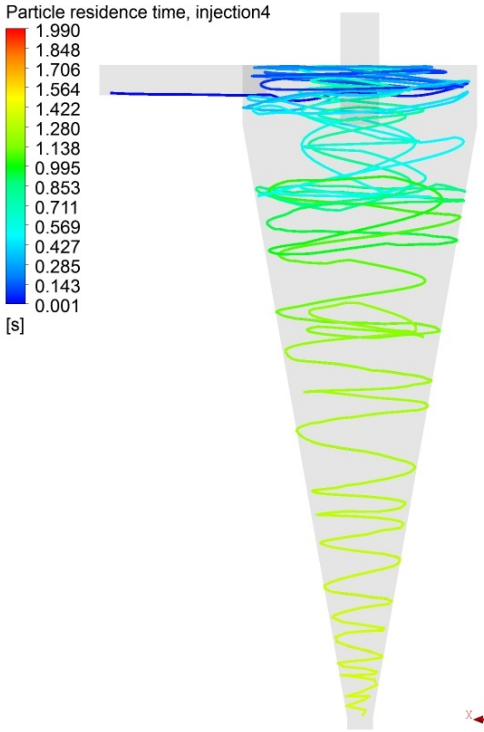

Figure 45: Particle tracks coloured by residence time (injection-4)

From the previous graphs is shown, that all the particles leave the flow domain through the spigot.

The pressure drop
Informations about the flow:

$$\dot{m}_1 = 5.9890281\frac{kg}{s};\ \dot{m}_p = 4.9893477\frac{kg}{s};\ \dot{m}_k = 0.99930278\frac{kg}{s}$$

$$p_{tot1} = 612846.63\ Pa;\ p_{totp} = 283810.06\ Pa;\ p_{totk} = 271589.44\ Pa$$

From equation (57):

$$p_{drop} = \frac{\dot{m}_1\, p_{tot1} - \dot{m}_p\, p_{totp} - \dot{m}_k\, p_{totk}}{\dot{m}_1} = 331093.5435\ Pa$$

From equation (54):

$$p_{drop} = p_{tot1} - p_{totp} = 329005.57\ Pa$$

The difference of mass flow rates $\Delta\dot{m} = \dot{m}_1 - \dot{m}_p - \dot{m}_k = 0.00037762\frac{kg}{s}$

$$\frac{\Delta\dot{m}}{\dot{m}_1} = 0.0063\%$$

The efficiency and total separability is evaluated from equations (48) and (49):

$$\varphi = \frac{5}{5} = 1$$

$$\eta_h = \varphi\frac{\dot{m}_{lp}}{\dot{m}_{l1}} = 0.833$$

This design has got a remarkable efficiency.

Variant d

The variant d is derived from the design of hydrocyclone number 2. However in this case the effect of the vortex finder length on pressure drop will be investigated. In this situation the length is 0,07m (for the original design see section 4.4.2).
The size of the computational mesh is the same as in the previous model.

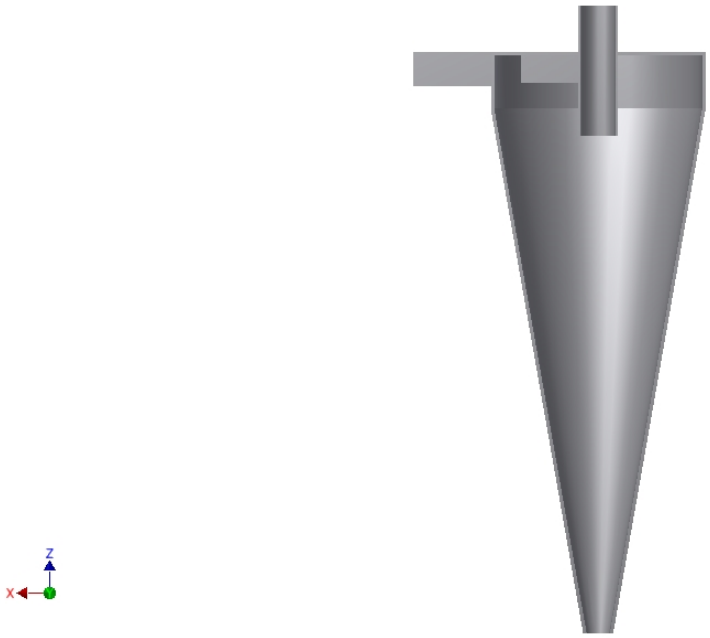

Figure 46: Model variant d

The flow character of this changed shape resembles the initial designs (hydrocyclone number), so it will not be displayed.

Informations about the flow:

$\dot{m}_1 = 5.9890281\frac{kg}{s}$; $\dot{m}_p = 4{,}99343\frac{kg}{s}$; $\dot{m}_k = 1.0067258\frac{kg}{s}$

$p_{tot1} = 643855.75\ Pa$; $p_{totp} = 285390.38\ Pa$; $p_{totk} = 291676.69 Pa$

From equation (57):

$$p_{drop} = \frac{\dot{m}_1\, p_{tot1} - \dot{m}_p\, p_{totp} - \dot{m}_k\, p_{totk}}{\dot{m}_1} = 356878.4132\ Pa$$

From equation (54):

$$p_{drop} = p_{tot1} - p_{totp} = 358465.37\ Pa$$

The difference of mass flow rates $\Delta\dot{m} = \dot{m}_1 - \dot{m}_p - \dot{m}_k = -0{,}0111277\frac{kg}{s}$

$$\frac{\Delta\dot{m}}{\dot{m}_1} = 1.11277\%$$

The DPM could not be carried out, due to the bug in FLUENT, therefore the calculation of efficiency is unable.

Variant e

This variant has got the longest vortex finder, the length is 0,09m. The size of the mesh is the same as in the previous modification.

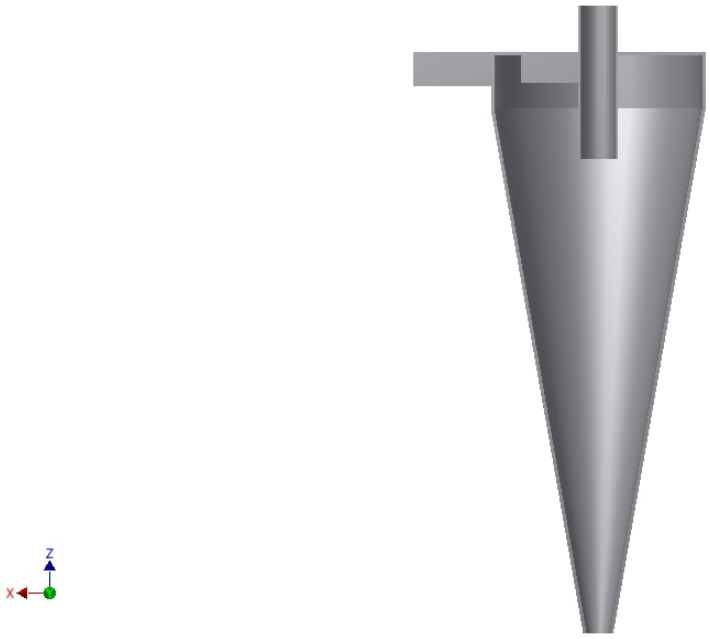

Figure 47: Intersection of variant e

Pressure drop
Informations about the flow:

$$\dot{m}_1 = 5{,}9890281\ \frac{kg}{s};\ \dot{m}_p = 5.0629332\frac{kg}{s};\ \dot{m}_k = 0.8902503\frac{kg}{s}$$

$$p_{tot1} = 705017{,}94\ Pa;\ p_{totp} = 349877.13\ Pa;\ p_{totk} = 341394{,}63\ Pa$$

From equation (57):

$$p_{drop} = \frac{\dot{m}_1\, p_{tot1} - \dot{m}_p\, p_{totp} - \dot{m}_k\, p_{totk}}{\dot{m}_1} = 358495{,}5834\ Pa$$

From equation (54):

$$p_{drop} = p_{tot1} - p_{totp} = 355140.81\ Pa$$

The difference of mass flow rates $\Delta\dot{m} = \dot{m}_1 - \dot{m}_p - \dot{m}_k = 0.0358\frac{kg}{s}$

$$\frac{\Delta \dot{m}}{\dot{m}_1} = 0.598\%$$

The DPM could not be carried out, due to the bug in FLUENT, therefore the calculation of efficiency was unable.

Summmary of the 3 designs

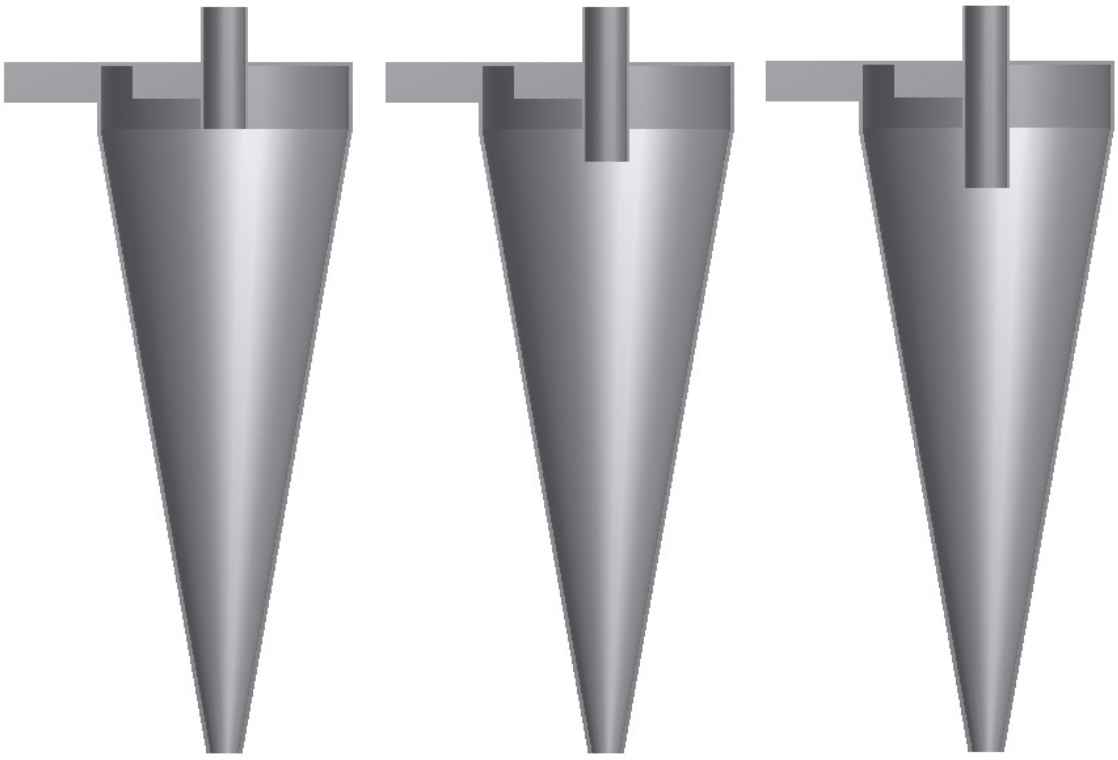

hydrocyclone number 2 variant d variant e

	Ratio of the vortex finder length	$p_{drop}\ [Pa]$
Hydrocyclone number 2	$\frac{0.0463}{0.0463} = 1$	331093,5435
Variant d	$\frac{0.07}{0.0463m} = 1.512$	356878.4132
Variant e	$\frac{0.09}{0.0463} = 1.944$	358495,5834

Chart 6: Summary of hydrocyclones

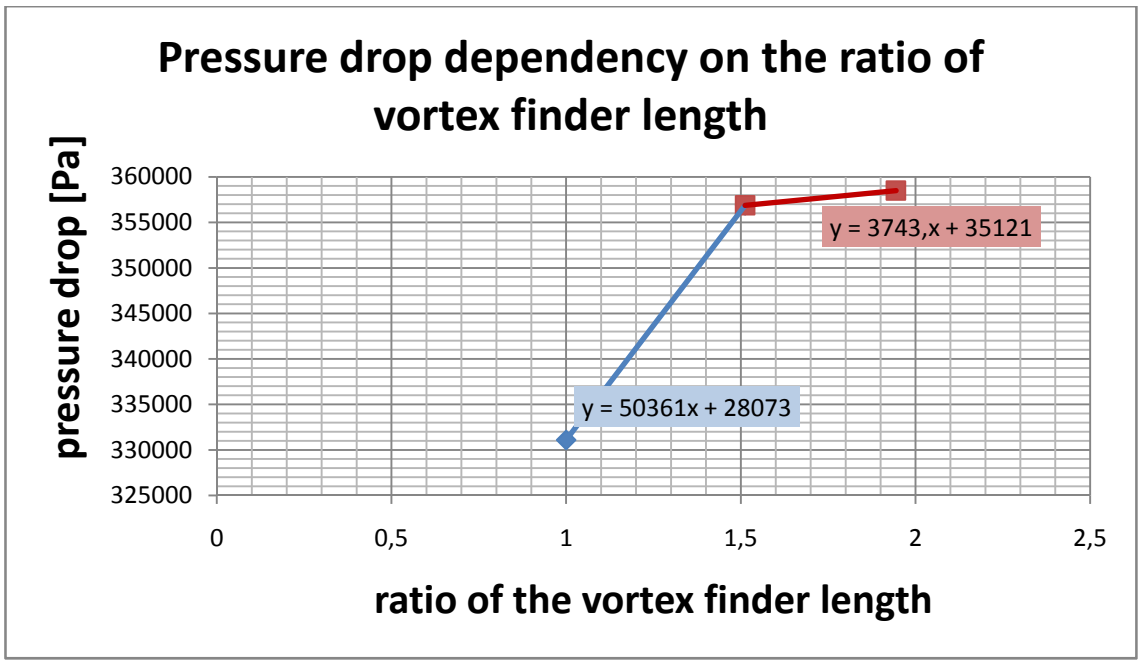

Graph16: Dependence of pressure drop on the ration of vortex finder length

The previous graph shows the longer the vortex finder is, the bigger is the pressure drop of the device.

7. Conclusion

This master thesis deals with the investigation of flow in a hydrocyclone, where difficulty of physics is present. The difficulty lies in solving a problem of the interaction of phases: water, air and dispersed solid particles. For this system the conception of Euler-Euler-Lagrange is used, where the first two fluids are treated as continuum. The practical application of such a hydrocyclone is mainly in separating materials. The first advantage of this device lies in the simplicity of its design, and secondly in the absence of moving parts. Due to the design, the suspension flows tangentially in, thus high swirling flow is gained. The mass of the water is squeezed to the walls, because of the big centrifugal force, in addition respecting the equation (34) static pressure decreases significantly along the axis of the hydrocyclone, and air is sucked in through the boundaries of under- and overflow (see figure 8 and 9), additionally air core is formed.
In chapter 3 the forces acting on the particle are deeply analyzed. Due to the absence of analytical solution of Navier-Stokes equation the tensors from fluid acting on the particle has to be substituted with forces and solved with the aid of numerical mathematics. Crucial problem is the calculation of the centrifugal force acting on the particle, because the trajectory and velocity is not known apriori (the radius and velocity distribution), therefore the simplification is applied to determine the equation for centrifugal force. This simplification presumes circular trajectory of the particle. The particle motion is assumed along the wall, hence the trajectory is quasi-known [11].
In chapter 4 a theoretical investigation is carried out of the flow in such a separator, however the disadvantage of these equations are that they have to be supplemented with empirical constants. From equations (39), (40), (41), (42), (43), (44), (45), (46) and some supplementing expressions from practice (64), (65) two designs were created. Where the first was called *hydrocyclone number 1*, and the second *hydrocyclone number 2.* Firstly the difference between them is in the design and secondly in respecting the approximation equations. *Hydrocyclone number 2* respects all the restrictions, whereas *hydrocyclone number 1* does not. In addition from the mathematical model presented in section 4.3.7 for both hydrocyclones the distribution of fractional separability was evaluated (see graph 1), the graph shows that for particles smaller than D_{50} a better separability can offer the hydrocyclone number 1, however for particles bigger than D_{50} the better variant is hydrocyclone number 2.
In chapter 5 are presented the governing equations implemented in FLUENT, a quick description can be found about the employed turbulent $k-\epsilon$ and Reynolds stress models. For modelling the two phase flow was used the volume of fluid model.
In the beginning of the calculation every hydrocyclone was initialized with $k-\epsilon$ model, then RSM, additionally VOF was adjusted. The papers show, that RSM shows quite good results on coarse meshes [24], [15]. In some situations the DPM was enabled too. Bounded Second Order Implicit scheme was set up, because the Second Order Implicit scheme has failed in some calculations. Challenging area was the determination of the appropriate time step. In the beginning it was computed with time step 0.001s, but it was shown that the results with this time step are unsatisfactory, then it was decreased to 0.0001, which showed better results.

From the original design three more modifications were created. The change was in the diameter of spigot and mesh quality. Variant a with spigot diameter 0.01m, variant b with spigot diameter 0.02m and variant c 0.025m. The reasoning was to establish the influence of the ratio of spigot and vortex finder diameter on pressure drop and the separability. It was shown that hydrocyclone number 1 has got significantly higher pressure drop then the three other variants, therefore it has been left out from the assessment (graph 13). This fact is caused by the quality of the mesh (figure 19).
The dynamical behaviour of the hydrocyclone was captured by monitoring static pressure at a point. Later fast Fourier transformation was applied to obtain the frequency of the phenomena. By the *hydrocyclone number 1* from pictures and videos was figured out, that the air core, which has got an elliptical shape is rotating, and its frequency was specified, the value is $f = 241.76Hz$. By the variant a and b pressure monitoring showed that it is almost a steady flow and no dynamical effects are present. In addition variant b was computed with both transient formulation schemes. The two graphs 9 and 10 are almost the same. However by the variant c the dynamical effects showed up. The same time steps were used out as in calculation of the hydrocyclone number 1, and the value of the frequency ($f = 219Hz$) was determined.
The distribution of static pressure is displayed in graph 6, furthermore it can be noticed that static pressure depends on the variable r, the contours shown in the figure are concentric circles, which conforms the theoretical findings. The distributions of static pressure, axial, radial and tangential velocity from simulations correspond with the distributions in the figure 12 and with results from other papers [14].
From graphs 13 and 14 it can be reported, that with increasing ratio of spigot and vortex finder diameter not only the pressure drops, but also the ratio of under- and inlet mass flow increases.
Modeling of the solid particle trajectories was realized with Euler-Lagrangian conception. The advantage of this method is that (DPM) identity is assigned to every single particle, therefore the trajectories can be determined. However for defining the separability and efficiency of the hydrocyclone it is not convenient, since large number of particles is necessary to obtain reliable values of these quantities. Simulations confirmed substantial effect of turbulent dispersion on particles depending mainly on the size of the particle. The smaller the particle is, the more the turbulent fluctuations influence its track (chaos theory).
The use of DPM was carried out for hydrocyclone number 1, variant b, variant c and for hydrocyclone number 2.

The hydrocyclone with the best parameters will be manufactured and used in the laboratories of *Victor Kaplan* Department of *Fluid Engineering.*

The most promising design is the variant c and hydrocyclone number 2.

Important parameters (pressure drop, efficiency, mass flow through spigot):

1. variant c: $\eta_h = 38.14\%$, $p_{drop} = 526160.658\ Pa$, $\dot{m}_k = 0.28977486 \frac{kg}{s}$
2. hydrocyclone number 2: $\eta_h = 83.3\%$, $p_{drop} = 331093{,}5435\ Pa$, $\dot{m}_k = 0{,}99930278 \frac{kg}{s}$

The advantage of variant c is the less mass flow rate through the spigot. Its design is smaller too, and the particles residence time is also shorter. However the hydrocyclone number 2 has got a smaller pressure drop and higher efficiency. The author would prefer hydrocyclone number 2.

8. Bibliography

[1] JIRCITANO, Alan J. Solutions. In: *Solution Chemistry* [online]. [cit. 2013-05-22]. Available: http://chemistry.bd.psu.edu/jircitano/solution.html

[2] . SaltInWaterSolutionLiquid. *File:SaltInWaterSolutionLiquid.jpg - Wikipedia, the free encyclopedia* [online]. 11 December 2004 [cit. 2013-05-22]. Available: http://en.wikipedia.org/wiki/File:SaltInWaterSolutionLiquid.jpg

[3] *Colloidal Solution* [online]. [cit. 2013-05-24]. Available: http://www.chemistrylearning.com/colloidal-solution-true-solution-and-suspension/

[4] *Colloid* [online]. [cit. 2013-05-24]. Available: http://www.britannica.com/EBchecked/topic/125898/colloid

[5] *Tyndall effect photography* [online]. [cit. 2013-05-22]. Available: http://veryphotography.com/tyndall-effect-photography/

[6] BRDIČKA, Miroslav, Ladislav SAMEK and Bruno SOPKO. *Mechanika kontinua*. 4. edit. Praha: Academia, 2011. ISBN 978-80-200-2039-0.

[7] HALLIDAY, David, Robert RESNICK, Jearl WALKER, Jana MUSILOVÁ, Jan OBDRŽÁLEK a Petr DUB. *Fyzika: vysokoškolská učebnice obecné fyziky. část 1, Mechanika: Mechanika*. 1. edit. Brno, Praha: VUTIUM: Prometheus, 2003. ISBN 80-214-1868-0.

[8] MENG, H. a C. W. M. VAN DER GELD. Liquid Solid Flows. *PARTICLE TRAJECTORY COMPUTATIONS IN STEADY NON-UNIFORM LIQUID FLOWS*. 1991, num. 118.

[9] VEJRAŽKA, Jiří. *Dynamics of bubbles / (drops) / (particles)* [internet, presentation]. 2012 [cit. 2013.5.23].

[10] DINTER, Oskar. *Hydrocyklóny a jejich použití*. Praha: SNTL, 1963.

[11] WANG, B., K.W. CHU a A. B. YU. Numerical Study of Particle - Fluid Flow in a Hydrocyclone. *Ind. Eng. Chem. Res*. 2007, num. 46.

[12] CLIFT, Roland, John R. GRACE a Martin E. WEBER. *Bubbles, drops, and particles*. New York, London: Academic Press, 1978. ISBN 012176950X.

[13] BATCHELOR, G. K. *An Introduction to Fluid Dynamics*. Cambridge University Press, 2000. ISBN 0521663962.

[14] NOWAKOWSKI, Andrzej F. a Michael J. DOBY. The Numerical Modelling of the Flow in Hydrocyclones. *KONA Powder and Particle Journal NO. 26*. 2008, num. 26.

[15] Davailles, Aurélien and Climent, Eric and Bourgeois, Florent *Fondamental understanding of swirling flow pattern in hydrocyclones*. (2012) Separation and Purification Technology, vol. 92. pp. 152-160. ISSN 1383-5866

[16] CHIH, Yuan Hsu, Jhih Wu SYUAN a Ming Wu ROME. Particles Separation and Tracks in a Hydrocyclone. *Tamkang Journal of Science and Engineering*. 2011, num. 14.

[17] RIEGER, František, Václav NOVÁK a Tomáš JIROUT. *Hydromechanické procesy*. Praha: Nakladatelství ČVUT, 2007. ISBN 978-80-01-03302-9.

[18] NOSKIEVIČ, Jaromír et al. *Mechanika tekutin*. 1. vyd. Praha: SNTL, 1987, 354 s.

[19] ŠOB, František. *Hydromechanika: studijní materiál pro I. stupeň magisterského studia, 2. a 3. ročník*. Brno: Akademické nakladatelství CERM s.r.o., 2002, 238 s. ISBN 80-214-2037-5.

[20] WENDT, John F. a John F. David ANDERSON. *Computational fluid dynamics: an introduction*. Berlin, Heidelberg: Springer, 1996. ISBN 9783540594710.

[21] VERSTEEG, H. K. a W. MALALESEKERA. *An introduction to computational fluid dynamics: The finite volume method*. Harlow, Essex: Longman Scientific and Technical, 1995. ISBN 0-582-21884-5.

[22] CHEN, Qun, Guangqing DAI a Haowu LIU. Volume of Fluid Model for Turbulence. *Journal of Hydraulic Engineering*. 2002, num. 683. DOI: 10.1061/(ASCE)0733-9429(2002)128:7(683). Available: www.paper.edu.cn

[23] ANSYS FLUENT User´s Guide. *ANSYS FLUENT 12.0 User's Guide - The Contents of This Manual* [online]. 2009 [cit. 2013-05-24]. Available: http://www.sharcnet.ca/Software/Fluent12/html/ug/node3.htm

[24] RUDOLF, Pavel. Simulation of multiphase flow in hydrocyclone. *EFM*. 2012.

[25] MEDRONHO, R. A., J. SCHUETZE a W. D. DECKWER. Numerical simulation of hydrocyclones for cell separation. Latin American Applied Research. 2005, number 8.

List of figures:

List of graphs:

List of charts: